A Novel Design Methodology for Air-based Building Integrated Photovoltaic/Thermal (BIPV/T) Systems with Coupled Modelling of Wind-driven and Channel Flow-driven Convective Phenomena

Efstratios Dimitrios Rounis

A Thesis
In the Department
of
Building, Civil and Environmental Engineering

Presented in Partial Fulfilment of the Requirements
For the Degree of
Doctor of Philosophy (Building Engineering) at
Concordia University
Montreal, Quebec, Canada

October 2021

CONCORDIA UNIVERSITY
SCHOOL OF GRADUATE STUDIES

This is to certify that the thesis prepared

By: Efstratios Dimitrios Rounis

Entitled: A Novel Design Methodology for Air-based Building Integrated Photovoltaic/Thermal (BIPV/T Systems with Coupled Modelling of Wind-driven and Channel Flow-driven Convective Phenomena

and submitted in partial fulfillment of the requirements for the degree of

Doctor Of Philosophy

complies with the regulations of the University and meets the accepted standards with respect to originality and quality.

Signed by the final examining committee:

Dr. Arash Mohammadi — Chair

Dr. Matthaios Santamouris — External Examiner

Dr. Marius Paraschivoiu — External to Program

Dr. Liangzhu Wang — Examiner

Dr. Hua Ge — Examiner

Dr. Andreas Athienitis — Thesis Supervisor (s)

Dr. Theodore Stathopoulos

Approved by

Dr. Mazdak Nik-Bakht — Chair of Department or Graduate Program Director

October 20, 2021
Date of Defence

Dr. Mourad Debbabi — Dean,

ABSTRACT

A Novel Design Methodology for Air-based Building Integrated Photovoltaic/Thermal (BIPV/T) Systems with Coupled Modelling of Wind-driven and Channel Flow-driven Convective Phenomena

Efstratios Dimitrios Rounis, Ph.D.

Concordia University, 2021

Open-loop air-based building integrated photovoltaic thermal (BIPV/T) systems have the potential to become integral elements of net-zero or near net-zero building design. In addition to on-site electricity generation, BIPV/T systems offer various options for producing useful heat when coupled with the building's HVAC system. Furthermore, when properly designed, they can fulfil building envelope functions for heat, moisture and air transfer, thus replacing the building envelope exterior layer, while offering superior architectural value compared to racked or building-applied photovoltaic (PV) systems.

Despite their potential, these systems comprise a very small share of PV applications and are not yet a mature technology. This can be attributed to several factors. Firstly, there are no standardised design guidelines, with the majority of realized systems being custom designs, not easily repeatable or scalable, and not adherent to established building techniques. Secondly, the documented performance of PV/T and BIPV/T systems is highly variable due to varying prototype designs and inconsistent testing conditions. Finally, the modelling of such systems is equally inconsistent, especially with regard to the wind-driven and channel flow convective heat transfer, elevating uncertainties in the prediction of a system's performance, further reducing confidence in such applications. The latter usually results in non-optimal thermal utilization and overheating of the PV panels that will affect their durability.

The main objective of this thesis is to set the foundation for a novel design and modelling approach for BIPV/T systems that can lead to increased share of applications of power generating envelopes (facades and roofs) for both new building constructions and retrofits, as well as enhanced system performance and durability.

This research consists of two main parts. The first part focuses on BIPV/T design considerations and investigates the adoption of curtain wall design techniques, modified for the BIPV/T systems. The purpose of this part is to address the lack of design standardization of BIPV/T and set the foundation for the adoption of common building practices in BIPV/T design, also incorporating concepts of modularity and prefabrication. To this end, the design, development and the indoor experimental testing of a modular BIPV/T curtain wall prototype is presented. The prototype was

conceived as part of a large façade application and was built using commercially available curtain wall mullion extrusions and frameless semi-transparent, glass-on-glass PV (STPV) modules with two levels of transparency. Furthermore, several thermal enhancement techniques deemed suitable for building integrated systems were incorporated, namely multiple air intakes, using transparent instead of opaque PV modules, as well as a specially built flow re-direction component. The prototype was tested in an indoor solar simulator facility under conditions representative of full-scale demonstration projects. It was found to have comparable or better thermal performance (26-32%) compared to other systems in literature (17-32%), with potential for further improvement if optimized in terms of its geometry and flow rate.

The second part of this work presents a novel approach for the modelling of convective phenomena, which takes into consideration the interlinked nature of wind-driven and channel flow-driven convection of air-based BIPV/T systems. Indeed, part of the reason for the lack of standards for BIPV/T systems is the lack of a widely accepted method for modelling convective phenomena. The key parameters that have been found to affect the thermal performance of a BIPV/T system, including the environmental (or boundary) conditions, are formulated into dimensionless groups and correlated to the ratio of wind-driven convective heat transfer over the system's heat recovery. This correlation was verified through solar-simulator testing of a modular BIPV/T system under varying environmental conditions, flow rate, channel aspect ratio and PV module opacity. Outlet air temperature predictions from the proposed modelling approach showed very good agreement with the experimental results (within ±0.4°C), as well as superior performance compared to commonly used modelling approaches (which have accuracy of ±3.0°C). Literature has shown that use of said approaches could result in up to more than 10°C error in the predicted outlet air temperature, resulting in poor thermal utilization and possible overheating of the PV panels.

This methodology can be tailored to individual systems via calibration through key temperature monitoring and can be instrumental in the optimal control and heat utilization for a coupled BIPV/T-HVAC system. In addition, it yields increased durability and performance of the PV installation through incorporation of more efficient cooling strategies, through accurate outlet air temperature and PV temperature predictions, respectively.

Acknowledgements

I want to express my utmost gratitude to my supervisors and mentors Prof. Andreas Athienitis and Prof. Theodore Stathopoulos. My academic journey and everything that followed has been a result of their trust, guidance and undivided support.

I would like to thank Olesia Kruglov for her assistance throughout the experimental process described in Chapter 3. The work presented in Chapter 5 was accomplished with the valuable critical input of Zissis Ioannidis, Harry Valianos and Anna Maria Buonomano, and the assistance of Anna Maria Sigounis. Many thanks to Erin Gaucher Loksts and Emil Calilov for their help in setting up the experiment.

Costa Kapsis has been a source of great guidance and support. Remi Dumoulin and Vasken Dermadiros have offered intuition and wit in great times of need. I would like to especially thank Sam Yip for the invaluable discussions, support and advice. To all my friends and colleagues from the lab, thank you for your help at various stages of my research.

A special thanks to Dr. Jiwu Rao, for his immense support throughout the experimental procedure, as well as valuable insight and advice in times of need.

Also, a special thanks to Prof. George Vatistas for the wonderful discussions and insight.

I would like to express my appreciation of Unicel Architectural Inc. and especially Samuel Doyon-Bissonnette for the technical support in the assembly of the BIPV/T prototypes, as well as Canadian Solar Inc. for the STPV modules.

I would also like to thank Véronique Delisle and Benjamin Roy form CanmetENERGY for a wonderful opportunity to work with them on BIPV modelling. Many thanks to the fellow researchers from IEA SHC Task 56 for the inspiring discussions.

My studies at Concordia University would not have been possible without the support from my family, as well as the encouragement from my inspiring Professors from Democritus University of Thrace, Dr. Minas Papadopoulos and Dr. Konstantinos Chalioris.

Most importantly, none of this would have been possible without the endless love and motivation from my wonderful wife Christina.

This work was funded by the Natural Sciences and Engineering Research Council of Canada (NSERC) through a NSERC/Hydro Quebec Research Chair and discovery grant, as well as the Gina Cody School of Engineering and Computer Science of Concordia University.

Table of contents

List of figures

List of tables

Abbreviations

BIPV	Building Integrated Photovoltaic
BIPV/T	Building Integrated Photovoltaic/Thermal
CFD	Computational Fluid Dynamics
CHTC	Convective Heat Transfer Coefficient
COP	Coefficient of performance
FIN	System with fins
HVAC	Heating, Ventilation and Air Conditioning
KPI	Key performance index
NOCT	Nominal operating cell temperature
PF	Packing factor
PV	Photovoltaic
PV/T	Photovoltaic/Thermal
RTD	Resistance temperature detectors
STC	Standard testing conditions
STPV	Semi-transparent photovoltaic
TMS	Thin metal sheet
UTC	Unglazed transpired collector

Nomenclature

<u>*Symbols*</u>

A_c	Collector area (m^2)
c_p	Specific heat of air (J/kg·K)
D	BIPV/T air channel depth (m)
D_h	Hydraulic diameter (m)
f	The Darcy friction factor (dimensionless)
F	View factor (dimensionless)
G	Solar irradiance (W/m^2)
$G_{available}$	Solar irradiance available for thermal conversion (W/m^2)
h_{ins}	Convective heat transfer coefficient for the insulation layer ($W/m^2 \cdot K$)
h_{PV}	Convective heat transfer coefficient for the PV layer ($W/m^2 \cdot K$)
h_{rad}	Radiative heat transfer coefficient ($W/m^2 \cdot K$)
h_{wind}	Wind induced heat transfer coefficient ($W/m^2 \cdot K$)
k	Thermal conductivity (W/(m·K))
K	Minor pressure loss coefficient
L	Length of collector or characteristic length of the flow (m)
$\dot{m}$	Mass flow rate (kg/s)
Nu	Nusselt number
P_{elec}	Electrical power produced by the PV (W/m^2)
Pr	Prandtl number
q_c	Recovered heat (W/m^2)
$q_{exterior}$	Heat transfer from the PV to the environment (W/m^2)
q_{rad}	Radiative heat transfer (W)
$q_{recovered}$	Recovered heat (W/m^2)
Q_{ratio}	Ratio of heat transfer to the environment over the heat recovered
R_{bot}	Thermal resistance of PV bottom layer ($m^2 \cdot K/W$)
R_{ins}	Thermal resistance of the insulation ($m^2 \cdot K/W$)
R_{top}	Thermal resistance of the PV top layer ($m^2 \cdot K/W$)
Re	Reynolds number
St	Stanton number
T_{air}	Average temperature of air inside the BIPV/T air channel (°C)
T_{amb}	Ambient temperature (°C)
T_{bot}	Temperature of the bottom surface of the PV module (°C)
T_{ins}	Temperature of the insulation (°C)
T_{out}	Outlet air temperature (°C)
T_{PV}	Temperature of the PV module (°C)
T_{sky}	Sky temperature (°C)
T_{STC}	PV cell temperature at standard testing conditions (°C)

T_{top}	Temperature of the top surface of the PV module (°C)
T_{zone}	Temperature of the zone adjacent to the BIPV/T system (°C)
V_{wind}	Wind velocity at reference height (m/s)
V_{avg}	Average BIPV/T channel air velocity (m/s)
w	Width (m)
W_{tot}	Total pumping power (W)
W_{fan}	Fan power (W)

Greek Symbols

α	Absorptance
β_{PV}	PV module temperature coefficient
ΔP	Pressure drop (Pa)
ΔT	Temperature difference (°C)
ε	Absolute roughness of surface (m)
ε_{ins}	Insulation layer emissivity
ε_{PV}	PV layer emissivity
ε_{tot}	Exergetic efficiency (%)
η_{el}	PV module electrical efficiency (%)
η_{STC}	PV module efficiency at standard testing conditions (%)
η_{th}	Thermal efficiency of the collector (%)
η_{th}^{*}	Modified thermal efficiency (%)
$\eta_{th\_equivalent}$	Equivalent thermal efficiency (%)
η_{tot}	Total hybrid system efficiency (%)
η_{power}	Power plant power conversion efficiency (%)
ρ	Density (kg/m^3)
σ	Stefan-Boltzman constant ($W/ m^2 \cdot K^4$)
τ	Transmittance

Chapter 1: Introduction

1.1 Background

The Paris Agreement on climate change has motivated many countries to develop legislation for the increased adoption of renewable energy systems and the reduction of greenhouse gas emissions (United Nations, 2015). Photovoltaic systems are expected to be one of the driving renewable energy technologies in the coming years (Xu et al., 2017) with a total installed capacity of 512 GW in 2018 (IEA PVPS, 2019a) and projections of 8.5 TW installed capacity by 2050 (IRENA, 2019), almost double from the projections of 2014 of 4.5 TW (IEA, 2014). For 2017 and 2018 the annual installed PV capacity was 100 GW (IEA PVPS, 2018), with the PV generated electricity having doubled its share in 2018 as compared to 2011 (IEA, 2017).

Currently the largest share of PV applications is held by utility size systems (IEA PVPS, 2019), at almost 62% of the total PV installed capacity. Regardless, distributed systems show significant growth potential, especially due to legislations and incentives promoting self consumption as well as the electrification of transportation, heating and cooling as part of the transition from fossil fuels.

Building integrated photovoltaic (BIPV) systems have been identified as one of the major tracks for large market penetration of PV (IEA PVPS, 2019), the other being price decrease, efficiency improvement, lifespan and electricity storage. Such systems can be ideal for densely built environments, where traditional ground-mounted systems cannot be easily used. The IEA PVPS Task 15, which is dedicated to the development of an enabling framework to accelerate penetration of BIPV in the global renewables market, has identified enormous growth potential for façade and roof BIPV applications. A considerable amount of research has been dedicated to the development of BIPV products with increased architectural value, such as coloured PV and semi-transparent (STPV) fenestration.

Building integrated photovoltaic/thermal (BIPV/T) systems constitute a branch of BIPV that in addition to on-site power generation, add the element of heat recovery, primarily through active cooling of the PV surface. BIPV/T systems are considered as one of the most promising applications for PV (Al-Waeli et al., 2017; Jelle & Breivik, 2012) with numerous studies showcasing the potential for waste heat exploitation and coupling with the building's HVAC, including but not limited to preheated ventilation air (Bambara et al., 2011; Dermadiros et al., 2019), heat recovery ventilator boosting (Ahn et al., 2015), air-source heat pump assistance (Delisle & Kummert, 2016; Kamel & Fung, 2014a; Huixing Li et al., 2015), as well as solar driven desiccant cooling (Guo et al., 2017). Recent studies have explored the coupled operation of BIPV/T, air-to-water heat pumps and active thermal storage, as a means to counter the intermittency of solar radiation and the fact that PV generated energy and heat may not be required at the time of production (Dumoulin et al., 2021; Rounis et al., 2018). Furthermore, a significant amount of on-going research is dedicated to the design of framing systems and heat enhancement techniques (fins, etc.) that maximize thermal efficiency, while avoiding excessive pressure drops, and facilitate installation (e.g. with curtain wall technologies) (Kruglov et al., 2017; Rounis et al., 2017, 2021a), modularity, scalability and easy of replacement/maintenance, as well as the integration of new PV technologies so as to optimize simultaneously both electrical efficiency and thermal efficiency and the establishment of archetype building categories with suited BIPV/T designs for different climates (Nibandhe et al., 2019).

Therefore, in addition to the requirements for self-consumption and electrification, BIPV/T systems can further contribute to two well recognized energy and grid related issues: the fact that building's themselves are responsible for almost 40% of the global energy consumption (IEA PVPS, 2019a), half of which is dedicated to space conditioning, and the mismatch between the time when PV power is generated and when power is needed. The latter is part of a larger subject, that of building energy flexibility; the ability of the building to enforce or delay energy consumption based on the requirements from the electrical grid.

1.2 Problem Statement

In spite of recent developments and their potential, BIPV and especially BIPV/T are not yet a mature technology and remain a niche market, holding only but a small share of PV applications (1-3%), with an equally small degree of commercialization (IEA PVPS 2019, Biyik et al., 2017; Debbarma et al., 2017; Joshi & Dhoble, 2018).

A case in point is the Varennes Library, located in Varennes, Quebec, Canada, which features a 110 kW roof PV installation. One fifth of that installation is a dedicated PV/T system used for the preheating of the fresh air supply (Fig. 1.1).

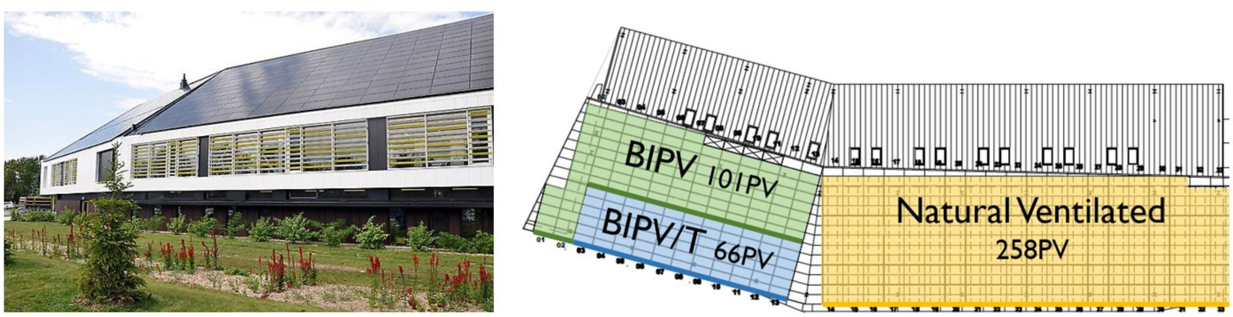

Figure 1. 1: The Varennes Library roof PV system. The southwest section implements mechanical ventilation and heat recovery.

Although characterized as a building-integrated system, both the naturally and the mechanically ventilated parts of the roof consist of regular framed PV modules, mechanically fixed on the metal roofing of an existing roof structure (Fig. 1.2), which qualifies as a building applied application (BAPV/T). Despite the almost seamless architectural result, this remains a custom solution for a specific building. Additionally, only a small portion of the total installation is exploited for heat recovery. The non-optimal design and controls of the system have led to an oversized geothermal system that caters for most of the heating demand of the building (Dermadiros et al., 2019).

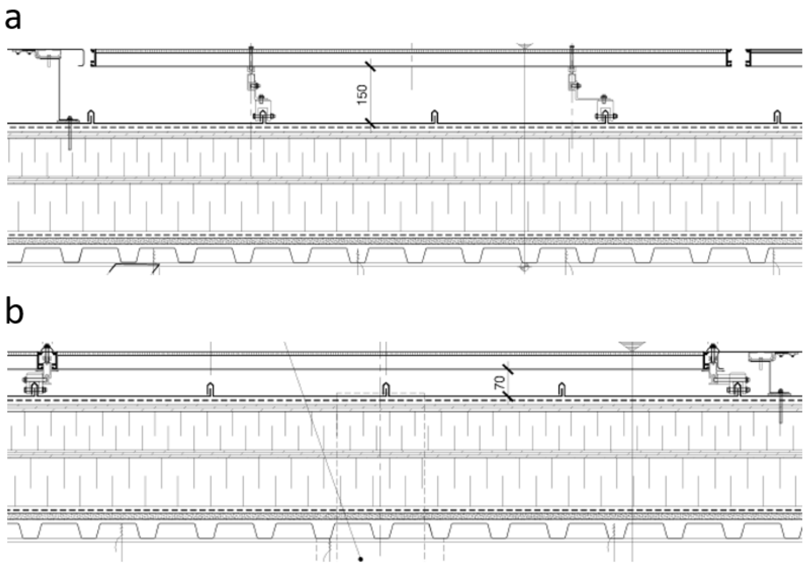

Figure 1. 2: Cross sections of the Varennes roof PV system: a. naturally ventilated section and b. mechanically ventilated section.

This can be generally attributed to three main factors, which can be summarized as follows:

1. There are no standardised design guidelines, with the majority of realized systems being custom designs, not easily repeatable or scalable, and not adherent to established building techniques. Similarly, there is no standard or guide regarding heat utilization and system design as integrated with the building's HVAC system optimized per building type and climate.

Consequently, there is small number of built projects and track record (Brahim & Jemni, 2017; Gaillard et al., 2014), which contributes to the lack of awareness of BIPV/T products. The lack of education and simple design guidelines further reduces confidence in such systems and may lead to conflict and confusion regarding professional jurisdiction and joint responsibility for architects, and structural, mechanical and electrical engineers. Additionally, the lack of design standardization results in expensive custom products, in which buyers are not willing to invest. Modularity, the implementation of the plug-and-play concept, and well-planned maintenance and repair have been recognized by the IEA Task 56 as ways to alleviate these costs (IEA SHC TASK 56, 2020).

2. The documented performance of PV/T and BIPV/T systems is highly variable due to varying prototype designs and inconsistent testing conditions. This lack of realized case studies forces engineers to rely primarily upon the documented experimental performance of PV/T and BIPV/T prototypes, which is highly variable due to varying prototype designs and inconsistent testing conditions that do not always reflect those of a full-scale installation coupled with a specific HVAC system (Rounis et al., 2021b). Gaillard et al. (2014) highlighted the need for full-scale field studies to validate the controlled laboratory studies of compact prototypes and noted that despite the

information numerical and laboratory studies may provide, they may not be adequate to describe the actual performance of a full-scale system.

3. The modelling of such systems is equally inconsistent, especially with regard to the wind-driven and channel flow convective heat transfer, elevating uncertainties in the prediction of a system's performance, further reducing confidence in such applications. The latter usually results in non-optimal thermal utilization and overheating of the PV panels that will affect their durability. Convective heat transfer has been regarded as one of the most complex and difficult modelling aspects of BIPV/T energy balance (Candanedo et al., 2011; Nemati et al., 2016a), with a multitude of expressions proposed achieving different levels of accuracy among studies. Expressions for wind-driven convection tend to be location and building type specific, while expressions used to evaluate the system heat recovery, primarily in the form of the Nusselt number, tend to be system type specific.

In air-based BIPV/T systems, the PV panels constitutes the only interface between the environment and the air channel, as opposed to glazed solar thermal collectors, where an added glazing provides a buffer between the absorber and the environment. Figure 1.1 demonstrates a typical BIPV/T cross-section and energy balance. Wind driven convection and channel convection could significantly affect one another (Rounis et al., 2021b). This can lead to highly varying convective heat transfer coefficients (*CHTC*) on either side of the PV depending on the environmental and operating conditions, and system design specifics. The effect of this interaction has not been investigated.

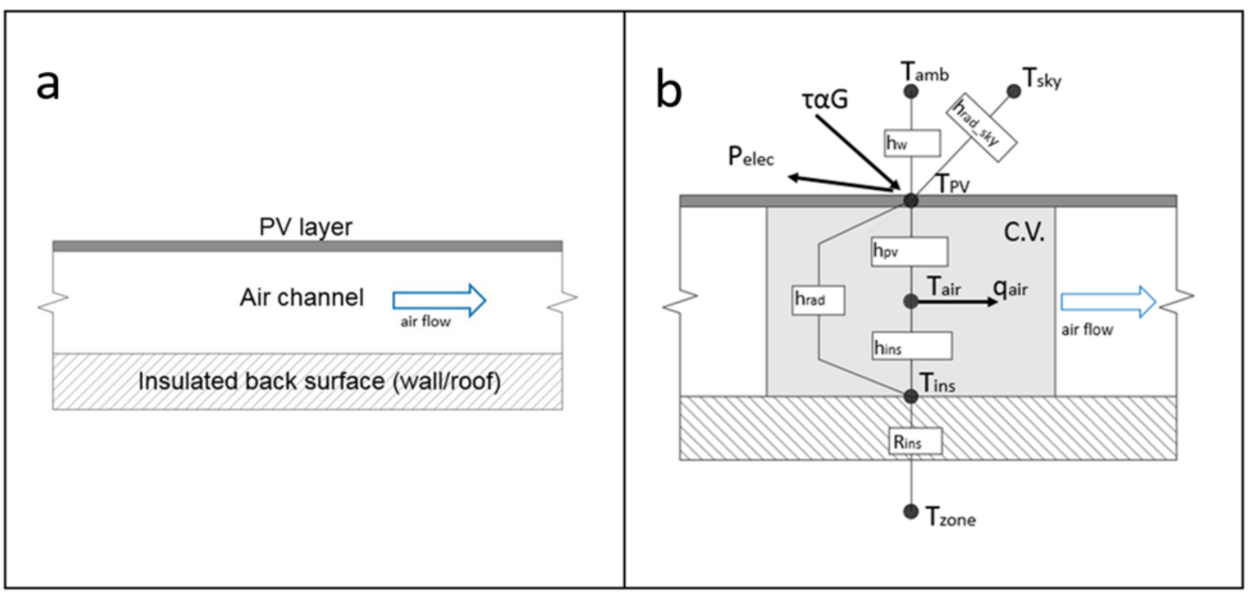

Figure 1. 3: a: common air-based BIPV/T system cross section and b: thermal network representation of its energy balance (Rounis t al 2021).

Modelling accuracy is desired but not crucial at the earlier design stages of a BIPV/T system, but can be detrimental for the optimal BIPV/T-HVAC operation, as well as the prediction of maximum PV panel temperature. This low accuracy can adversely affect the system's durability.

1.3 Thesis scope

The research presented in this thesis consists of two main parts; The first part addresses the issue of design standardization for BIPV/T systems and aims to set the foundation for the implementation of common building practices in BIPV/T design. To this end, the design, development and the indoor experimental testing of a modular BIPV/T curtain wall prototype is presented. The prototype was conceived as part of a large façade application and was built using commercially available curtain wall mullion extrusions and frameless semi-transparent, glass-on-glass PV (STPV) modules with two levels of transparency. Furthermore, several thermal enhancement techniques deemed suitable for building integrated systems were incorporated, namely multiple air intakes, using transparent instead of opaque PV modules, as well as a specially built flow re-direction component. The prototype was tested in an indoor solar simulator facility under conditions representative of full-scale demonstration projects. It was found to have comparable or better thermal performance (26-32%) compared to other systems in literature (17-32%), with potential for further improvement if optimized in terms of its geometry and flow rate.

While there are issues that need to be further addressed, including, but not limited to, the function of PV as building materials, safety issues, facilitation of wiring and continuity of the building envelope, this study shows that there is significant potential in the implementation of the curtain wall building techniques as a more standardized system design approach to allow higher penetration of BIPV/T in the market. This design technique is not introduced as a sole solution of standardized BIPV/T design but aims to set the basis on the adoption of common building practices and their modification into standardized BIPV/T elements.

The second part of this work presents a novel approach for the modelling of convective phenomena, which takes into consideration the interlinked nature of wind-driven and channel flow-driven convection of air-based BIPV/T systems. The key parameters that have been found to affect the thermal performance of a BIPV/T system, including the environmental (or boundary) conditions, are formulated into dimensionless groups and correlated to the ratio of wind-driven convective heat transfer over the system's heat recovery. This correlation was verified through solar-simulator testing of a modular BIPV/T system under varying environmental conditions, flow rate, channel aspect ratio and PV module opacity. Outlet air temperature predictions from the proposed modelling approach showed very good agreement with the experimental results (within ±0.4°C), as well as superior performance compared to commonly used modelling approaches (which have accuracy of ±3.0°C). Literature has shown that use of said approaches could result in up to more than 10°C error in the predicted outlet air temperature, resulting in poor thermal utilization and possible overheating of the PV panels.

This methodology can be tailored to individual systems via calibration through key temperature monitoring and can be instrumental in the optimal control and heat utilization for a coupled BIPV/T-HVAC system. In addition, it yields increased durability and performance of the PV installation through incorporation of more efficient cooling strategies, through accurate outlet air temperature and PV temperature predictions, respectively.

1.4 Thesis overview

This thesis follows the chapter-based format although big part of the content of several chapters has been presented in several journal publications, as reported in the relevant footnotes. The thesis is composed of 6 chapters including the introductory.

- Chapter 2 presents a comprehensive literature on several aspects of BIPV/T, including performance affecting parameters, thermal enhancements, testing, modelling, thermal applications and design issues.
- Chapter 3 presents the design, development and experimental investigation of a BIPV/T curtain wall prototype which aims to set the foundation for standardized design options adhering to existing building practices.
- Chapter 4 presents a study on the effect of the use of the different expressions for wind-driven and channel convection commonly used in PV/T and BIPV/T modelling, on the numerical prediction of the channel air temperature rise.
- Chapter 5 introduces a novel approach for the modelling of the aforementioned convective phenomena, where wind-driven and channel convection are treated together in the form of a dimensionless ratio and correlated to other dimensionless numbers derived from the analysis of the important parameters that affect the thermal performance of a hybrid system.
- Finally, chapter 6 summarizes the main conclusions and contribution of this thesis, discusses research needs and provides suggestions for future work.

Chapter 2: Literature Review[1]

2.1 Introduction

This chapter presents an overview of various subjects regarding BIPV/T systems and consists of two main sections. Sections 2.3-2.5 deal with the parameters that affect the performance of air-based PV/T and BIPV/T systems, thermal enhancing techniques that have been introduced as means of overcoming the poor thermophysical properties of air as a coolant, as well as realized and theoretical thermal applications. Relevant design issues are discussed from a building integration perspective. The remaining sections focus on the lack of standardized testing and modelling procedures for such systems. A comprehensive review of experimental studies is presented which demonstrates that PV/T and BIPV/T systems' testing can be highly inconsistent making performance comparison of various system types very difficult. Similarly, there is a multitude of approaches on PV/T and BIPV/T modelling, which is also highly inconsistent, especially as far as the convective phenomena are concerned.

2.2 PV/T and BIPV/T

PV/T is a general term used to describe any type of hybrid photovoltaic-thermal system that cogenerates electricity and heat, by using a fluid medium to extract that heat from the PV/absorber surface. The original PV/T prototypes were essentially solar thermal collectors with pasted PV cells (Florschuetz, 1979; Wolf, 1976), with early studies focusing on maximizing the system's thermal performance (Fig. 2.1).

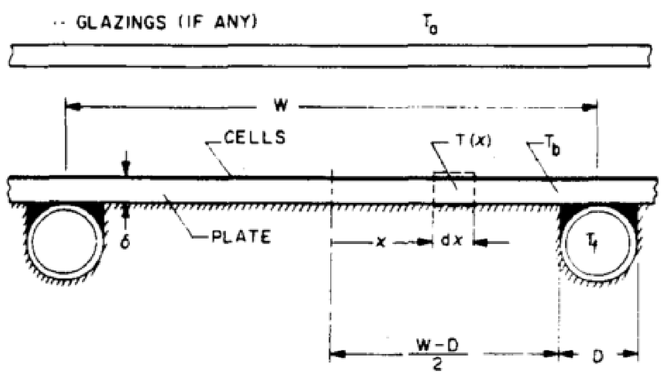

Figure 2. 1: Early solar thermal collector of the sheet and tube configuration, with pasted PV cells (Florschuetz, 1979).

In practice, the term PV/T or PV/T collector is attributed to stand-alone hybrid photovoltaic-thermal units that have a format similar to that of flat plate solar thermal collectors (Figure 2.2). PV/T collectors can be installed individually as add-on systems on the roofs of buildings or used in other applications as i.e. greenhouse driers (Tiwari et al., 2018).

[1] Part of the literature review has been included in: Rounis, E. D., Athienitis, A., & Stathopoulos, T. (2021). Review of air-based PV/T and BIPV/T systems - Performance and modelling. *Renewable Energy*, *163*, 1729–1753.

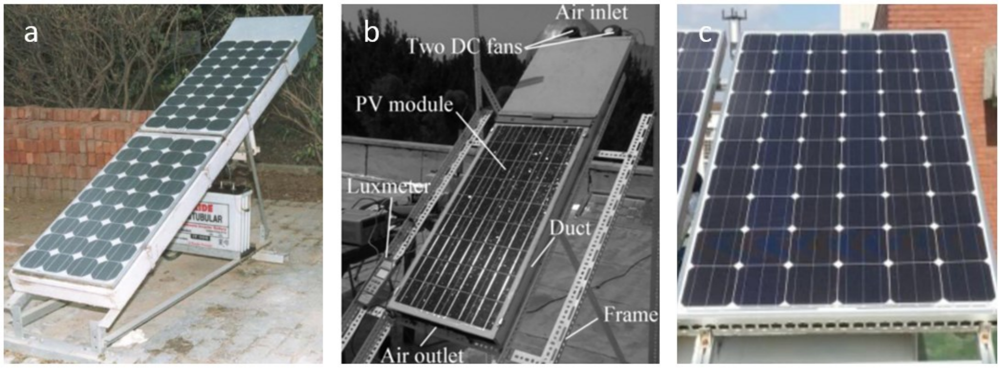

Figure 2. 2: PV/T stand-alone collectors (Adeli et al., 2012; Kim et al., 2014; A. Tiwari et al., 2006).

Depending on the cooling medium, PV/T can be primarily categorized as air-based or water-based, although there are systems which combine air and water (Bakar et al., 2014), use nanofluids or phase changing materials (PCM) (Malvi et al., 2011; Nahar et al., 2017). Depending on the PV/absorber morphology there are flat-plate and concentrating collectors. PV/T distinctions have been comprehensively presented in the review studies of Joshi & Dhoble (2018), Lamnatou & Chemisana (2017), Xu et al. (2017) and Yang & Athienitis (2016) among others.

BIPV/T systems constitute a branch of PV/T systems through the integration of the PV/T concept with the building itself. BIPV/T is also part of the wider category of building integrated photovoltaic (BIPV) which encompasses all different ways of integrating PV with the building such as semi-transparent PV (STPV) windows, façade/roof integrated PV, PV overhangs, double-skin façade STPV applications etc. In practice, the term BIPV is usually used to signify integrated PV applications without active heat recovery.

Building integration itself suggests the implementation of a PV/T system which is structurally and architecturally integrated with the building, maintains the building envelope functions and replaces common building envelope materials. The term is often loosely attributed to systems that are applied on an existing building envelope (building applied PV/T or BAPV/T) (Yang & Athienitis, 2016a), which however exhibit seamless aesthetic integration, such as the roof BIPV and BIPV/T system of the Varennes Library in Quebec, Canada (Dermadiros et al., 2019).

According to the IEC 63092-1 and -2 standard on BIPV systems, a BIPV system should employ PV modules that "provide one or more of the functions of the building envelope" (IEC 61730-1, 2020; IEC 61730-2, 2020). This standard covers the electrotechnical and building related requirements such as mechanical resistance and stability, and primarily safety aspects, but does not include best practice guide for the actual design and neither does it cover the design and HVAC integration for BIPV/T.

The fundamental design and operation concept for air-based PV/T collectors and full-scale BIPV/T systems is the same. The main difference is the system size, with BIPV/T covering a large section of a building's façade or roof, as well as its added building function (structural and architectural integration, mechanical integration with the HVAC and building envelope function). Figure 2.3

presents the basic air-based PV/T and BIPV/T design with the PV/absorber on the outer layer, an air channel for air circulation and an insulated back surface.

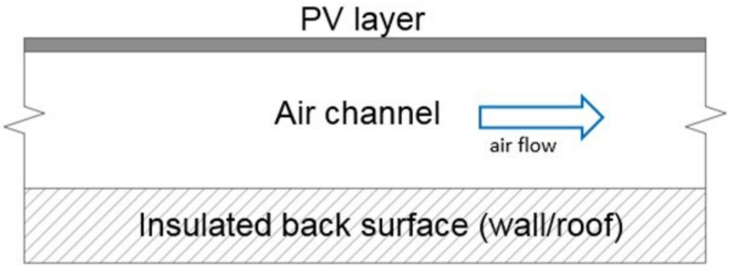

Figure 2. 3: Basic air-based PV/T and BIPV/T design (Rounis et al., 2017).

Figure 2.4 presents some notable BIPV/T systems. The John Molson School of Business (JMSB) building of Concordia University features a unique façade BIPV/T system on its penthouse, which consists of custom p-Si PV modules set upon an unglazed transpired collector (UTC) cladding (Bambara et al., 2011). The shape and orientation of the PV modules was designed to match the modulation of the building's curtain wall, as well as reduce temperature stratification in the vertical axis. The recovered heat is used for ventilation air preheating during the heating season and is rejected during the summer. This hybrid system constitutes the first form of a multiple-inlet BIPV/T system.

Figure 2. 4: Full-scale BIPV/T systems, from left to right: the EcoTerra house roof system, the JMSB façade system, roof BIPV/T of the Varennes library and roof BIPV/T with integrated skylight of the Deep Performance Dwelling.

The Varennes Library building features a large roof PV installation, one section of which is naturally and one mechanically ventilated (Dermadiros et al., 2019). This is practically an add-on system with framed PV modules fixed with supports upon a metal roof which achieves almost seamless architectural integration with the building. Approximately one fifth of the PV installation serves as a BIPV/T system, with the recovered heat used for ventilation air preheating.

The roof BIPV/T systems installed in the EcoTerra house (Chen et al., 2010), one of the first net-zero energy buildings in Canada, and the Deep Performance Dwelling (DPD) (Dumoulin et al., 2021; Rounis et al., 2018), which was the design entry by Team Montreal for the 2018 Solar Decathlon competition in China, can be prime examples of the potential for standardization in BIPV/T design. The former introduced a prefabricated modular design where the whole roof assembly including the BIPV/T (a-Si modules pasted on metal roofing) was pre-assembled and shipped to location. The latter featured a curtain wall design approach based on the system discussed in the present study, which allowed for seamless building integration, as well as the incorporation of an integrated skylight.

Table 2.1 summarizes the basic features of the four BIPV/T systems.

Table 2. 1: Full scale BIPV/T systems

Case Study	Building Type	System Type	Integration Type	System (peak power, installation area)	Thermal application
EcoTerra (Chen et al., 2010)	Residential	Roof	Flexible a-Si modules pasted on metal roofing, wooden roof structure	2.84 kW 55 m^2	Outlet air used passed through ventilated concrete slab
JMSB (Bambara et al., 2011)	Institutional/ Office	Façade	Custom p-Si modules over UTC cladding	24.5 kW 288 m^2	Preheated ventilation air
Varennes Library (Dermadiros et al., 2019)	Institutional/ Library	Roof	Framed p-Si modules braced on corrugated metal roof	110 kW 711 m^2	Preheated ventilation air
DPD (Dumoulin et al., 2021)	Residential	Roof	BIPV and BIPV/T curtain wall frame fixed on roof.	12.4 kW 80 m^2	Air/water heat exchanger to cold tank of 2-tank heat pump system

A major distinction among PV/T systems refers to the heat transfer medium. Water-based PV/T systems use a closed loop of water or a mixture of water/glycol in cold climates as the medium, while air-based systems use air primarily in an open loop configuration. Comprehensive reviews of water-based PV/T studies can be found in (Al-Waeli et al., 2017; S. S. Joshi & Dhoble, 2018; Michael et al., 2015). Such systems can achieve higher fluid temperatures and are usually used for domestic hot water (DHW) applications (Bigorajski & Chwieduk, 2018) but may extend to solar assisted heat pump and industrial applications for water desalination.

Notwithstanding their thermal efficiency and performance, water-based systems are arguably better suited as stand-alone units rather than fully integrated systems to avoid the risk of freezing and leakage than can lead to corrosion at the building envelope level. Conversely, air-based systems are arguably better suited for building integration due to their simpler design and greatly reduced need for maintenance. Furthermore, the necessary elements of the building envelope (air/moisture transfer control, insulation, cavity ventilation) can be readily facilitated, while existing building techniques such as the curtain wall can be easily modified to incorporate the BIPV/T concept. The focus of the present thesis is solely on air-based BIPV/T systems.

2.3 Thermal performance parameters

The following section reviews the various parameters that affect the electrical, thermal and hydraulic performance of PV/T systems, as documented in the literature. These include environmental parameters (irradiance, ambient temperature, wind velocity), operating conditions (mass flow rate), parameters inherent to the design of the system (length, width, depth, tilt angle) and use of heat transfer enhancements (fins, glazing, double-pass configurations etc.). The latter are discussed in more detail in section 3. Elbreki et al. (2016) performed a review of such parameters, which has been further extended and analyzed in the present paper, with focus on the building integration context.

2.3.1 Environmental parameters

2.3.1.1 Solar irradiance

Solar irradiance is probably the most critical environmental factor for the performance of a hybrid photovoltaic/thermal system. The higher the insolation on the PV/T, the higher the electrical and thermal output. The electrical efficiency itself may decrease due to the fact that the PV cell temperature increases linearly with increasing solar irradiance. This causes a slight increase in the cell's short circuit current (I_{sc}) and corresponding generated electrical power but decreases the open circuit voltage (V_{oc}) with a consequent decrease in the cells fill factor (*FF*) (Hamrouni et al., 2008). This, in turn, has a direct impact on the cells electrical efficiency which decreases with increasing irradiance levels (Figure 2.5). The thermal efficiency increases, as is the outlet air temperature (T_{out}), due to the larger amount of available heat from the PV boundary. The effect of solar irradiance has been documented in various experimental studies in PV/T literature (Adeli et al., 2012; Kaiser et al., 2014; Kim et al., 2014; Koech et al., 2012; Kumar & Rosen, 2011b; M. Y. Othman et al., 2007; Sopian et al., 2000).

It is therefore critical for BIPV/T systems to receive the maximum amount of solar radiation. However, it should be noted that contrary to stand alone PV/T collectors, BIPV/T placement may be limited and dictated by the building's shape and orientation, especially for the case of retrofits.

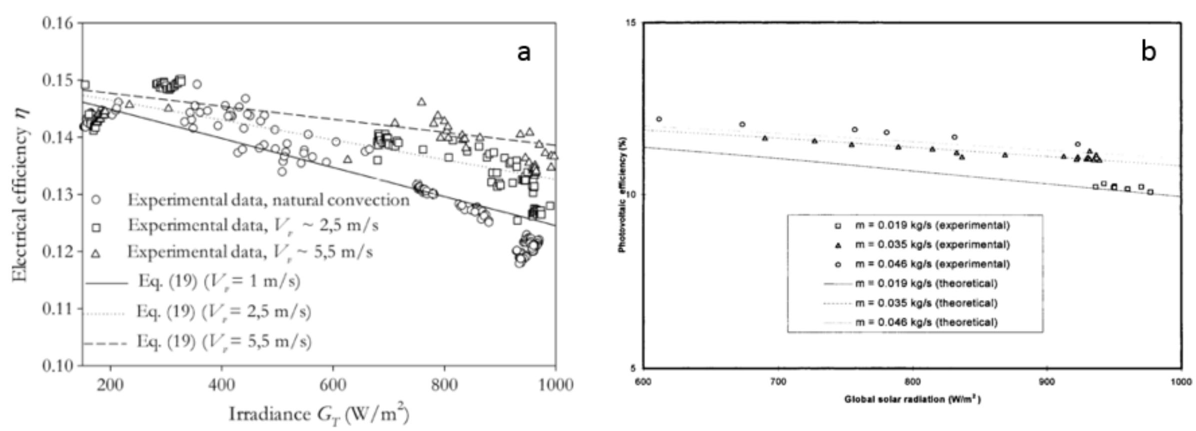

Figure 2. 5: Linear decrease of electrical efficiency with increasing solar irradiance (a: Kaiser et al, 2014, b: Sopian et al, 2000)

2.3.1.2 Wind

The wind effect on BIPV/T is critical, as the PV (absorber) interfaces directly with the ambient environment, as opposed to glazed solar thermal collectors. Furthermore, in contrast with small, stand-alone type collectors, local wind velocity distributions may have a more significant effect on large BIPV/T installations both in terms of local convective phenomena, as well as pressure distributions for the case of multiple-inlet systems (Rounis et al., 2016).

Wind has a cooling effect on the PV modules which increases the electrical efficiency of the system, but reduces the thermal output and efficiency due to the reduced PV temperature, T_{out} (Adeli et al., 2012; Hussain et al., 2013; Mekhilef et al., 2012; Yang & Athienitis, 2014). Figure 2.6 demonstrates the thermal efficiency of an experimental PV/T system for varying flow rate and three wind velocities (Yang & Athienitis, 2014).

The relation between wind and the external convective heat transfer coefficient has primarily been found to be linear in most studies as documented by Palyvos (2008), Vasan & Stathopoulos (2014) and Ladas et al. (2017).

Although important, the wind effect on PV/T collectors and BIPV/T systems has been poorly documented, due to the complexity introduced. Furthermore, contrary to solar thermal collector, the addition of a glazed cover over the PV/absorber should be avoided, as it can lead to PV cell overheating, as well as reduction of incident solar irradiation, transmitted through the transparent cover.

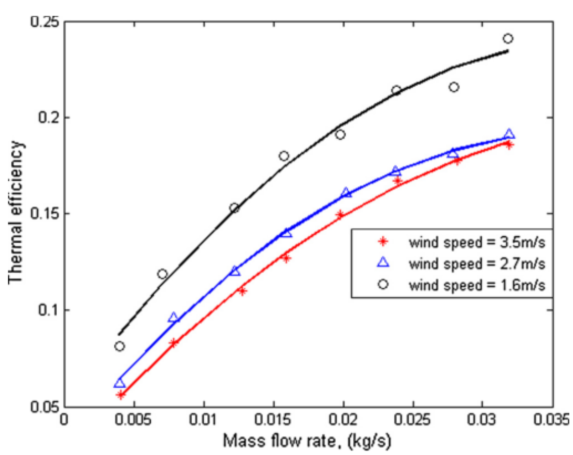

Figure 2. 6: Thermal efficiency versus mass flow rate for three different wind velocities (Yang & Athienitis, 2014).

2.3.1.3 Ambient temperature

The effect of irradiation and wind on the PV cell temperature is always relative to the ambient temperature. Therefore, an increase or decrease in ambient temperature will reflect upon the PV cell temperature accordingly. The effect of the ambient temperature on the air temperature rise (ΔT) and the thermal efficiency is a more difficult subject, especially in the field, as it is difficult to maintain constant combination of the other parameters (irradiation and wind), while indoors studies usually involve a constant ambient (room) temperature with small variations around it.

A solar simulator study on a hybrid UTC-PV/T system by Bambara et al. (2011) indicated that the temperature rise normalized by the irradiation for spring and winter conditions for a mass flow rate is the same, although only the irradiation level was varied (Fig. 2.7).

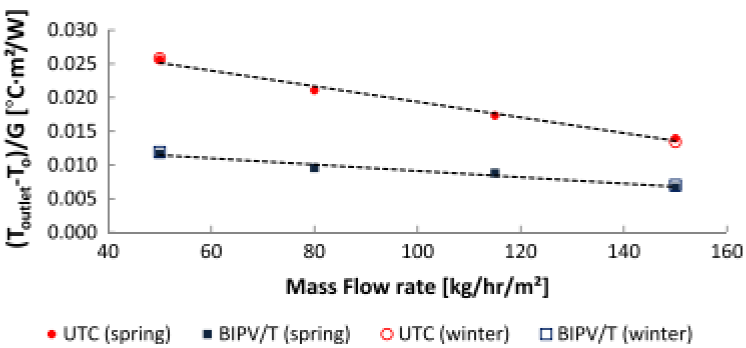

Figure 2. 7: Inlet/outlet temperature difference, normalized by the solar irradiance, vs the normalized mass flow rate (Bambara et al., 2011).

2.3.2 Mass flow rate and channel geometry

The air flow rate is another critical factor for the hybrid system's performance and has been studied extensively in PV/T literature (Bambrook & Sproul, 2012; Bergene & Løvvik, 1995; Dubey et al., 2009; Hegazy, 2000; Koech et al., 2012; M. Y. Othman et al., 2007; Sopian et al., 2000; A. Tiwari et al., 2006; Tonui & Tripanagnostopoulos, 2006, 2007; Yang & Athienitis, 2014a).

The air flow rate highly affects the convective heat transfer within the air channel. Increasing the flow rate, the convective heat exchange increases, and this enhances both the thermal and the electrical efficiency by reducing the PV cell temperature. The rate of increase in electrical and thermal efficiency drops rapidly with increasing flow rate, until both reach a maximum (Fig. 2.8a). This is due to the fact that as the PV and coolant temperatures get closer, the heat exchange between the two decreases. Furthermore, with increasing flow rate, heat is dissipated in a larger body of air and therefore the temperature rise is smaller, as is the outlet temperature (Fig. 2.8b).

As far as the hydraulic performance is concerned, increasing mass flow rate (and average channel air velocity) also increases the frictional pressure drop inside the air channel and consequently the fan consumption. The additional fan power has to be deducted from the PV generation to obtain the net electrical gains.

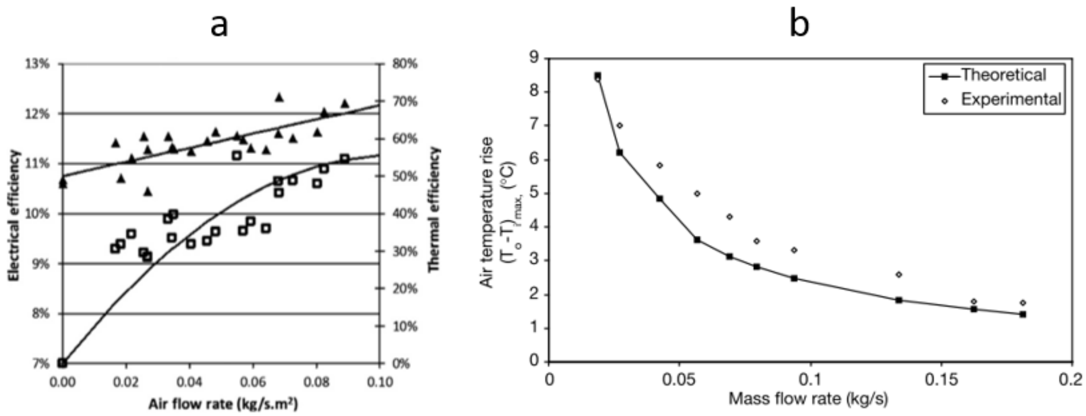

Figure 2. 8: a. Increase of electrical and thermal efficiency with increasing mass flow rate (Bambrook & Sproul, 2012), b. effect of mass flow rate on max air temperature rise (Othman et al, 2007)

Studies have also shown that with increasing collector length, the air temperature and thermal efficiency increase, up until a plateau is reached (A. S. Joshi et al., 2009; Koech et al., 2012; A. Tiwari & Sodha, 2007; Tonui & Tripanagnostopoulos, 2007). This is due to the fact that as the air temperature rises, the convective heat exchange efficiency with the absorber (PV) decreases. A reduced channel depth, *D*, increases the flow velocity and therefore the heat extraction from the PV surface, for the same flow rate. This causes an increase in both the electrical and a small increase in the T_{out}. Furthermore, as the velocity increases, the pressure drop increases, as does the fan consumption (Kumar & Rosen, 2011b; Tonui & Tripanagnostopoulos, 2007).

It should be noted that the effect of varying flow rate and channel geometry is most times studied performing a numerical parametric analysis, after having established mathematical models for specific channel configurations, and not experimentally.

Suggestions for optimal channel length and depth vary among studies. Tonui & Tripanagnostopoulos (2006) suggested a collector's length between 6-8 m to balance the thermal output, the electrical efficiency drop due to the consequent increased PV temperature, and the pressure drop and fan consumption. Tonui & Tripanagnostopoulos (2007) suggested an optimal channel depth of 0.15 m to minimize pressure drop and fan consumption, considering a 5-10 m long installation. Tiwari et al (2006) reported an optimum channel of 0.03-0.06 m for a 1.2 m long system. Farshchimonfared et al. (2015) found that the optimum channel depth increases with increasing ratio of length over width (*L/W*) of the collector within a range of 0.026-0.09 m. Adeli et al (2012) performed an optimization study for a 1 m long PV/T system and found that a channel depth between 0.109-0.148 m maximizes the electrical and thermal output. (Agrawal & Tiwari, 2010) investigated the effect of connecting PV/T channels in series and in parallel. They found that for a given flow rate, a series configuration, which essentially increases the length of the collector, will increase the thermal efficiency and outlet temperature, but will decrease the electrical efficiency.

For building integrated systems, the channel length and depth should be designed based on the flow rate range needed for efficient coupling with the HVAC system, along with other potential building restrictions. The optimization of these features should consider the net gains from the coupled BIPV/T and HVAC system performance, including fan consumption, while also considering requirements on PV temperatures.

2.3.3 Material thermal and optical properties

Apart from the specific geometry of the air channel, the thermal performance of a hybrid system can be highly affected by the properties of the materials that constitute the boundaries of the channel.

The efficiency of the PV cell and the PV module's packing factor (PF), along with the optical properties of the materials (reflectance, transmittance and absorptance) will define the fraction of solar irradiance that will be available for thermal conversion. The effect of the packing factor, as well as the use of semi-transparent PV (STPV) instead of opaque PV modules has been studied by several researchers (Guiavarch & Peuportier, 2006; Sandnes & Rekstad, 2002; Vats et al., 2012; Yang & Athienitis, 2015). For the same PF, the use of STPV can highly benefit the thermal performance, as a fraction of the solar irradiance is transmitted and absorbed by the rear surface of the channel. Additionally, the electrical performance is also enhanced, since less irradiance is absorbed by the part of the module not covered by PV cells, resulting in an overall lower PV module temperature.

Yang & Athienitis (2015a) reported a 7.6% increase in thermal efficiency when using STPV instead of opaque PV modules of the same PF for an experimental PV/T prototype. This indicates the potential of utilizing STPV even for opaque applications, to the benefit of both the electrical and thermal performance of the system.

Several researchers have studied the effect of the thermal conductivity on either side of the PV cell encapsulation. A thermally conductive PV substrate could function as a heat sink and increase heat transfer in the air channel, whereas, a thermally insulated superstrate, as is the case for glazed collectors, can reduce heat loss to the environment and possible PV overheating.

Tiwari & Sodha (2007) reported that PV modules without tedlar on the back performed better thermally in an experimental investigation of a PV/T air system. Joshi et al (2009) reported better thermal, electrical and overall efficiency for a PV/T air collector with glass-to-glass versus glass-to-tedlar PV modules. Koech et al (2012) showed that with increasing conductivity of tedlar, both the thermal and electrical efficiencies of the system increase. A similar effect is caused by the thermal resistance of the bonding materials between the PV and the substrate, or the absorber for the cases of pasted PV cells on a thermal absorber (Zondag, 2008).

The combination of thermal conductivities of the materials on either side of the PV cell could create a unique effect on the external and internal convective heat transfer of a specific system.

This can be especially important for building integrated systems where typical substrate materials may not meet building code standards.

Glass-on-glass modules could be well suited for such applications, while PV modules specifically designed for BIPV/T applications with a thermally conductive substrate (potentially aluminum) could be an interesting subject of research. A similar concept was applied on the BIPV/T roof of the EcoTerra (Chen et al, 2010), in which case flexible a-Si modules were pasted on the metal roofing. From a modelling perspective, this can also introduce additional uncertainties in the use of commonly used expressions for wind-driven and channel convection, as the thermal resistance of the material in either side of the PV cell are added in series with the respective air film resistance.

2.4 Thermal Enhancements

In order to bypass the issue of lower thermal performance, there are various methods of enhancing the thermal performance of air-based PV/T systems proposed in the relevant literature. These include the use of a glazed cover which reduces wind-driven thermal losses (Agrawal & Tiwari, 2011; Hegazy, 2000; Pei et al., 2008; Sopian et al., 2000; A. Tiwari et al., 2006; Tiwari & Sodha, 2007; Tonui & Tripanagnostopoulos, 2007), double-pass configurations (Amori & Abd-AlRaheem, 2014; Hegazy, 2000; M. Y. Othman et al., 2007; Saygin et al., 2017; Sopian et al., 2000), which combine a top glazing section with increasing the available area for convective heat transfer through the formation of air channels on either side of the PV, as well as the use of fins, thin metal sheets and other porous media (Hussain et al., 2015; Kumar & Rosen, 2011b; M. Y. Othman et al., 2007; Tonui & Tripanagnostopoulos, 2006, 2007; Tripanagnostopoulos, 2007). These added elements increase the available area for convective and radiative heat transfer and/or can induce turbulence.

Arguably, these methods may not always be suitable for systems intended for building integration, due to increased complexity of the design, potential PV overheating and partial shading (glazed covers, double pass), or high pressure drop and resulting fan consumption increase (fins, porous media). Generally, thermal enhancements for BIPV/T should be easily implemented at minimal additional cost, without affecting the building envelope function or the electrical performance.

The following section presents the various thermal enhancement techniques, followed by a discussion on the suitability of each method for building integration.

2.4.1 Use of top glazing

The use of a top glass cover has been studied extensively in solar thermal collectors and PV/T systems experimental prototypes that focus on maximizing the thermal output, by reducing the convective losses from the top surface. A layer of still air is encapsulated between the PV/absorber surface and a top glazing (Fig. 2.9). By reducing the wind-driven convective losses, more heat is transferred to the air channel, resulting in higher outlet temperature and increased thermal efficiency. However, the electrical efficiency drops due to the increased PV cell temperature, as well as the reduced solar irradiance due to the addition of the top cover (Bakari et al., 2014; Sandnes & Rekstad, 2002).

Tonui & Tripanagnostopoulos (2007) reported an increase of 30% in thermal efficiency and 16% optical losses for a glazed vs a reference system. They suggested that the primary purpose of a PV/T is electricity generation and the resulting high temperatures of glazed systems should be avoided. Chow et al. (2006) suggested that glazed systems enhance the thermal performance and, reversely, unglazed ones enhance the electrical. The choice of system type depends on the intended use. Bakker et al. (2005) indicated that unglazed systems produce low T_{out} and should be combined with heat pumps.

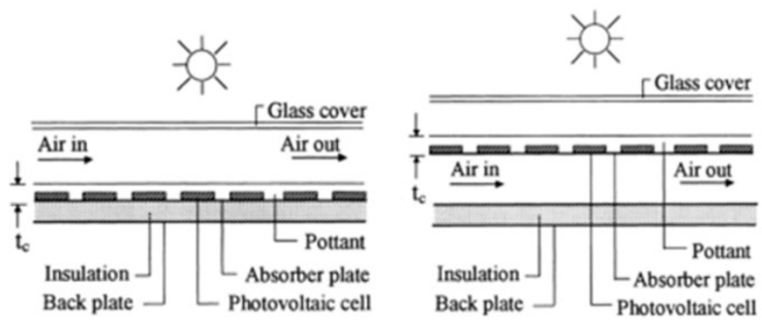

Figure 2. 9: Glazed PV/T configurations (Hegazy, 2000).

2.4.2 Double-pass

A system with a double pass configuration has the PV/absorber set within the air gap, with a glazed cover set on top, and flow on both sides of the PV. The upper and lower flow can be either separate, forming two individual channels (double-duct, Figure 2.10a), or it can continue from the top to the bottom section (single-duct, Figure 2.10b).

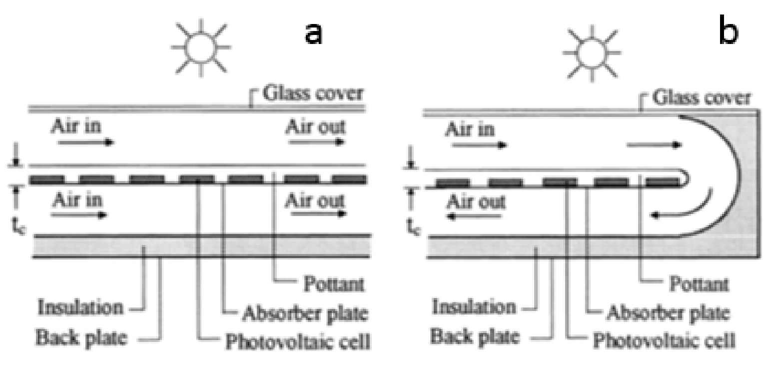

Figure 2. 10: (a) Double-pass, double-duct PV/T (b), and double-pass, single-duct PV/T (Hegazy, 2000).

The same effects of having a top cover are implied for this type of configuration (reduced wind-driven losses and reduced optical properties), but with the added benefit of top heat extraction in addition to that from the rear side of the PV. Enhanced electrical and thermal efficiency for double-pass systems have been reported in literature (Amori & Abd-AlRaheem, 2014; Hegazy, 2000; M. Y. Othman et al., 2007).

Saygin et al. (2017) proposed a modified glazed, double-pass PV/T air collector with air entering through a slot in the middle of the top glazing and was collected from an outlet located beneath the center of the PV module. The distance from the top glazing to the PV varied and it was found that a 3 cm gap maximized the collector's thermal efficiency, for a flow rate of 0.037 kg/s (η_{th_max}=48%, η_{el_max}=7.7%, ΔT=8-10ºC).

An inherent issue with both glazed and double-pass systems is that of self-shading from the collector's side walls, due to the fact that the PV layer is set lower than the top surface of the collector.

2.4.3 Channel added elements and porous media

Several researchers have incorporated the addition of elements within the air channel which can increase convective and radiative heat transfer, or act as heat sinks for the PV.

2.4.3.1 Fins

Fins can increase heat transfer from the PV/absorber surface either as turbulence inducing elements (Tonui & Tripanagnostopoulos, 2006, 2007; Tripanagnostopoulos et al., 2002) (Fig. 2.11a), heat sinks when in touch with the PV (Jin et al., 2010; M. Y. Othman et al., 2007) (Fig. 2.11b), or a combination of the two (Kumar & Rosen, 2011) (Fig. 2.11c). Furthermore, when fins are in contact with the PV, they also enhance the radiative heat transfer from the PV surface. Tonui & Tripanagnostopoulos (2006) reported an increase in thermal efficiency from 25% to 30% when using fins attached to the insulation surface. Kumar & Rosen (2011b) found that using fins in contact with the PV on the lower channel of a double pass system lowered the PV temperature from 82ºC to 66ºC.

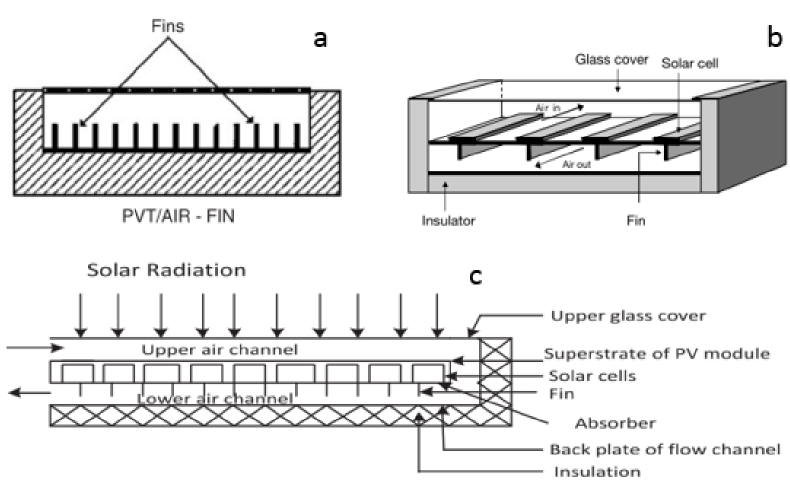

Figure 2. 11: PV/T with fins as: a. turbulence inducers (Tonui & Tripanagnostopoulos, 2006), b. heat sinks (Othman et al, 2007) and c. combination of the two (Kumar & Rosen, 2011).

A similar effect was reported by Yang & Athienitis (2015a), who used metal supports for the PV of an experimental PV/T setup, which also acted as fins.

2.4.3.2 Thin metal sheet (TMS), porous media, V-grooves, rectangular channels, honeycomb

Added porous media increase the available surface for radiative and convective heat exchange within the air channel (Othman et al., 2013). A thin metal sheet (TMS) suspended in the middle of the air channel increases radiative heat exchange with the PV. This also creates a double pass configuration which further increases convective heat transfer from the TMS surface. The suspended TMS reduces radiation to the back surface, forming a cooler back boundary. Tonui & Tripanagnostopoulos (2006) found that a PV/T with a TMS had 3% higher thermal efficiency compared to a reference system (Fig 2.12a). Similar results were reported by (Shahsavar & Ameri, 2010).

Othman et al. (2009) introduced a single-pass PV/T prototype with V grooves (Fig 2.12b). Such a technique has been applied in a solar thermal collector by Karim & Hawlader (2006) with a resulting 12% increase in its thermal efficiency. Hussain et al. (2015) found that an experimental PV/T air collector equipped with a hexagonal honeycomb heat exchanger had a 60% increase in its thermal efficiency and a marginal increase in its electrical efficiency (Fig 2.12c). Sopian et al. (2009)investigated experimentally a double pass PV/T air system with porous material on the lower channel. It was found that the porous material increased the thermal efficiency and outlet temperature, with a typical thermal efficiency of 60-70%. Jin et al. (2010) studied a PV/T collector with rectangular tunnel absorbers (Fig 2.12d). The prototype system showed improved performance versus a one without the rectangular absorbers, with a thermal, electrical and overall performance of 54.7%, 10.02% and 64.72% respectively, under solar irradiance of 817.4W/m^2, ambient temperature of 25^{o}C and 0.0287 kg/s mass flow rate.

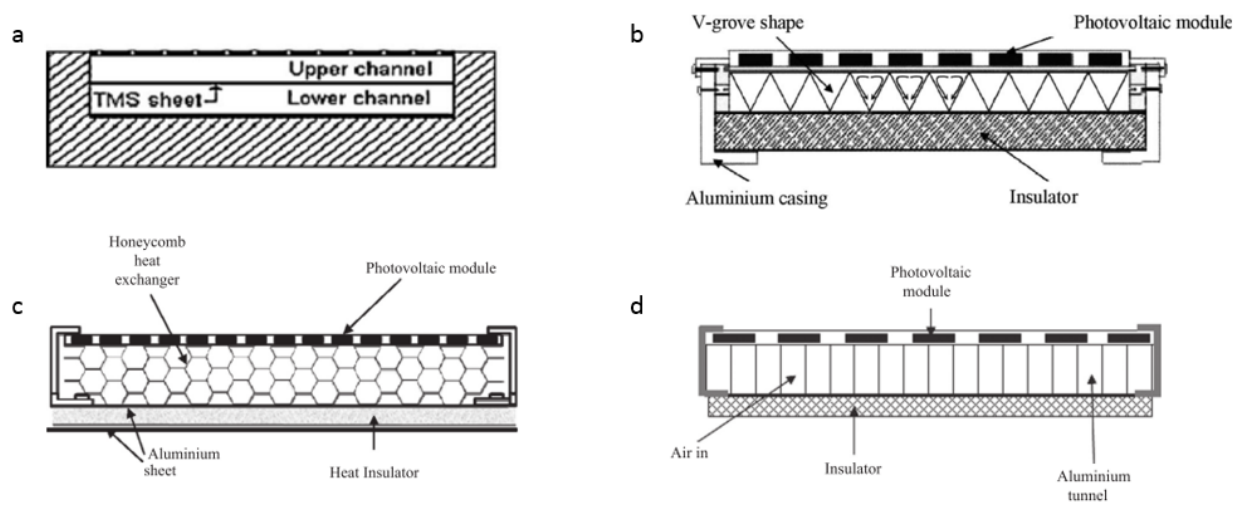

Figure 2. 12: a. Rectangular tunnel absorbers (Jin et al, 2010), b. hexagonal honeycomb heat exchanger (Hussain et al, 2015), c. suspended thin metal sheet (Tonui & Tripanagnostopoulos, 2007) d. V-grooves (Othman et al, 2009)

2.4.4 Multiple-inlets

The concept of multiple-inlets evolved from the hybrid UTC-PV/T system designed by Bambara et al. (2011) and relies upon the introduction of several intakes of fresh air and the disruption of the thermal boundary layer over the PV surface by introducing additional entrance effects. As opposed to all other cases of PV/T configurations, where a temperature stratification always occurs on the PV surface, resulting in non-uniform electrical performance, in a multiple-inlet system the PV modules can be uniformly cooled. This is possible with regulation of the flow entering the inlets of the system.

Yang & Athienitis (2014, 2015) found that a two-inlet system (Fig. 2.13) had 5% higher thermal and marginally higher electrical efficiency as compared to a single-inlet reference system. Similar results were found from the experimental investigation of a BIPV/T curtain wall prototype (Fig. 2.14) (Rounis et al, 2017; Kruglov et al, 2017). Mirzaei et al. (2014) investigated experimentally the role of cavity flow on the performance of BIPV placed on inclined roofs. The experimental configurations included a flat and a stepped arrangement, which was essentially a multiple-inlet formation. The cavity was naturally ventilated and no mechanical air collector potential was investigated; however, it was found that the PV temperatures were significantly lower for the stepped configuration (multiple-inlet) cases, as opposed to the flat roof, indicating that the additional opening provided enhanced heat transfer within the air channel. Rounis et al. (2016) developed a flow distribution model for the sizing of inlets and Athienitis et al. (2018) investigated through simulations the optimal number of inlets for a 30 m high façade integrated system, considering a single flow rate and channel depth.

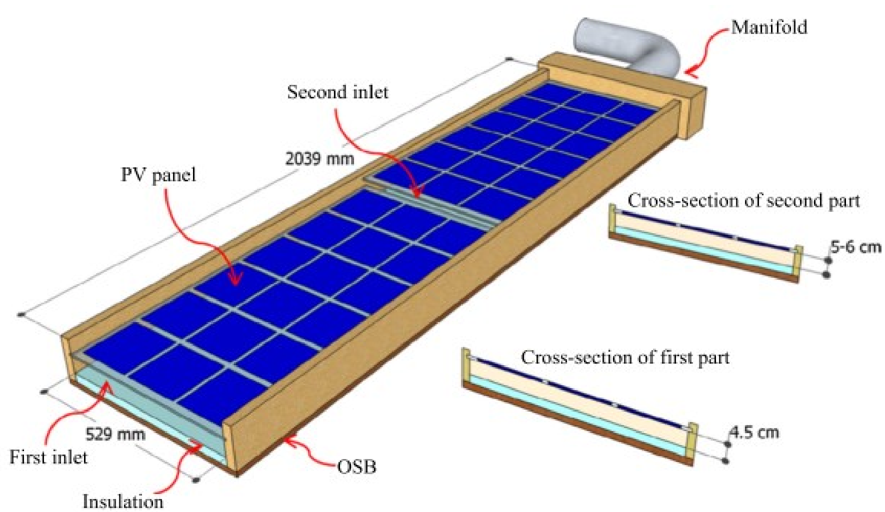

Figure 2. 13: Two-inlet PV/T system (Yang & Athienitis, 2015)

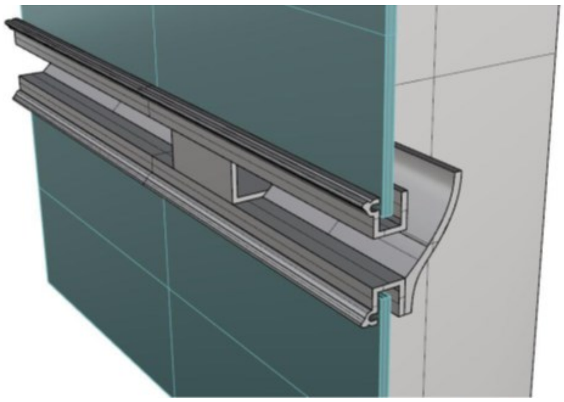

Figure 2. 14: Detail from middle inlet in BIPV/T curtain wall prototype (Rounis et al, 2017)

2.4.5 Added glazed section

Yang & Athienitis (2014) and Pantic et al. (2010)investigated through simulations the option of adding a glazed thermal collector section in series with a roof BIPV/T system (Fig. 2.15). The addition of the glazed section was found to increase the thermal efficiency of the system by 8-20%. With the addition of the glazed thermal collector, higher outlet temperatures can be achieved without affecting the operating temperatures of the PV.

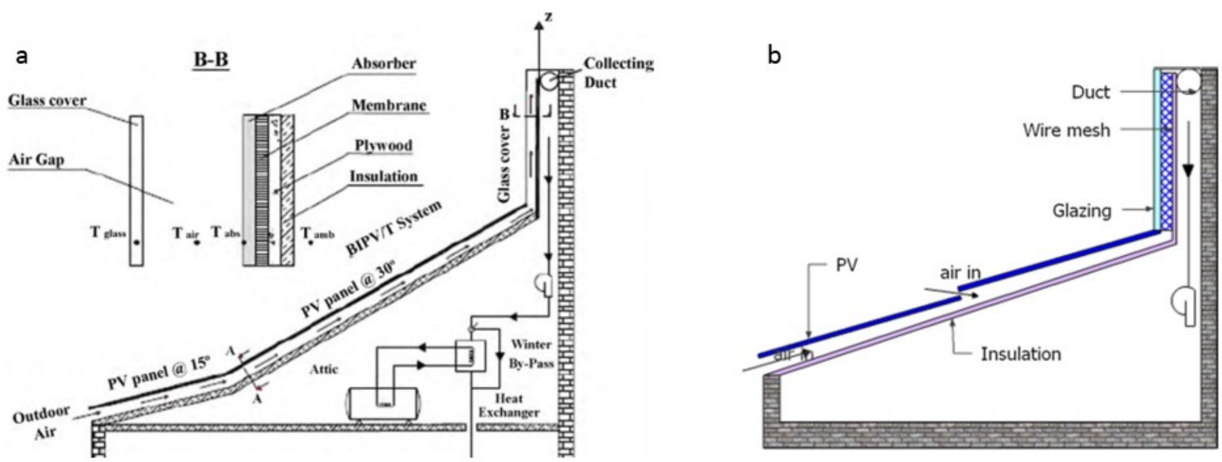

Figure 2. 15: a. Single-inlet BIPV/T with added glazed section (Pantic et al, 2010), b. Double-inlet BIPV/T with added glazed section (Yang & Athienitis, 2014).

2.4.6 Concentrating parabolic collectors (CPC)

PV/T concentrator systems use reflectors to increase the radiation intensity on the PV cells. With concentrating collectors, less PV area is needed, which is replaced by lower cost reflectors or lenses. In the case of air-based concentrators, the high air temperatures within the collector undermine the PV efficiency. Although the heat output is high, there is a trade-off between maximizing electricity hot air production (Garg & Adhikari, 1997; M. Y. H. Othman et al., 2005). In order to increase heat extraction, concentrating collectors may employ fins and double pass channels (Fig. 2.16a), but mainly a liquid is used for higher heat exchange efficiency, while such systems are primarily used for high-temperature industrial applications.

2.4.7 Impinging jets

Brideau & Collins (2012) developed a PV/T air heating collector employing impinging jet as a means to enhance heat transfer to the working fluid (Fig. 2.16b). This concept consisted of a perforated plate below the PV layer, with air entering in the sub-channel formed between the plate and the back surface, then being directed through the perforations towards the PV layer and collected at the outlet. It was found that with increasing PV coverage, the electrical output of the system increased while the thermal output decreased due to the lower absorptivity of the solar cells versus the absorber plate.

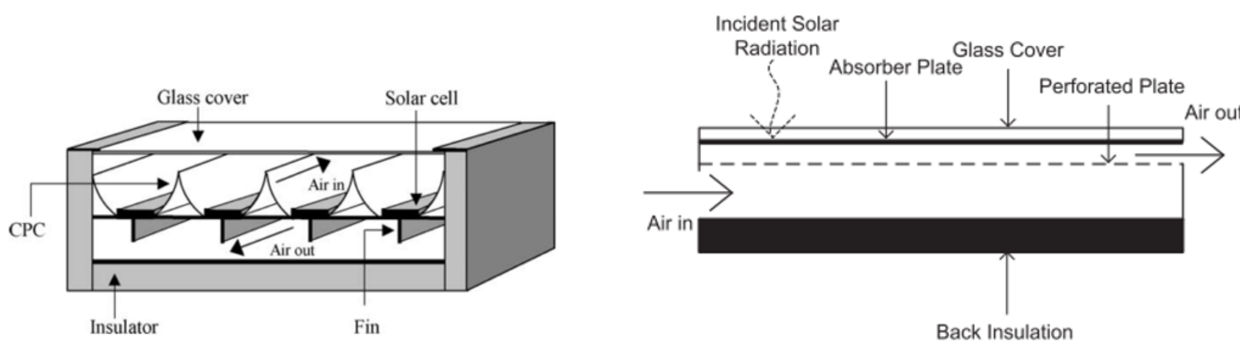

Figure 2. 16: a. Double pas CPC collector with fins (Othman et al, 2005), b. Impinging jets (Brideau & Collins, 2012)

2.4.8 Discussion

According to the observation made from the review of these methods, the following can be said in terms of their applicability for building integration:

A reference system is the simplest design, and has great potential for standardization and modularization, as well as adaption to existing building practices. It is the least efficient thermally but performs better electrically from its glazed counterparts due to wind-cooling. This is also the easiest system to design within the building integration context, adaptable to many existing building techniques (curtain wall, wood structure, DSF, etc.) and involving the least number of parts.

Adding a glazed cover increases the thermal performance by reducing convective heat losses, but at the cost of the electrical performance and potentially the PV modules' durability (delamination). The electrical efficiency is further reduced due to the optical losses introduced by the added glazing and there is an inherent issue of shading as the PV is set lower than the top surface. There is also the cost and installation for the extra glazing, as well as need for specialized supporting structure for building integration. Double pass systems entail the same issues, but with more efficient PV cooling.

The use of fins is an interesting option. It could be combined with an aluminum substrate to provide rigidity (for building codes) as well as enhance the thermal and electrical performance. On the downside, this might involve the development of new type of PV modules for building integration, with the requirements of certification a new product implies.

The use of other porous media (grooves, ducts, mesh, TMS etc.) can increase the cost and fabrication/installation complexity. Furthermore, for installations with large flow channels, the pressure drop might and resulting fan consumption be considerable. Concentrating systems, impinging jets, middle slots etc., are probably the least suitable for large scale building applications.

Multiple-inlet systems have high potential of enhanced performance with only the requirement of modified inlets with varying openings/porosities (and rated flow *ΔP* for design). Their design needs to account for rain penetration and may be sensitive to wind flow distributions for wind >2-3m/s. Such a system also has the potential for standardized design and it is the only type of thermal enhancement that addresses the PV temperature stratification and non-uniform electrical performance.

Finally, the addition of a glazed collector in series with the system may reduce the available PV installation area, however, it can highly boost the thermal output without affecting PV performance. Such a design can be the subject of coupled BIPV/T-HVAC system optimization (energy generation and energy saved by boosting thermally the operation of the HVAC)

Table 2.2 summarizes the various methods of thermal performance enhancement and their resulting effects on the electrical and thermal output, as well as PV and outlet temperatures.

Table 2. 2: Thermal enhancement techniques

Enhancement technique	**PV temperature**	**Air temperature rise**	**Electrical efficiency**	**Thermal efficiency**	**Pressure drop**	**Comments regarding building integration**
Top glazing	↑	↑	↓	↑	N/A	Generally, it should be avoided for BIPV/T due to resulting PV overheating. It may however have application in cold climates.
Double pass	↑	↑	↓	↑	↑	Improved cell temperatures vs the top glazing, but there are still shading issues and it may be impractical as a construction for large installations
Fins, TMS, porous elements	↓	↑	↑	↑	↑	This can be a practical and efficient solution, however when applied to long channels, there may be

						significant pressure drop imposed.
Multiple inlets	↓	↑	↑	↑	N/A	Very efficient thermal enhancement for integrated systems in terms of performance. It needs careful flow distribution planning, which may be affected by wind and there need to be provisions for a watertight rear surface.
Added glazed collector	N/A	↑	N/A	↑	↑	This can highly boost the thermal performance without affecting the electrical, especially when used to cover an area that would not be covered by PV anyway.

2.5 BIPV/T + HVAC

There are numerous studies that showcase BIPV/T system's potential for waste heat exploitation through various ways of coupling with the HVAC system of the building, such as ventilation air pre-heating, boosting the performance of a heat recovery ventilator, air-source heat pump assistance and solar driven desiccant cooling. More recent studies have explored the potential contribution of BIPV/T systems to the building energy flexibility through the coupled operation of BIPV/T, air-to-water heat pumps and active thermal energy storage. Despite the numerous options, there is no standardized design procedure or best practice guide for the optimal coupling of BIPV/T and HVAC systems for different applications, building types and climates. The following section provides an overview of the various thermal applications, followed by a discussion on relevant design considerations and research needs.

2.5.1 Ventilation air pre-heating

One of the simplest and most efficient thermal applications for BIPV/T is preheating the supply air through the BIPV/T, thus reducing the ventilation thermal load for the HVAC system. Depending on the BIPV/T outlet temperature and the setpoint indoor temperature, the BIPV/T can either fully supply pre-heated ventilation air or boost the operation of the heating system by supplying air at higher temperature. In the case that the outlet air temperature is higher than the setpoint, it can be mixed with cool fresh air to reach the required temperature.

For this type of application, all the heat recovered by the system can be directly utilized without heat exchange losses. The temperature of the collector's outlet air can be further optimized by regulating the flow rate and mixing ratio with unheated fresh air. Such systems have been implemented in the Varennes Library (Fig. 2.17) and the John Molson School of Business (JMSB) building of Concordia University (Fig. 2.18). In both systems, the preheated air is directed to the fresh-air supply during the heating season and vented to the environment during summer.

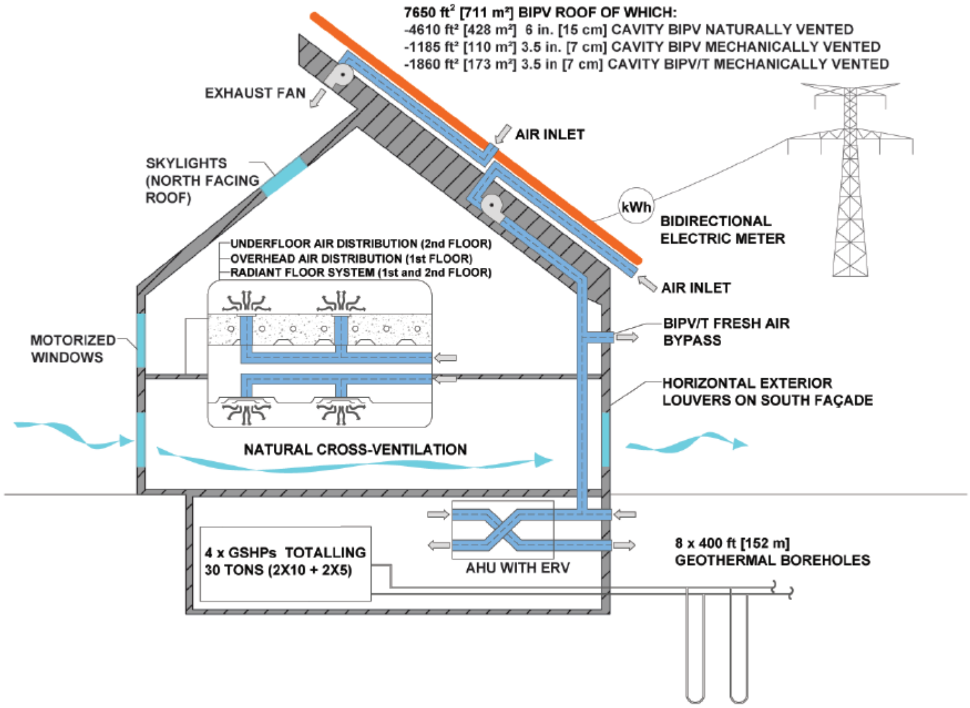

Figure 2. 17: The Varennes Library BIPV/T system schematic (Dermadiros et al., 2019).

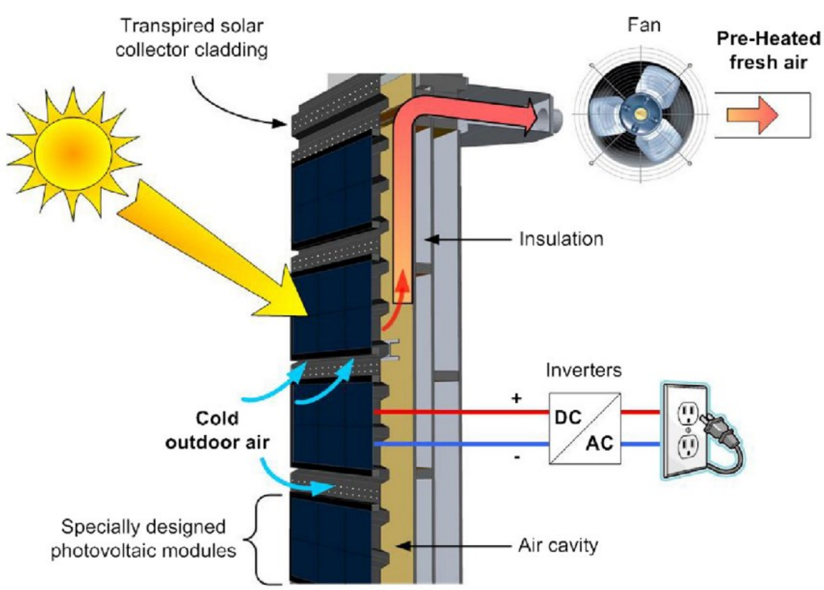

Figure 2. 18: Schematic of the JMSB building BIPV/T system (Bambara et al., 2011).

2.5.2 Heat recovery ventilator (HRV) boosting

Like ventilation air pre-heating, the recovered heat can be used to pre-heat the supply air side of a heat recovery ventilator system, thus enhancing the performance of the HRV itself, as the BIPV/T outlet air supply has higher enthalpy than outdoor air and is closer to that of warm return air. This type of application can further reduce the risk of condensation and frost for the HRV unit.

Figure 2.19 shows a BIPV/T-HRV configuration, studied by Ahn et al. (2015). In said study, it was found that by using the pre-heated air from a roof BIPV/T system improved the efficiency of an HRV by about 20%, with a peak BIPV/T thermal efficiency f 23% at 100 kg/h constant air supply. The temperature difference between the inlet and outlet temperature of the PV/T ranged between 7-15ºC, depending on the irradiance level, with an outdoor temperature of around 0ºC.

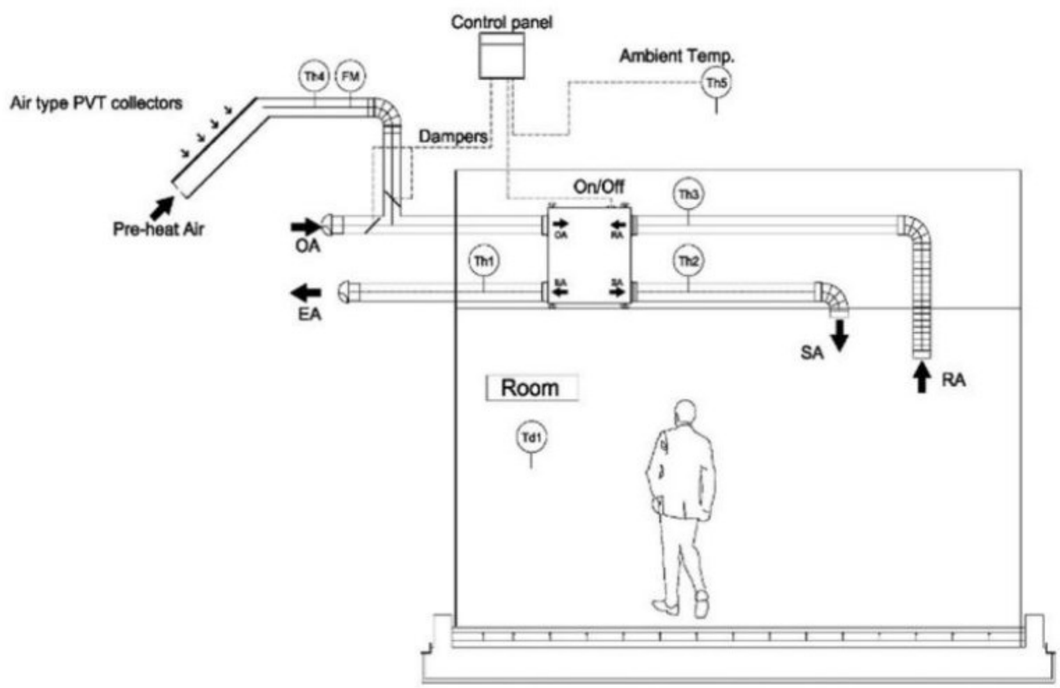

Figure 2. 19: Air BIPV/T coupled with HRV (Ahn et al, 2015)

2.5.3 Solar assisted air-source heat pump

Heat pumps incorporate a basic vapor compression cycle to pump heat from a lower temperature source to a higher temperature depository. There are several categories of heat pumps, namely air-source, water-source and ground-source, depending on the heat source (or depository in cooling mode) for the outdoor coil which can be the ambient air, a body of water or the ground (via underground water loops), respectively. The heat can then be delivered to the conditioned space either directly through the indoor (condenser) coil, or indirectly, through thermal storage.

Low-grade heat introduced on the outdoor/evaporator side can greatly enhance the coefficient of performance (COP) of the heat pump. Air-source heat pumps are usually placed under a snow-protective cover near the building’s exhaust openings to take advantage of the building’s waste heat. In a similar manner, heat pumps can benefit from heat delivered through a dedicated solar thermal collector, PV/T collector or BIPV/T system. Such a configuration is referred to as a solar assisted heat pump (SAHP).

According to Kamel et al. (2015) the majority of studies on SAHP systems involve water-based collectors integrated in the water loop of water-based heat pumps, acting as the evaporator coil (Figure 2.20)

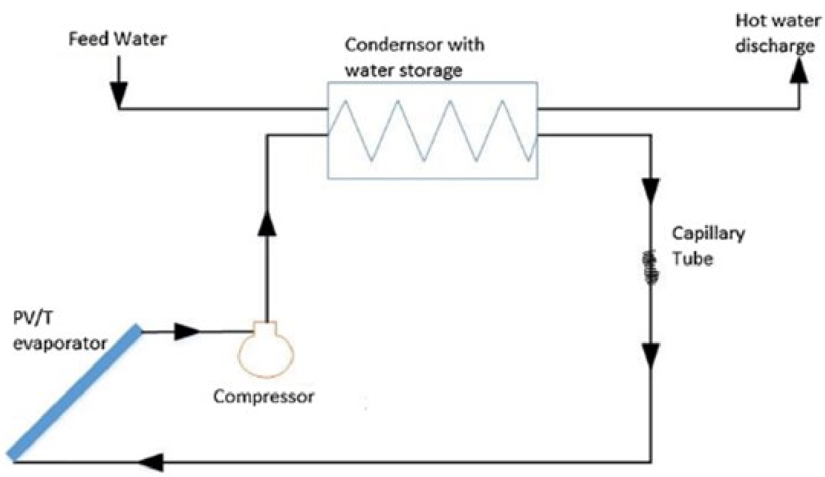

Figure 2. 20: Schematic of a water-based PV/T/ASHP system (Kamel et al., 2015).

Nevertheless, there is significant potential for the coupling of air-based BIPV/T with air-source heat pumps to save more energy than each system alone (Badescu, 2002). The coupling of BIPV/T and air-source heat pumps can have multiple benefits such as reducing the risk of frost and condensation for the outdoor coil, especially in cold climates, while reducing the defrost cycles, generally enhancing the COP of the heat pump and supplementing the irregular heat delivery of the BIPV/T by the parallel operation of the heat pump. Furthermore, by incorporating thermal storage (water tank, seasonal storage) the effect of available irradiation intermittency can be further reduced, and the stored thermal energy can be used as source for the heat pump at night too (Bakirci & Yuksel, 2011; Gang et al., 2007; Kuang et al., 2003). The potential of such coupling has been demonstrated in several studies.

Kamel & Fung (2014b) developed a TRNSYS model to simulate the performance of an open-loop roof PV/T system integrated with a two-stage, variable capacity ASHP in an Archetype Sustainable House. The pre-heated air from the PV/T was used as the heat source for the heat pump. The simulated seasonal performance of the integrated ASHP + PV/T system was compared to the base case of just the ASHP system for different regions, in terms of overall electricity cost reduction and GHG emissions. The results showed an annual saving of 500$ in electricity bills and a GHG emission credit of 1734.7 kg CO2 from renewable energy generation.

Badescu (2002)analyzed the model of an ASHP integrated with a solar air heater. The COP of the integrated system was found to be higher than that of the heat pump alone. Badescu (2002, 2003) investigated air thermal storage for heating purposes. Energy collected by solar collector was used for thermal energy storage (TES) when space heating was not required. If space heating was required, part of the output of the collector was used for storage and part for driving the heat pump. If irradiance was not adequate, TES was used as source for the heat pump. If again TES was not adequately charged, the heat pump operated by itself. Electrical savings were evaluated between 20-50%, depending on the level TES was charged.

Liang et al. (2011) proposed a system for space heating consisting of an ASHP and a solar collector connected in series with the condenser of the heat pump to supply hot water of 45ºC. Li et al. (2015) investigated numerically a coupled BIPV/T + ASHP closed loop system for the local climate of Shenyang. The outlet of the BIPV/T system was linked to the supply of the ASHP and the cool air exiting re-entered the façade BIPV/T system. It was found that for a supply rate of 2.82 kg/s the COP of the heat pump reached 4.6, while the ΔT of the air channel was 6ºC for a 12 m long system, at 400 W/m^2 solar irradiance and ambient temperature of -5ºC.

More recently, Dumoulin et al. (2021), studied the energy flexibility potential of a residential building with an air-based BIPV/T system coupled to an air-source heat pump and linked to a thermal storage tank (Fig 2.21).

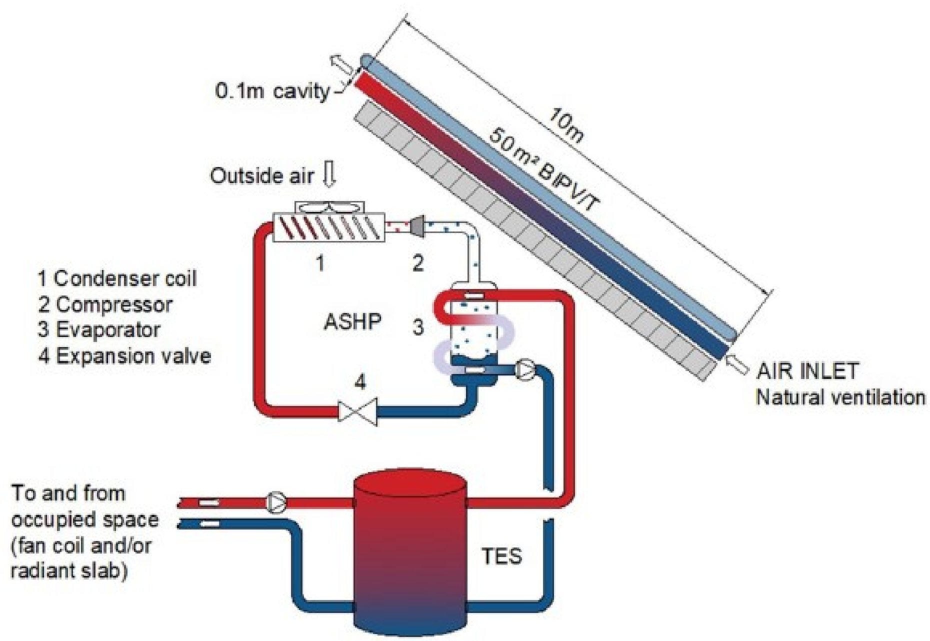

Figure 2. 21: Solar assisted air-source heat pump coupled with BIPV/T system and water source thermal energy storage (TES) (Dumoulin et al., 2021).

The study investigated how rule-based controls for the coupled system could reduce and shift electrical energy demand during peak demand periods, taking advantage of on-site electricity and heat generation by the BIPV/T system. It was found that the energy consumption of the building was reduced by more than 40% during peak demand events. Additionally, it was reported that the

COPV of the heat pump was improved by more than 22% on a weekly average when coupled with the BIPV/T and by more than 50% during peak sun conditions.

2.5.4 Desiccant cooling

Desiccant cooling is a cooling technology based upon reducing the moisture content of the supply air before passing it through an evaporator cooler. This eliminates the need for a first cooling stage for the supply air below its dew point and then reheating it to thermal comfort levels. The basic cycle of a solid desiccant cooling system involves a rotary desiccant dehumidifier, an evaporative cooler and an auxiliary heat source for the regeneration of the desiccant agent.

Desiccant cooling has generally high COP and requires lower operating temperatures for the heat source (around 60-65ºC), compared to other cooling methods (Fong et al., 2010; Gommed & Grossman, 2007; H. Li et al., 2011). The heat from a BIPV/T system can be utilized for the regeneration of the desiccant agent, either directly or through preheating of the auxiliary heating source, depending on the outlet temperature and relative humidity.

(Guo et al., 2017) reviewed recent advances in thermally driven cooling systems that could reduce the required heat source for desiccant cooling to the range of 50-60ºC, including isothermal dehumidification (or 2-stage/internal cooled dehumidification) and pre-cooling of the entry air with ambient heat sinks (indirect evaporative cooling), which could lead to more thermodynamically efficient utilization of the heat recovered by the PV/T for desiccant regeneration.

A coupled BIPV/T façade and a desiccant cooling system is installed in a library building in Mataro, Spain (Infield et al., 2006). The facade consists of a 55 kW PV/T system (525 m^2) with a 105 m^2 added solar thermal collector to boost the outlet temperature. The desiccant cooling system is operated to condition a 510 m^2 room. When the room temperature goes over 25ºC, an auxiliary cooling system takes over.

Beccali et al. (2009) performed a theoretical investigation of a coupled PV/T + desiccant cooling system in TRNSYS, for the local climate of Palermo, Italy. They found that the outlet temperature of the PV/T (40-50ºC) resulted in poor desiccant regeneration and overall system performance, but by using an added solar thermal section in series with the PV/T, the system's performance was highly improved (with outlet temperatures 60-70ºC).

Nibandhe et al. (2019) performed a simulation study to investigate the performance of several configurations of a BIPV/T assisted solid desiccant cooling system for a warm and humid climate, employing a direct-indirect evaporative cooling cycle (Fig. 2.22). The study showed that a BIPV/T outlet air temperature over 50ºC could be maintained for over 40% of the daylight hours, indicating the potential for thermal exploitation.

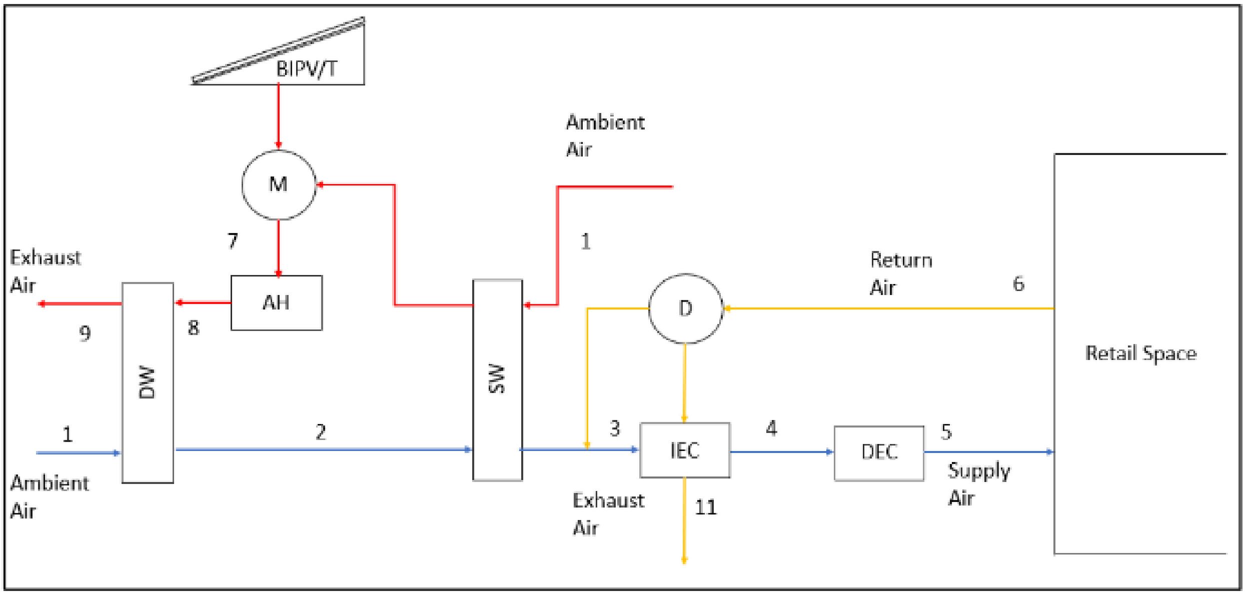

Figure 2. 22: Direct-indirect evaporative cooling (DINC) cycle for a BIPV/T assisted desiccant cooling system (Nibandhe et al., 2019).

2.5.5 Building integrated thermal energy storage (BITES) charging

One of the first applications where a BIPV/T system coupled with thermal energy storage was considered involved using the outlet air to charge a ventilated concrete slab for a near net-zero residential building in Quebec, as demonstrated in Figure 2.23 (Chen et al., 2010). If the outlet air temperature was 3ºC or higher than that of the concrete slab it would be directed within a ducting system of the concrete slab, which would then give of the stored heat at a later time in the day. Furthermore, the outlet air could be used for clothes drying, when heating was not needed and when its temperature and RH were over 15ºC and less than 50% respectively, or for DHW if temperature was at least 5ºC higher than that of the storage tank. From the monitored data, it was found that the BIPV/T system has a typical thermal efficiency of 20%, while its annual space heating energy consumption is about 5% of the national average.

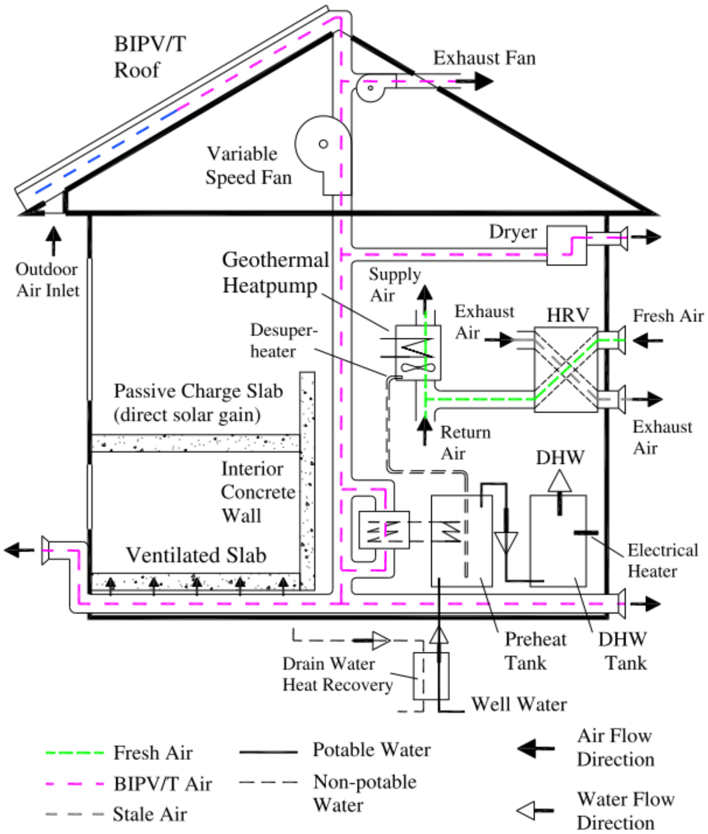

Figure 2. 23: Schematic of BIPV/T and ventilated concrete slab integration (Chen et al., 2010)

2.5.6 Discussion

The major trends in the energy sector include decentralization of power generation with integration of distributed renewable energy sources, electrification of heating with heat pumps and transportation with electric vehicles, as well as smart grid integration by using building energy flexibility.

BIPV/T systems fit well and support the trends above and there is significant room for integrated applications (BIPV/T plus heat pumps plus energy storage and the building as a smart prosumer trading energy with a smart grid), given that both the retrofit and new building markets are very large.

Indicatively, according to Canada Green Building Council [120], in order to achieve a 30% reduction in Canada's emissions by the year 2050, there are several steps that need to be followed, including recommissioning in 60% of very large buildings (over 200,000 ft^2) and 40% of large buildings (25,000 to 200,000 ft^2), deep retrofits in 40% of buildings over 35 years old and installation of on-site renewable energy system in 30% of buildings (in carbon intensive locations). An early study by CANMET Energy (Natural Resources Canada) indicated that roof PV applications on residential buildings could potentially supply roughly 46% of electricity consumption in Canada [121].

The utilization of BIPV/T systems for fresh air preheating [13, 14] or as a heat source for heat pumps during the heating season in most of Canada and the Northern US [16, 17] is particularly promising because of the widespread adoption of forced air systems in which this heat source can be readily connected.

The intermittency of power generation and the fact that electricity and heat may be readily available when least needed (i.e. during peak sun hours in the winter) can be alleviated with optimized grid integration strategies and demand response scenarios. Recent studies [20] have shown that a BIPV/T assisted air-source heat pump connected to a thermal storage tank could significantly increase the energy flexibility of a residential building and reduce energy consumption during peak demand period in winter by up to 40%.

Regarding the coupling of air-based BIPV/T and HVAC, the following can be noted:

- The literature shows that there are numerous options for the integration of air-based BIPV/T and HVAC. There are however no relevant guidelines or standards for such coupling and integrated performance.
- The intermittency of the incident solar radiation is a crucial factor which affects the degree of thermal utilization of the system. There will never be a constant outlet temperature and therefore whether the preheated air can be used as is or needs to be further heated by an auxiliary source, depends on the type of BIPV/T and HVAC coupling.
- The coupling options with the greatest simplicity and degree of thermal utilization are direct preheated fresh air supply, boosting the operation of an HRV and boosting the evaporator intake of an air-source heat pump. The efficiency of these options is due to the fact that the outlet air of the BIPV/T replaces the ambient intake of each system, reducing thus the heating load.
- Increasing the complexity of the system with added equipment increases the initial and maintenance cost but may provide further options for thermal utilization. The design option of a BIPV/T boosting an air-to-water heat pump, also connected to a storage tank allows for further thermal flexibility in interacting with a smart grid and utilization when there is no incident solar radiation. This can also be beneficial from the grid peak shaving standpoint.
- As far as thermally driven cooling systems are concerned, BIPV/T has great potential to be coupled with desiccant cooling systems that require low regeneration temperatures. Limiting factors for that are the complexity of the system, which increases with more extreme climates, as well as the intermittency of incident radiation that renders an auxiliary heat source necessary.

Comments regarding the system design:

- Several studies have established that PV/T systems should not be treated as solar thermal collectors, as their primary function is electricity generation (Gautam & Andersen, 2017; Yang, 2015), and should therefore be intended for low temperature applications (Tonui and Tripanagnostopoulos, 2006; Thomas, 2001; Kamel et al 2014). An important factor to take into consideration is PV module degradation at high operating temperatures (Yang, 2015) (Rebecca), as well as the thermal boundary for the building that is created and the impact on the heating/cooling load of the building.

- The design of the BIPV/T should not be done independently but considering the integration with the HVAC (in addition to the structural and building envelope requirements). The designated HVAC system may impose constraints on the system's flow rate and required outlet temperature. This may in turn affect the system's geometric design (thermal and hydraulic performance) and may dictate the need for an auxiliary heating source.

- In the end, the design of a BIPV/T system is a trade-off and optimization procedure depending on the climate, system type, thermal needs and application, electrical needs, thermal enhancement. Enhancements like use of glazing may be unsuitable for warm climates but a good solution for cold climates. It is therefore important to map the potential thermal applications, with emphasis on the ones that require low temperature input. The presence of thermal storage and its use to store heat for later use can help develop flexibility in the interaction with a smart grid by displacing heating loads to off-peak hours and take advantage of dynamic tariffs.

- Evaluation and control of the outlet air temperature can be critical for the optimal coupled operation of the BIPV/T and the HVAC system.

2.6 Documented performance of PV/T and BIPV/T systems

The following section presents a review of key indoor and outdoor experimental studies of PV/T prototypes, as well as full scale BIPV/T systems that have been instrumented and monitored. The objective is to get an overview of a system's performance in terms of electrical and thermal output, as well as PV and outlet temperatures (or air temperature rise) with respect to the system design, configuration and size, and the operating/testing conditions. The review showed that the majority of experimental studies involve small-scale PV/T prototypes of the stand-alone format, usually tested under conditions that are not representative of full-scale BIPV/T systems, while the cases of instrumented full-scale BIPV/T systems are very few. The varying testing conditions render a direct performance comparison of the various systems difficult, while the convective phenomena may exhibit significantly different behavior depending on the system type and size.

The selection of studies was done according to the wealth of information these could provide regarding the testing conditions (solar irradiance, ambient temperature, wind velocity and flow rate), the system's configuration data (geometric features, thermal enhancements, PV type) and performance (electrical and thermal performance, surface and air temperatures and fan operation when applicable), as well as convective correlations used in the modelling of the system, when applicable.

The performance of hybrid PV/T and BIPV/T systems is usually described by the electrical and thermal efficiency of the system. For crystalline, silicon-based PV, the electrical output is highly dependent on the operating PV temperature (cell or module), according to the well-established correlation (Florschuetz, 1979; Wolf, 1976):

$$\eta_{PV} = \eta_{STC}(1 - \beta_{PV}(T_{PV} - T_{STC})) \tag{2.1}$$

The thermal output is given by:

$$q = \dot{m}C_p\Delta T \tag{2.2}$$

And the thermal efficiency is defined as:

$$\eta_{th} = \frac{q}{A_c G} \tag{2.3}$$

where q indicates the total heat flow output by the collector and ΔT is the temperature difference between inlet and outlet temperature of the air flow. The thermal efficiency, η_{th}, can be a useful indicator when comparing the thermal performance of different design configurations for systems operating under the same conditions (environmental conditions, flow rate). However, for building integrated systems, and depending on the coupled BIPV/T – HVAC configuration, the thermal efficiency may not be an adequate indicator of the overall system performance since the usable recovered heat is needed to describe the overall system performance.

Table 2.3 presents several indicative investigations of PV/T systems in literature and includes a brief description of the system (geometric and other features), testing and operating conditions (ambient conditions, flow rate, and the critical values measured in each study (PV, back surface and outlet air temperatures, electrical and thermal output, fan consumption). These studies can be summarized as follows.

2.6.1 Single pass PV/T with and without glazing

Tiwari et al. (2006) developed an unglazed PV/T air collector consisting of two 75 W (η_{STC}=12%) PV modules (Fig. 2.24) and evaluated its performance experimentally under three flow modes; natural flow, forced flow with single and forced flow with double fan. For the case of forced channel flow, combined efficiencies of up to 43% were reported. However, these corresponded to cases of high channel flow with insignificant temperature rise, which may not be usable for building and HVAC integrated systems. The experimental study was extended to include a glazed configuration (A. Tiwari & Sodha, 2007), as well as PV modules with and without tedlar, as the substrate material which supports the PV cells. It was found that the glazed collector employing PV modules without tedlar had the best overall performance, due to the increased conductive heat transfer from the substrate side. This indicated the importance of the thermal conductivity of the material placed between the PV cells and the air channel.

Figure 2. 24: PV/T system by Tiwari et al. (2006).

Bambrook & Sproul (2012) designed an experimental, 3.92 m long unglazed single-pass PV/T collector with a 0.1 m air channel gap (Fig. 2.25), with the aim of maximizing its electrical and thermal output, while achieving lower fan consumption than the additional energy generated. The PV/T system, which employed large ducts in order to minimize the hydraulic resistance, was tested outdoors in Sydney, Australia and it was found that for flow rates in the range of 0.03-0.05 kg/s/m^2 the additional energy output from the PV cooling was in excess of the fan power demand. The thermal and electrical efficiencies of the system were found to increase with increasing air mass flow rate. The study concluded that a control system which optimizes the outlet air temperature, also considering the fan operation, should be investigated.

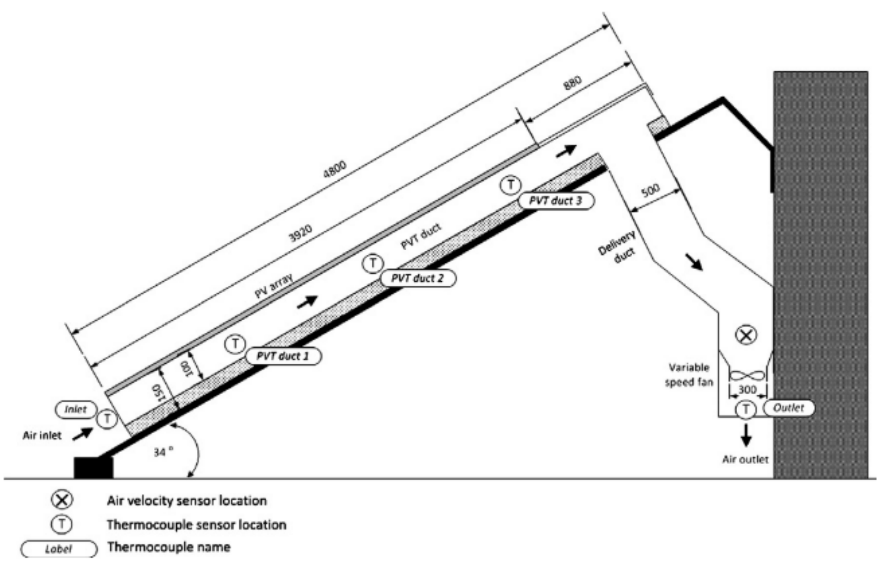

Figure 2. 25: Single pass PV/T air collector studied by Bambrook & Sproul (2012).

Adeli et al. (2012) studied the performance of a single pass PV/T collector (0.997 m x 0.462 m, 5 cm channel gap) with a m-Si PV module (Fig. 2.26a). The experiments were conducted outdoors in Iran under a constant flow rate of 0.18 $kg/s/m^2$ and the measured data were used for the development of a mathematical model to be used for the simultaneous electrical and thermal optimization of the collector. Kim et al. (2014) studied a similar collector (Fig 2.26b) featuring a single 250Wp m-Si PV module (1.645 m x 0.983 m, 6cm channel gap) and found a 5ºC air temperature rise with an average thermal efficiency of approximately 22%. The collector was tested outdoors with a constant channel flow rate of 240 m^3/hr (0.05 $kg/s/m^2$). The study suggested that the heated air from the system could be supplied to the ventilation system as pre-heated fresh air, although the system geometry and flow rate did not represent a specific thermal application.

a b

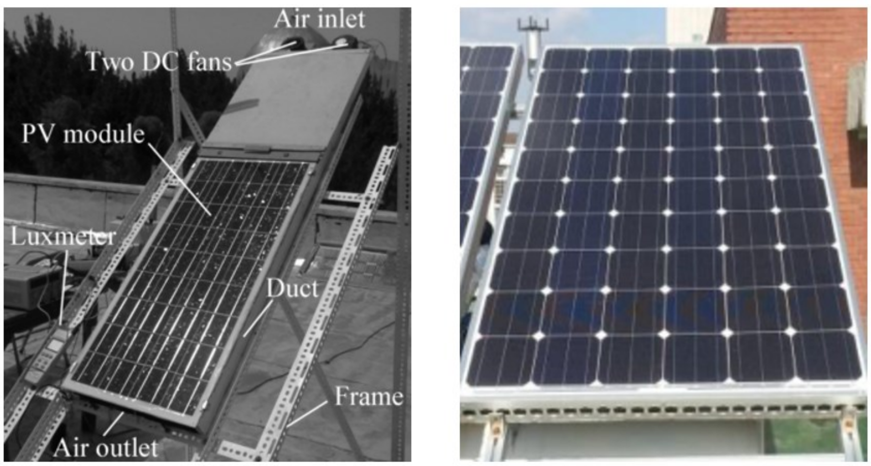

Figure 2. 26: Single pass PV/T collectors by: a. Adeli et al. (2012), b. Kim et al. (2014).

Kaiser et al. (2014) studied experimentally the effect of gap size on the PV cell temperature and PV efficiency for an unglazed, single-pass PV/T collector consisting of a single 270 Wp PV module, for the case of forced and natural ventilation. The system was 1.96 m long and the channel gap size could vary between 0.1 and 0.16 m. Results showed that a critical aspect ratio (duct depth/duct length) of about 0.11 was found to minimize the PV cell temperature for the case of natural ventilation. With increasing channel air velocity (forced ventilation) smaller aspect ratios could be used, while for a constant aspect ratio it was found that the induced air velocity highly affected the PV cooling. Finally, an increase of 19% in the power output was observed from the natural ventilation case (V_{avg}=0.5 m/s) to the forced ventilation case of V_{avg}=6 m/s. The flow resistance and consequent fan consumption were not included in that study, while velocities of this magnitude would not be applicable for building integrated systems.

2.6.2 Double-pass PV/T

Sopian et al. (2000) developed and tested a double-pass PV/T intended for solar drying applications (Fig. 2.27). The system featured a 1.476 m x 0.66 m PV module (η_{STC}=14%) with a top and a bottom air channel (5 cm channel height each), and with the flow path starting at the top channel and continuing to the bottom one. A mathematical model of the system was developed and validated against experimental results. The system was tested outdoors for various flow rates (0.018-0.04 kg/sm^2) and it was found that with increasing mass flow rates the electrical and thermal efficiencies of the system increased. The main aspect investigated was the thermal performance with equal value assigned to both the electrical and thermal efficiencies. The temperature rise of the PV cells and the fan operation were not investigated.

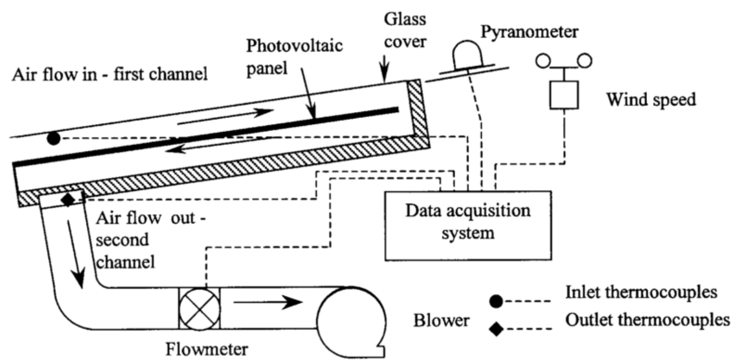

Figure 2. 27: Experimental setup of the double pass PV/T collector (Sopian et al., 2000).

Othman et al. (2007) studied a double-pass PV/T solar air heater system consisting of monocrystalline Si cells pasted on an absorber plate with fins attached to the other side of the absorber (Fig. 2.28a) in an indoor solar simulator facility. The system was 1.22 m long, 0.83 m wide, with an upper channel height of 0.165 m and a lower channel that could vary between 0.03-0.12 m. It was found that with increasing mass flow rate, the temperature rise in the air collector dropped, while the electrical and thermal efficiencies increased. The recorded temperature rise was in the range of 7-12ºC with respective thermal efficiencies between 40-60% for relatively high mass flow rates (0.18 kg/s/m^2). The study concluded that fins should be an integral part of the absorber to enhance the thermal and electrical output of the system, without considering though the effect on fan consumption for a large application.

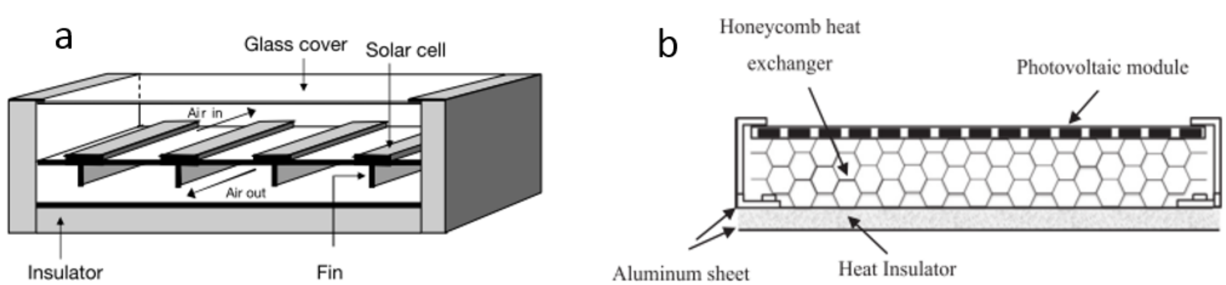

Figure 2. 28: PV/T with fins (Othman et al., 2007) (a) and honeycomb (Hussain et al., 2015) (b).

Kumar & Rosen (2011a) investigated a double pass PV/T solar air heater with and without fins installed normal to the flow on the lower air channel (Fig. 2.29). The effects of system, climatic and operating parameters (irradiation levels, upper and lower channel gap size, mass flow rate) on air temperature rise, cell temperature, electrical and thermal efficiency, and total equivalent efficiency were assessed. The fins improved the heat extraction from the PV cells, reducing their temperature and increasing the electrical, thermal and overall system efficiency. The total equivalent efficiency and air temperature rise were higher for smaller gap sizes, the effect being more dependent on the lower channel gap size. The size of the system tested was 1 m long and 1 m wide with the flow entering from the 0.1 m high upper air channel and continued to the 0.03 m high lower channel. the PV temperature rise of a larger installation and resulting system performance was not considered, neither was the effect of fins on the flow resistance.

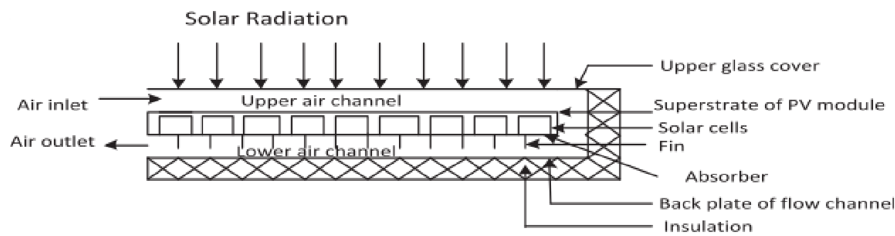

Figure 2. 29: Double pass PV/T air heater with fins on the lower channel (Kumar & Rosen, 2011a).

Amori & Abd-AlRaheem (2014) performed a comparative study of three PV/T configurations and investigated the effect of climatic conditions and air flow rate on the PV and air temperatures, power production and fan consumption. The 2.97 m long and 0.58 m wide PV/T configurations featured 2 45 Wp p-Si PV modules and included a single-duct/single-pass (3.5 cm channel gap), a double-duct/single pass and a double-duct/double-pass collector with a 3.5 cm and 2.4 cm upper and lower channel gap respectively (Fig. 2.30). The single-pass/double-duct configuration was found to have the highest overall efficiency, while the other two configurations resulted in the lowest pressure drop and fan consumption. Each PV/T configuration was tested against a regular racked PV system of the same size on three different times of the year and compared in terms of electrical performance and PV temperatures, although there was no side-by-side comparison of the three PV/T configurations.

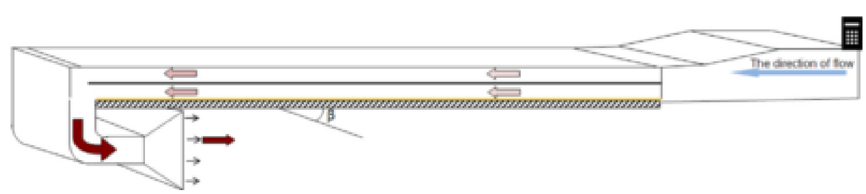

Figure 2. 30: Double-duct/double-pass system studied by (Amori & Abd-AlRaheem, 2014).

Saygin et al. (2017) investigated a modified glazed, double-pass PV/T collector in Instabul, Turkey. The 1.115 m long collector features a slot in the middle of the glass cover as an air inlet with air collected from an outlet located behind the PV module (Fig. 2.31). Measurements were carried out to investigate the optimal distance from between the PV and the glass cover to maximize the electrical output for the PV. It was found that a 5 cm distance between the PV and the glass cover and 0.021 kg/s mass flow rate yielded the highest electrical efficiency as compared to a case with no PV cooling (with a bottom channel kept at 7 cm gap size). Such a configuration might be more suited as a stand-alone collector application but would probably be impractical for building integrated systems.

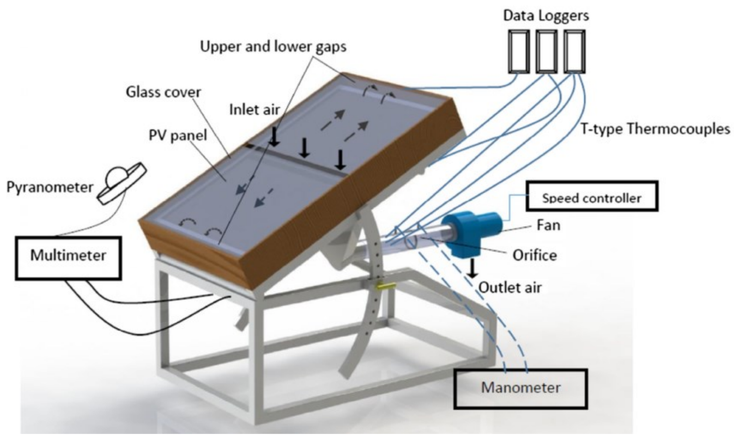

Figure 2. 31: PV/T with center slot (Saygin et al., 2017).

2.6.3 PV/T with fins and porous media

Tonui & Tripanagnostopoulos (2006) compared three experimental PV/T systems, one equipped with a thin metal sheet (TMS) suspended in the middle air channel, one with fins (FIN) on the back wall (Fig. 2.32a) and a reference system with no modifications. The overall system dimensions were 1 m x 0.45 m, with a 15 cm channel gap and featuring a single PV module. The tests were carried outdoors in Greece and each set of experiments included side by side testing of the reference system with either the FIN or the TMS system (but not all at the same time). They later included the glazed counterparts of these systems (Fig. 2.32b) (Tonui & Tripanagnostopoulos, 2007). It was found that for all systems there was an exponential rise of thermal efficiency with mass flow rate, with the FIN system performing best, followed by the TMS system and finally the reference system. The TMS and FIN systems were found to have slightly lower PV and back wall temperature and higher outlet air temperature than the reference system. Finally, the pressure drop of all systems was found to be less than 10 Pa (for a 1 m long system) and the fan consumption less than 1% of the power produced by the PV and a channel depth of 15 cm was proposed as a balance point for larger BIPV/T systems (5-10m). This, however, should be the result of an optimization study maximizing the heat extraction and net electrical output, as a very large channel gap can significantly reduce the convective heat transfer for a given flow rate. The glazed systems had higher thermal efficiency, due to the reduced losses, but lower electrical efficiency. The authors argued that unless the system is optimized for thermal output, glazed PV/T systems are not recommended due to the reduced electrical efficiency.

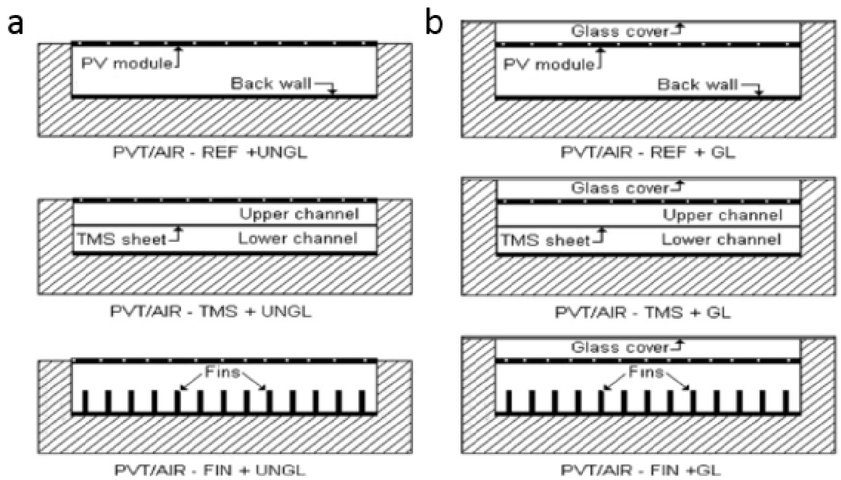

Figure 2. 32: Unglazed (a) and glazed (b) PV/T with TMS and fins (Tonui & Tripanagnostopoulos, 2006, 2007).

Hussain et al. (2015) introduced an improved unglazed, single-pass PV/T solar collector with a hexagonal honeycomb (Fig. 2.28b) heat exchanger installed horizontally in the channel to enhance heat extraction from the PV. The system was tested with and without the honeycomb at constant irradiance and flow rates ranging between 0.02-0.13 kg/s. For a mass flow rate of 0.11 kg/s the honeycomb increased the thermal efficiency from 27% to 87%, while the electrical efficiency was improved by 0.1% for all mass flow rates. The temperature rise for such a flow rate was less than 3ºC, which highlights the fact that the thermal efficiency by itself is not an adequate indicator of the recovered heat that can be actually utilized.

Mojumder et al. (2016) performed indoor testing of a single-pass PV/T collector with fins (Fig. 2.33). Different fin configurations (0-4 fins) attached on the rear surface of the air channel, mass flow rates (0.02-0.14 kg/s) and irradiation levels (200-700 W/m^2) were considered. The maximum thermal efficiency (56.19%) was obtained for the configuration with 4 fins and the max flow and irradiation settings. It should be noted that there was no external wind present, while the mass flow considered is significantly high for a collector of this size (0.63 m long, 0.51 m wide with a 13 cm channel gap).

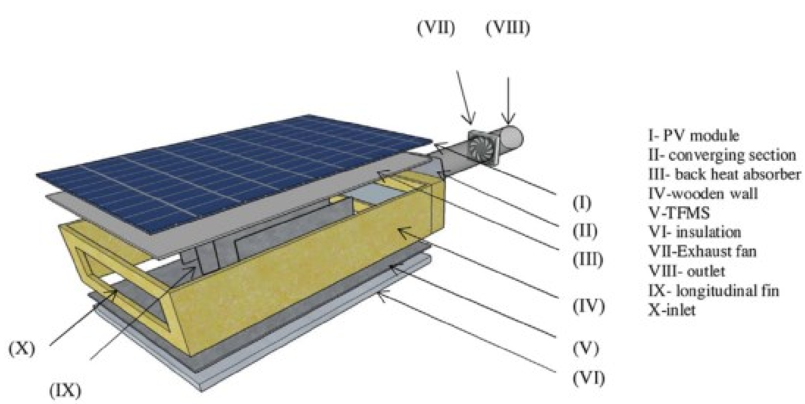

Figure 2. 33: PV/T collector with fins (Mojumder et al., 2016).

2.6.4 BIPV/T prototypes, multiple inlets and full-scale systems

In one of the rare cases of a monitored full-scale BIPV/T system, Chen et al. (2010) presented the measured performance of a prefabricated roof BIPV/T system with a-Si PV modules pasted on metal roofing (Fig. 2.34). The system was installed on a prefabricated, two-storey, detached, low-energy house and linked to a ventilated concrete slab. This study provided detailed system performance in terms of PV, air and insulation temperatures, as well as thermal and electrical output for clear sunny and overcast days during the winter. A typical temperature rise of 30-35°C was observed for a sunny day with a flow rate of 250 L/s (0.006 kg/s/m^3, average channel velocity: 0.75 m/s). The system featured 6.2 m long a-Si PV modules, 0.038 m channel gap and an air channel net cross sectional area of 0.332 m^2.

Construction of BIPV/T roof module (ready to attach metal roof layer)	Spray foam insulation applied on ducting manifold	BIPV/T roof module delivered on site for assembly of house

Figure 2. 34: Prefabricated roof BIPV/T system (Chen et al., 2010).

Bambara et al. (2011) developed an Unglazed Transpired Collector (UTC) – PV/T hybrid prototype (Fig. 2.35). 70% of the UTC area was covered by custom made PV modules. This BIPV/T concept was applied to the mechanical penthouse of an institutional building in Montreal, Canada. Long, narrow PV modules were chosen to reduce temperature stratification in the vertical axis, while heat was recovered both by the PV and the exposed UTC area. The UTC-PV/T prototype (2.4 m x1.375 m, 15cm channel height) was tested outdoors in Montreal, Canada, side by side with a UTC thermal collector of the same dimensions, at flow rates ranging between 0.014-0.042 kg/sm^2. The combined efficiency of the hybrid system was found to be 7-17% higher than that of the UTC thermal system, with the assumption that electricity is approximately 4 times more valuable, based on a heat pump COP of 4. Although the combination of the UTC and the PV could be considered redundant, this set the foundation for the concept of multiple inlets and more efficient heat extraction from the absorber by disrupting the thermal boundary layer.

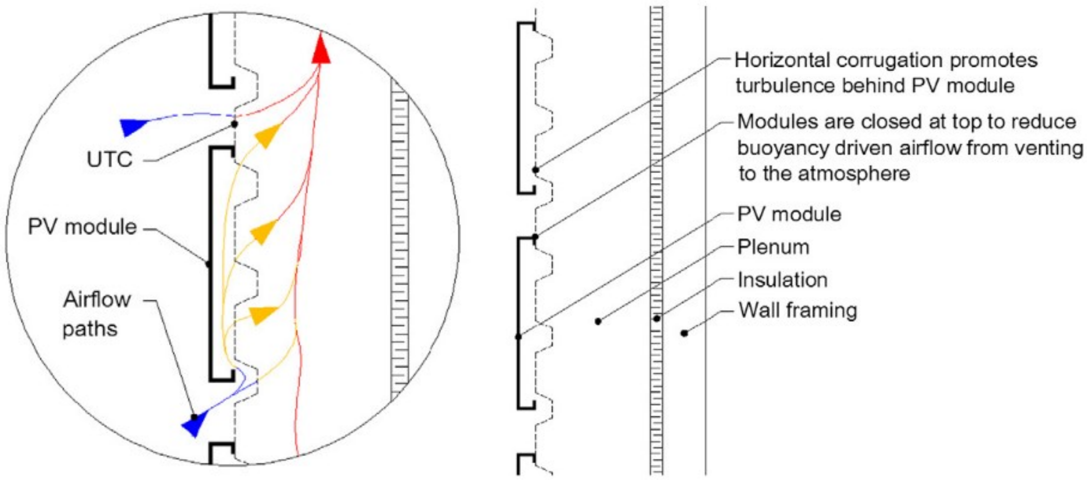

Figure 2. 35: Hybrid UTC-PV/T system (Bambara et al., 2011).

(Candanedo et al., 2011) investigated experimentally a BIPV/T sample, tested outdoors (Fig. 2.36). The subject represented part of the full-scale BIPV/T application studied by Chen et al. (2010), with a-Si modules pasted on metal roofing. The researchers developed Nu numbers for the top and bottom part of the air-channel for Re between 250-1060, highlighting the heating asymmetry of the two channel boundaries. The normalized flow rates used (0.0043-0.023 kg/s.m^2) were representative of the EcoTerra BIPV/T system (Chen et al., 2010).

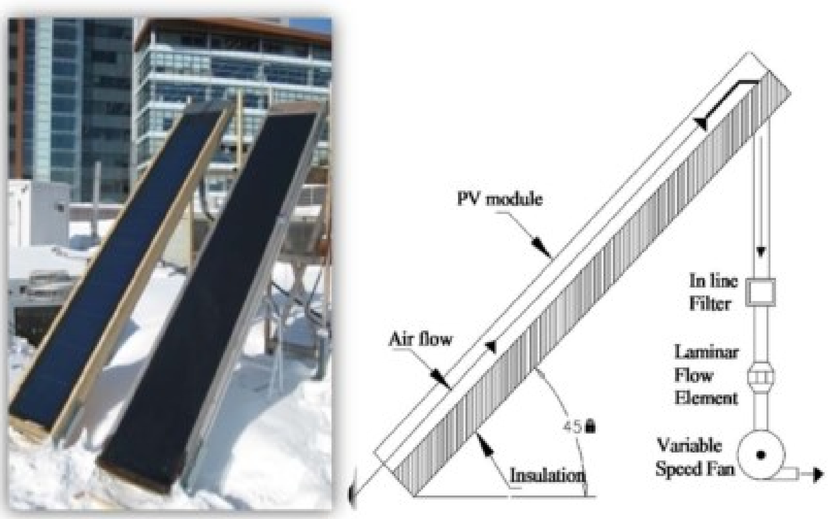

Figure 2. 36: BIPV/T prototype with a-Si PV (Candanedo et al., 2011).

(Yang & Athienitis, 2014) performed a solar simulator study of the EcoTerra system, with the goal of developing local Nu correlations for the top and bottom surface of the air channel. The 2.9 m long sample, with a 0.038 m channel depth and equipped with a-Si PV was tested under constant irradiation (1080 W/m^2), with varying mass flow rate (0.0043-0.025 kg/s/m^2) and wind velocity (1.6-3.2 m/s) and provided detailed PV, air and insulation temperature profiles.

In a following study, a double-inlet PV/T prototype (Fig. 2.37) was investigated (Yang & Athienitis, 2015a). The addition of the second inlet increased the thermal efficiency of the system by 5% and it was also found that using semi-transparent PV modules further increased the thermal efficiency by 7.6%. It was suggested that the use of multiple inlets is an efficient means to improve the performance of a BIPV/T, easily applied and with no significant cost added. The measurements were used for the development of Nu numbers for the single and double-inlet configuration.

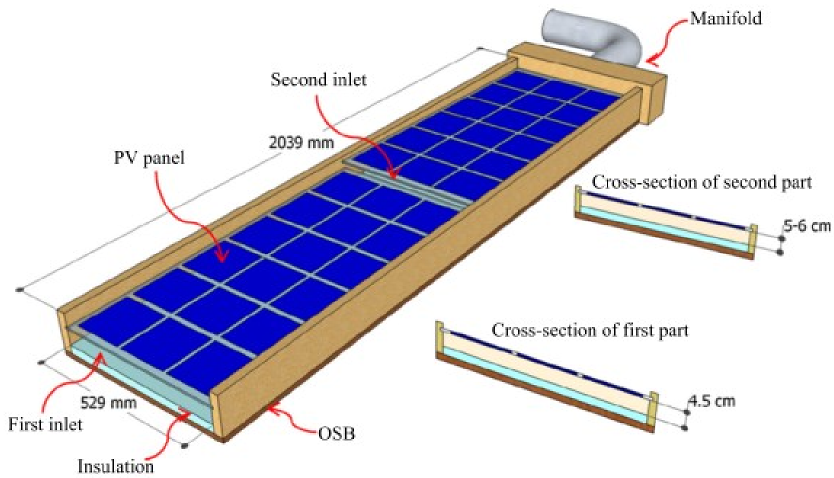

Figure 2. 37: Two-inlet PV/T (Yang & Athienitis, 2015a).

A BIPV/T curtain wall prototype was designed, developed and tested at Concordia University in Montreal, Canada, in order to combine the PV/T concept with a standardized building technique (Rounis et al., 2021a). The prototype was treated as a building block of a modular BIPV/T design (Fig. 2.28) and was tested under nominal operating cell temperature conditions in an indoors solar simulator facility, with flow rate between 0.025-0.038 kg/s/m^2. The prototype featured two frameless PV modules and a 9 cm channel gap. Thermal enhancements such as multiple inlets, flow director equipment and varying PV transparency were considered. The monitored performance showed a thermal efficiency between 26 and 32%, with a respective air temperature rise of 7-9°C for a 2 m long channel.

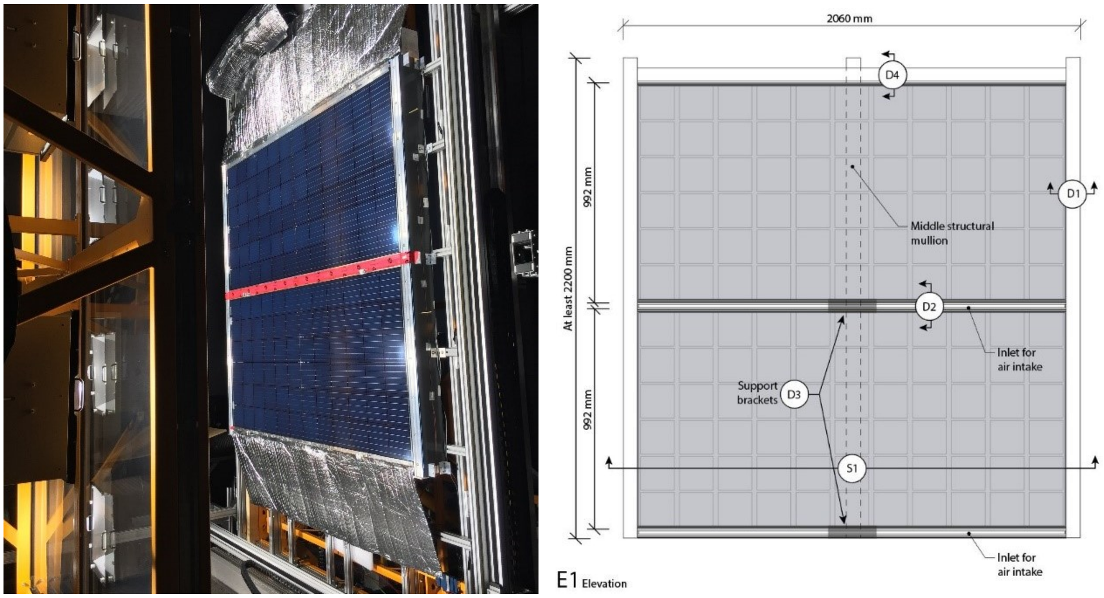

Figure 2. 38: Testing of a BIPV/T curtain wall prototype and its schematic at the Concordia Solar Simulator – Environmental Chamber (SSEC) laboratory; the lamps and artificial sky are on the left (Rounis et al., 2021a).

2.6.5 Discussion

With few exceptions, most of the studies presented in this section and summarized in Table 2.3 involve compact systems, which usually facilitate 1-2 commercial PV modules, with channel lengths between 1-2.4 m and channel depth between 0.02-0.15 m. A typical mass flow rate per collector area ranges between 0.03-0.05 kg/s m^2. Reynolds numbers are usually within the transitional area (2300<Re<10000), there are however studies including laminar (Re<2300) and fully turbulent flows (Re>10000). It is also important to notice that most of researchers choose low to no wind conditions (0-1.5 m/s) for their experiments. Air temperature rises are typically within the 5-20ºC range and respective thermal efficiencies in the 20-50% range. It should be noted that the highest recorded thermal efficiencies corresponded to cases with very high mass flow rate, which is impractical for a small stand-alone collector and in most cases leads to very small air temperature rise. The resulting channel velocities would be too high for practical applications, with potential noise, vibrations and significant pressure drop issues. Although experimental testing should investigate a range of flow rates and channel velocities, these should reflect reality and practical applications.

From the analysis of the above studies, several issues become evident:

1. There is no standard testing procedure for hybrid PV/T systems. The electrical and thermal efficiency of the system and the temperatures of the various layers highly depend on the ambient and operating conditions. These conditions, as well as each prototype's unique features vary considerably from study to study, and this renders the direct comparison of the various systems' performance very difficult.

2. The experimental prototypes are designed and optimized primarily as stand-alone collectors with few exceptions (Bambara et al., 2011; Candanedo et al., 2011; Chen et al., 2010; Rounis et al., 2021a; Yang & Athienitis, 2014b). The dimensions of the subjects, as well as the use of thermal enhancements vary considerably (depth to length ratio) and there is no suggested way of extrapolating results to larger building integrated systems. Furthermore, there is no holistic thermal performance approach, considering coupling with an HVAC system, which would induce constraints in terms of flow rate, as well as usable temperatures.

3. An important issue relevant to both the performance and the modelling of air-based systems is the poor representation of wind effects. In most of the experimental studies, low to zero wind conditions are considered and it is therefore difficult to quantify the effect of wind on the system. However, the effect of wind in terms of convective heat transfer can be critical for the performance of BIPV/T systems, since the use of a top glazing should generally be avoided, and the absorber is in direct contact with the ambient environment.

Table 2. 3: Experimental PV/T and BIPV/T studies (monitored performance and operating conditions).

Author	System description	Testing	PV type	Dimensions LxWxD (m)	Tilt (°)	Flow rate (kg/s m^2)	Vavg (m/s)	Re	G (W/m2)	Tamb (°C)	Vwind (m/s)	TPV (ºC)	ΔT (inlet-outlet, ºC)	η_{el} (%)	η_{th} (%)	ΔP (Pa)	Fan (W)
Single-pass PV/T with and without glazing																	
(Tiwari et al., 2006)	Single pass, unglazed PV/T collector, tested	Outdoor	75Wp, η_{STC}=12% PF=0.83	1.2 x 0.45 x N/A	30	N/A	1.6-3.33	N/A	23-677	9-22	0-1.27	12-43	1.3-3.4	N/A	N/A	N/A	N/A
(A. Tiwari & Sodha, 2007)	Single pass PV/T collecote, with and without glazing	Outdoor	75Wp, η_{STC}=12% PF=0.83	1.2 x 0.45 x N/A	30	N/A	2.83-4.83	N/A	300-660	31-36	0-1.52	42-54.7	1.5-4	10	40	N/A	N/A
(Bambrook & Sproul, 2012)	Unglazed, single-pass PV/T collector	Outdoor	m-Si, 110Wp, frameless	3.92 x N/A x 0.1	34	0.03-0.05	N/A	N/A	800-850	15-17	N/A	56 (no fan), 26 (with fan)	~5 (m=0.05kg/sm^2)	9-12	28-55	6-80	6-82
(Adeli et al., 2012)	Unglazed, single-pass PV/T collector	Outdoor	pc-Si, 45Wp	0.997 x 0.462 x 0.05	N/A	0.18	3	20000	830	32-36	1-1.5	48	7	9	32-37	N/A	N/A
(Kim et al., 2014)	Unglazed, single-pass PV/T collector	Outdoor	m-Si, 250Wp	1.645 x 0.983 x 0.06	35	0.05	1.14	8613	910	-1.6-9.5	N/A	N/A	5	15	22	N/A	N/A
(Kaiser et al., 2014)	Unglazed, single-pass	Outdoor	270Wp	1.956 x N/A x 0.10-0.16	N/A	N/A	2.5-6	N/A	100-1000	N/A	<3	30-45	N/A	19% increase	N/A	N/A	N/A
Double pass PV/T																	
(Sopian et al., 2000)	Double-pass PV/T collector for solar drying	Outdoor	η_{STC}=14% PF=0.87	0.66 x 1.476 x 0.05/0.05	N/A	0.018-0.046	0.5-1.3	2973-7597	900-1000	31	1-3.5	N/A	20-22	11	38-40	N/A	N/A
(M. Y. Othman et al., 2007)	Double pass PV/T air heater with fins attached below the absorber	Sol. Sim.	Cells pasted on absorber	1.22 x 0.83 x 0.165/0.03-0.12	N/A	0.027-0.18	0.16-1.07	3094-20630	400-700	31-32	N/A	N/A	7-12	N/A	40-60	N/A	N/A
(Kumar & Rosen, 2011b)	Double-pass PV/T solar air heater with and without fins on the lower channel	N/A	η_{STC}=18	1.00 x 1.00 x 0.10/0.03	N/A	0.03-0.15	N/A	N/A	500-1000	25-45		65-85	2-15	14-15	45-61	N/A	N/A
(Amori & Abd-AlRaheem, 2014)	Single and double-pass PV/T collector,	Outdoor	pc_Si, 60Wp	2.37 x 0.58 x 0.035/0.024	5, 23, 44	0.024-0.06	2.6-6	8670-20000	0-1000	10-31	N/A	40-75	1.5-8.5	9-12	36-62	15-75	N/A
(Saygin et al., 2017)	Glazed double-pass PV/T collector with middle slot as air intake	Outdoor	pc-Si, 80 Wp	1.115 x 0.706 x 0.05/0.07	31	0.015-0.046	0.2-0.6	1690-5184	660	32	N/A	38-45	8-18	6.9-7.7	Max: 48	1.2-6	N/A
PV/T with fins and porous media																	
(Tonui & Tripanagnostopoulos, 2006)	Unglazed PV/T collector with TMS and fins	Outdoor	46Wp, η_{STC}=12.7 %	1.0 x 0.4 x 0.15	40	0.045	0.25	4000	590-720	25-35	N/A	55	5-15	10	25 (ref) 28 (TMS) 30 (FIN)	N/A	N/A
(Tonui & Tripanagnostopoulos, 2007)	Glazed/ unglazed PV/T collector with TMS and fins	Outdoor	46Wp, η_{STC}=12.7 %	1.0 x 0.4 x 0.15	40	0.0031-0.0493	0.02-0.28	250-4040	800	25	1.5	45-71 (unglazed) 45-100 (glazed)	12-38 (unglazed) 12-51 (glazed)	10-12	36 (ref) 40 (TMS) 50 (FIN)	N/A	N/A
(Hussain et al., 2015)	Single pass PV/T with honeycomb	Solar Simulator	N/A	N/A	N/A	0.02-0.13 kg/s	N/A	N/A	591-906	N/A	N/A	N/A	3-7.5	7	27-87 (m=0.11 kg/s)	N/A	N/A

	installed in the air channel																
(Mojumder et al., 2016)	Unglazed, single-pass PV/T collector with 2-4 fins attached on the rear surface of the air channel	Solar Simulator	Pc-Si, 40Wp, PF=0.81	0.63 x 0.51 x 0.13	15	0.06-0.44	0.24-1.78	3347-24543	700	N/A	no	N/A	1-5	13.55-14.03	49-56	N/A	N/A
BIPV/T prototypes, multiple inlets and full-scale systems																	
(Chen et al., 2010)	Roof BIPV/T with a-Si flexible modules pasted on metal roofing	Full-scale	a-Si, η_{STC}=6%	6.2 x 8.4 x 0.038	30	0.006-0.01	0.75-0.82	3900-4370	0-750	(-4)-(-10)	3-9	25-35 above ambient	Up to 30 (m=0.006kg/sm^2)	6%	20%	N/A	N/A
(Bambara et al., 2011)	BIPV/T prototypeconsisting of PV/T-UTC hybrid, tested outdoors	Outdoor, full-scale	pc-Si, 70Wp	2.4 x 1.375 x 0.15	90	0.014-0.042	0.2-0.56	3370-10100	570-930	2.7-4.4, 15.8-16.8, 25.6	N/A	15-22 above ambient	6-9	6-7	23-33	N/A	N/A
(Candanedo et al., 2011)	Roof BIPV/T experimental prototype with a-Si flexible modules pasted on metal roofing	Outdoor	a-Si, η_{STC}=6%	2.89 x 0.38 x 0.038	45	0.0043-0.024	0.26-1.5	7400	800-1000	0	0.5-1.5	35-40	5 (for v=0.3 m/s)	6-7	11	N/A	N/A
(Yang & Athienitis, 2014a)	Roof BIPV/T experimental prototype with a-Si flexible modules pasted on metal roofing	Solar Simulator	a-Si, η_{STC}=6%	2.89 x 0.38 x 0.038	45	0.0043-0.024	0.26-1.5	1230-7400	1080	21	1.6-3.2	55-62	12-20	5	17-21 (m=0.024 kg/s m^2)	N/A	N/A
(Yang & Athienitis, 2015a)	Unglazed single pass PV/T prototype with 2-inlets	Solar Simulator	m-Si, opaque, STPV	2.04 x 0.53 x 0.045/0.055	45	0.03-0.95	0.7-3	1453-19034	1040	21	2.1-3.1	N/A	8-11	N/A	27-58	N/A	N/A
(Rounis et al., 2021a)	Unglazed, BIPV/T curtain wall prototype with single and multiple-inlets, and frameless PV	Solar Simulator	Pc-Si, STPV	2.12 x 2.06 x 0.09	90	0.025-0.038	0.55-0.8	6200-9070	842	21	1	52-54	7-9	11.4-12.7	26-32	N/A	N/A

2.7 BIPV/T Modelling

The modelling of hybrid air-based photovoltaic-thermal (PV/T) and BIPV/T systems has been the subject of multiple studies. The main modelling approaches for BIPV/T systems are the following, as summarized by Yang & Athienitis (2016):

- Use of a modified Hottel-Whillier model.
- Analytical solutions of the governing differential equations.
- Use of a finite difference scheme and an iterative solution method for the resulting system of equations.
- Computational fluid dynamics (CFD analysis)

Early studies of water-based PV/T systems suggested a modified Hottel-Whillier model, originally developed for flat-plate solar thermal collectors (Florschuetz, 1979). This approach has been adopted in several later studies (Bazilian & Prasad, 2002; Bigaila & Athienitis, 2017). The modification of the model relies upon the deduction of the PV cell electrical generation from the absorbed irradiation by the collector. This electrical efficiency is itself evaluated as a linear function of the PV cell temperature according to the well-known equation (2.1).

The modified Hottel-Whillier model for hybrid PV/T collector's is presented in detail in Florschuetz (1979) and is commonly used for (but not limited to) liquid-based PV/T systems of the tube and sheet configuration.

Very commonly, BIPV/T systems are represented by thermal (nodal) networks, discretized by a finite-difference scheme (Yang & Athienitis, 2016). Figure 2.39 demonstrates a typical air-based BIPV/T system cross section and the thermal network representation of its energy balance. A common modelling assumption is that of one-dimensional heat transfer, with no temperature variation across the width of the air channel (Candanedo et al., 2011; Yang & Athienitis, 2016).

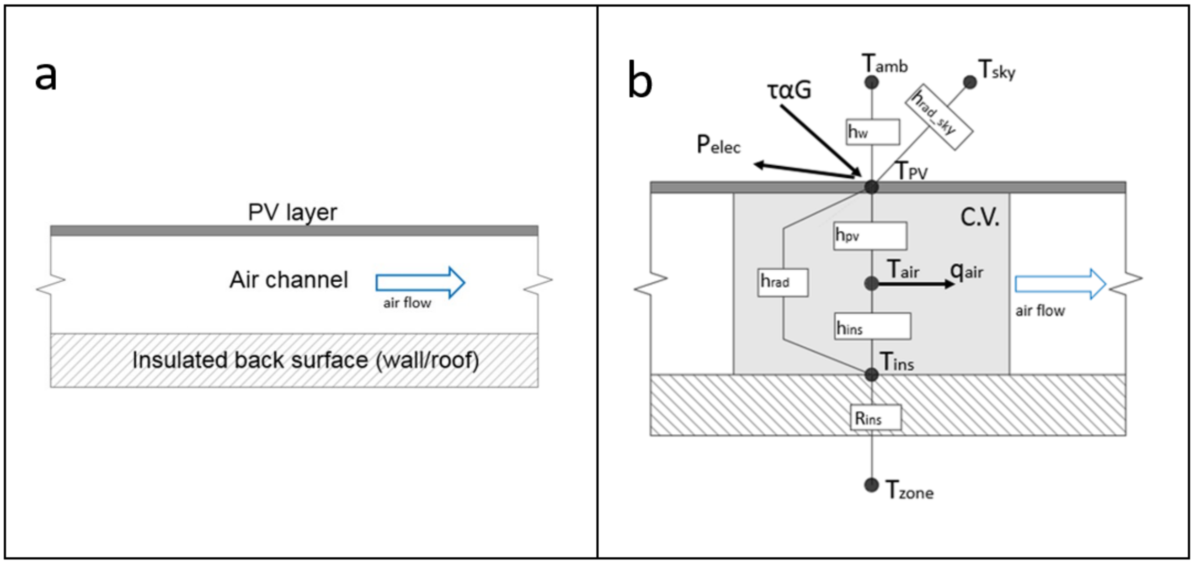

Figure 2. 39: a: common air-based BIPV/T system cross section and b: thermal network representation of its energy balance (Rounis et al., 2021b).

The PV layer is most times treated as a single node, due to its small thickness. The thermal capacitance of the PV is usually neglected for the same reason and a steady state approach is followed. These assumptions are valid for PV modules where the PV cells are sandwiched between a thin top glass cover (usually around 3 mm) and a very thin PET or tedlar backing stratum.

The following are the governing equations for a steady state model of a BIPV/T system energy balance:

Top PV surface node

$$\frac{1}{R_{top}}(T_{PV} - T_{top}) + h_w(T_{amb} - T_{top}) + h_{rad_{sky}}(T_{sky} - T_{top}) + h_{rad_{sur}}(T_{sur} - T_{top}) = 0 \tag{2.4}$$

PV cell node

$$\frac{1}{R_{top}}(T_{top} - T_{PV}) + \frac{1}{R_{bot}}(T_{bot} - T_{PV}) + \alpha\tau G - \eta_{PV} G = 0 \tag{2.5}$$

Bottom PV surface node

$$\frac{1}{R_{bot}}(T_{PV} - T_{bot}) + h_{PV}(\bar{T}_{air} - T_{top}) + h_{rad}(T_{ins} - T_{bot}) = 0 \tag{2.6}$$

Insulation node

$$h_{ins}(\bar{T}_{air} - T_{ins}) + h_{rad}(T_{PV} - T_{ins}) + \frac{1}{R_{ins}}(T_{zone} - T_{ins}) = 0 \tag{2.7}$$

Air node

$$[h_{PV}(T_{bot} - \bar{T}_{air}) + h_{ins}(T_{ins} - \bar{T}_{air})]wdx = \dot{m}C_p dT \tag{2.8}$$

The following are common assumptions in PV/T modelling. The majority originates from the modelling of solar thermal collectors (Duffie et al., 2003):

- Due to the small thermal resistance of the PV module, a single temperature is usually assigned to the PV layer. There are however studies showing that there can be up to 3-5^{o}C difference between the upper and lower PV surface (Amori & Abd-AlRaheem, 2014; Candanedo et al., 2010).
- In the vast majority of studies, 1-D heat transfer is assumed, normal to the surfaces and the flow path. Two of the rare cases where 2-D heat transfer was considered was in Chen et al (2010) and Athienitis et al. (2018).
- Quasi-steady state is usually assumed due to the negligible thermal capacitance of the PV module. Candanedo et al (2010) developed steady and transient PV/T models to simulate the daily performance of an experimental PV/T setup. The results showed that in terms of hourly performance, both models gave almost identical predictions of hourly-averaged temperatures. However, the transient model followed closer and without extreme fluctuations the measurements taken with 1 second time step. It was argued that a transient model would be suitable for a flow control algorithm for the system but redundant for the evaluation of the system's performance.
- Radiative heat transfer between the PV and the back surface is usually considered assuming a view factor of 1. Studies that have considered the view factors between the two surfaces are those of Charron & Athienitis (2006) and Athienitis et al. (2018).
- Convective heat transfer coefficients (CHTC) are usually assumed constant for the whole collector length. Several studies (Candanedo et al., 2011; Hegazy, 2000; Yang & Athienitis, 2014a) have incorporated local CHTC (or Nusselt number) expressions, which account for the entrance effects of the flow.

The temperatures can be evaluated either by analytical solutions of the governing differential equations or following a finite difference scheme. Regardless of the solution method, the wind-driven convection from the top cover and the convective heat transfer coefficients from the PV module surface and the insulated back surface to the channel air have to be evaluated as well. Both top and interior convective phenomena constitute a large portion of the energy balance of the BIPV/T.

Several studies provide analytical solutions for the evaluation of the fluid temperature rise (Garg & Adhikari, 1997). This is done by solving equations 2 through 5 (or accordingly for additional layers) for the PV (or PV module/air channel interface temperature), and the insulation temperature and replacing these values in equation 6 for the channel fluid. The resulting differential equation can then be solved by assigning the boundary conditions of ambient temperature at the inlet (x=0). This methodology relies upon the assumption of uniform temperature over the PV and insulation layers.

Very commonly, the set of equations can be solved through a finite difference scheme. This approach has been extensively used by several researchers (Candanedo et al., 2010, 2011; Yang & Athienitis, 2014a). The collector is divided into smaller control volumes and the radiative heat transfer coefficients are linearized by initial guesses for the PV and insulation temperatures. The linearized set of equations is solved for each control volume through an iterative scheme until the required convergence is achieved. The inlet air temperature for each successive control volume is assumed as the outlet temperature of the previous. This approach can provide more detailed temperature profiles of the various layers, along the flow path of the coolant.

Finally, CFD analysis can provide detailed two or three-dimensional temperature and flow fields, through the solution of energy conservation, mass conservation and the Navier Stokes equations. These temperature and velocity fields can then be used to deduce the local and/or average convective heat transfer coefficients and their correlation to the fluid flow. CFD analysis can be very useful for geometry optimization or investigation of thermal enhancements, as well as understanding/visualizing flow and heat transfer patterns (Ghani et al., 2012; Karava et al., 2012; Zogou & Stapountzis, 2012). However, it can be very expensive computationally and is not practical for the modelling and control of extensive installations.

2.7.1 Convective heat transfer

Convective heat transfer has been recognized as the part of the energy balance that can cause the greatest uncertainty in the modelling of PV/T and BIPV/T systems (Candanedo et al., 2011; Nemati et al., 2016a). Except for CFD analysis, all other modelling approaches for BIPV/T systems require the convective heat transfer coefficients to evaluate the following:

- The wind-driven convective heat transfer from the PV (or outermost layer) to the ambient temperature node
- The convective heat transfer within the air channel, from the PV (or interface of the PV layer with the air channel) to the air stream
- The convective heat transfer within the air channel, from the insulation (or interface of the rear surface with the air channel) to the air stream

2.7.1.1 Channel convection

Convective heat transfer within the air channel is usually represented by the Nusselt number, which indicates the ratio of convective over conductive heat transfer and is defined as:

$$Nu = \frac{hL}{k} \qquad (2.9)$$

Where: h is the convective heat transfer coefficient, L the characteristic length (the hydraulic diameter for heat transfer in duct flow) and k the conductivity of the fluid. Most Nu correlations in the literature is given as a function of the Reynolds and the Prandtl number (and on several occasions the ratio of hydraulic diameter over the collector length, when the entrance effects are considered). The flow within the air channel resembles that between parallel plates (plane-Poiseuille flow), while the flow regime, as seen in Table 2.3, can vary from laminar to turbulent, but is primarily within the transitional region.

Table 2.4 presents the most used Nu expressions in PV/T modelling, as well as the conditions for which they were originally developed.

Table 2. 4: Nusselt number expressions used in PV/T literature

Author	Correlation	Conditions	Re	Used by
LAMINAR FLOW				
(Mills, 1999)	4.364	Fully developed laminar flow in smooth tube with uniform wall heat flux	Re<2300	(TESSLibs 17, 2017)
(Mercer et al., 1967)	$Nu = 4.9 + \frac{(0.0606[RePr(D/L)]^{1.2})}{1+0.0909[RePr(D/L)]^{0.7}Pr^{0.17}}$	Laminar flow and asymmetric heating	Re<2800	(Kamel & Fung, 2014a)
TRANSITIONAL AND TURBULENT FLOW				
(Gnielinski, 1983)	$Nu = \frac{(Re-1000)\mathrm{Pr}\,(f/8)}{1+12.7\sqrt{f/8}\,(Pr^{2/3}-1)}$	Average Nu for smooth tubes, fully developed flow and symmetrical heating	3000<Re<50,000, 0.5<Pr<2000	(Candanedo et al., 2009; Charron & Athienitis, 2006)
(Petukhov, 1976)	$Nu = \frac{(Re-1000)\,\mathrm{Pr}(f/8)}{1+12.7\sqrt{f/8}\left(Pr^{\frac{2}{3}}-1\right)}(1 + \left(\frac{D_h}{L}\right)^{\frac{2}{3}})$	Includes adjustment for developing flow.	Re>3000	(Mei et al., 2003; Pantic et al., 2010; Teo et al., 2012)
(Tan & Charters, 1969)	$Nu = 0.0182Re^{0.8}Pr^{0.4}\left[1+S\left(\frac{D}{L}\right)\right]$ $S = 14.3\log\left(\frac{L}{D}\right) - 7.9$	Forced convection, including entrance length effects, for short ducts		(Shahsavar & Ameri, 2010; Tonui & Tripanagnostopoulos, 2006, 2007)
(Tan & Charters, 1970)	$Nu = 0.0158Re^{0.8} + (0.00181Re + 2.92)e^{-0.0379(\frac{L}{D})}$	Asymmetrical heating in horizontal duct. Adjustment for developing flow	Re>9500	(Amori & Abd-AlRaheem, 2014; Garg & Adhikari, 1997; Hegazy, 2000; Rajoria et al., 2016)
(Dittus, 1985)	$Nu = 0.023Re^{0.8}Pr^{0.4}$	Average Nu for smooth pipes, symmetrical	Re>10,000,	(Sohel et al., 2014; TESSLibs 17,

		heating, fully developed flow	L/D>10,0.7<Pr<160	2017; Zogou & Stapountzis, 2011)
(Malik & Buelow, 1973)	$Nu = \frac{0.0192Re^{0.75}Pr}{1 + 1.22Re^{-0.125}(Pr-2)}$	Asymmetric heating in rectangular channel	10,000<Re<40,000, L/D>162	(Othman et al., 2007)
(Kays, 1996)	$Nu = 0.0158Re^{0.8}[1 + \frac{C_x}{L/D_h}]$ C_x=6 for abrupt contraction entrance			(Kamel & Fung, 2014a; Kumar & Rosen, 2011a)
CORRELATIONS DEVELOPED FOR BIPV/T				
(Candanedo et al., 2010)	$h = 10.2$ (W/m^2.K), 0.4<V_{avg}<0.6 $h = 12V_{avg} + 3$ (W/m^2.K), V_{avg}>0.6	Empirical correlation linking average convective co. to average channel velocity	3900<Re<4370	(Candanedo et al., 2010)
(Candanedo et al., 2011)	Top: $Nu = 0.052Re^{0.78}Pr^{0.4}$ Bottom: $Nu = 1.017Re^{0.471}Pr^{0.4}$	Average Nu for top (PV) and bottom (insulation) surface	250< Re<7500	(Candanedo et al., 2011)
(Yang & Athienitis, 2015a)	1st section: $Nu = 0.0149Re^{0.9}Pr^{0.43}$ 2nd section: $Nu = 1.451Re^{0.44}Pr^{0.4}$	Averagde Nu for 1st and 2nd section of a two-inlet PV/T	1453<Re<14322 (1^{st}) 3600<Re<19034 (2^{nd})	(Yang & Athienitis, 2015a)

One commonly used correlation is that by Dittus-Boelter, which has been developed for heat transfer in smooth circular pipes for fully developed turbulent flow (*Re*>10000). The accuracy of the Dittus-Boelter correlation diminishes with large temperature difference across the fluid. Furthermore, the smooth duct assumption is not valid for PV/T systems. Regardless of its inaccuracy, the Dittus-Boelter correlation has been implemented for the modelling of PV/T systems in commercial software like TRNSYS (TESSLibs 17, 2017).

Comparison of Nu expression developed from the experimental findings of Liao et al. (2007), Candanedo et al. (2011), Chen et al. (2010), and Nemati et al. (2016) showed that commonly used correlations (Dittus, 1985; Gnielinski, 1983; Petukhov, 1976; Tan & Charters, 1969, 1970) generally under-predict the in-channel convective heat transfer by 25-75%. Similar findings were reported by Bazilian & Prasad (2002). This has been attributed to the assumptions under which the original expressions were developed, primarily the duct smoothness and fully developed flow. Local and average Nu have been specifically developed by Candanedo et al. (2011) and Yang & Athienitis (2014), for the same experimental prototype for indoor and outdoor testing respectively. Even these were found to vary considerably. Several of the most commonly used expressions from Table 2.4 are plotted in Figure 2.40 against Re (up to Re=20,000), including the expressions specifically developed for PV/T.

It becomes evident that Nu numbers developed for PV/T are always higher than the typical Nu developed for smooth ducts. These differences become more pronounced with increasing Re, although it should be noted that the validity of the expressions developed for PV/T has been tested within the transitional range (up to approximately Re=10,000).

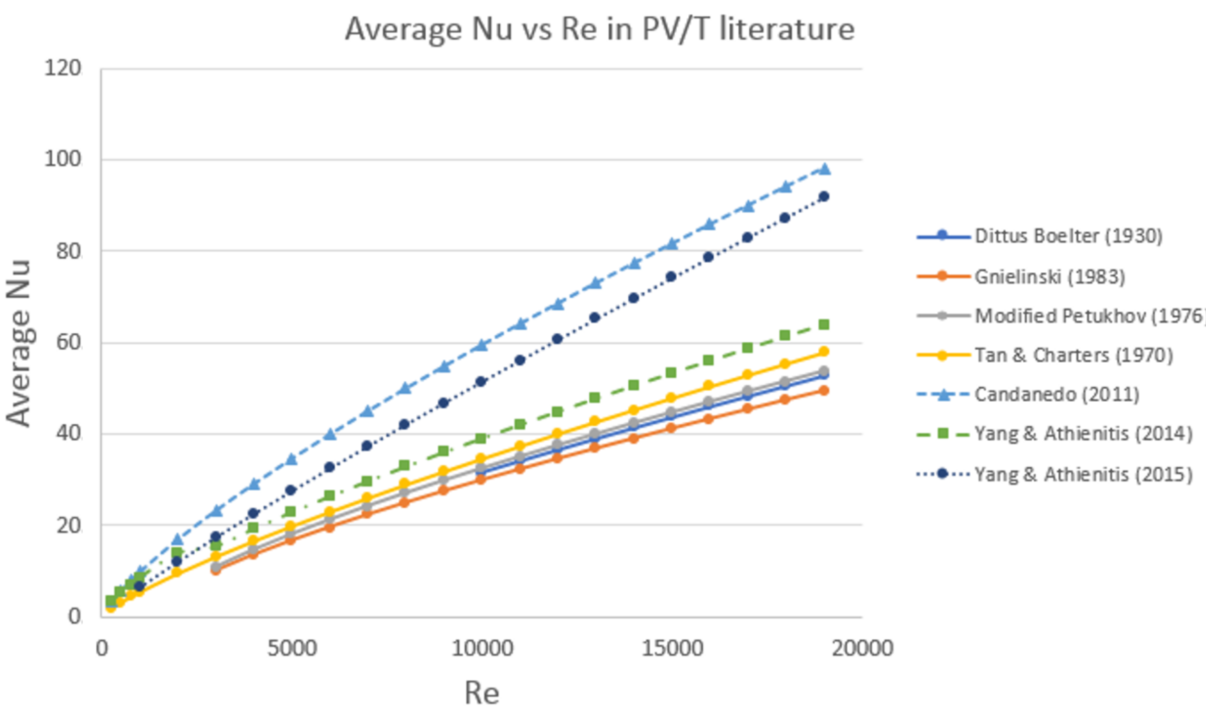

Figure 2. 40: Average Nu vs Re in literature plotted based on the experimental prototype by Yang & Athienitis (2014).

2.7.1.2 Wind-driven convection

Wind-driven convective heat transfer accounts for the largest part of the PV/T energy balance for unglazed systems. Vasan & Stathopoulos (2014) and Ladas et al. (2017) have presented an extensive review of wind-driven CHTC (or h_{wind}) correlations in literature, developed for flat-plate solar thermal collectors. They stated that most of these correlations demonstrate a linear correlation between the h_{wind} and a reference wind velocity, V_{wind} (usually at a height 10 m above the collector) but vary considerably. They also found that assigning a single reference wind speed for a large installation area can create errors in the estimation of convective heat losses over a large installation, as opposed to considering the local velocity distributions over the installation area. Accurate evaluation of wind-driven convection is rendered even more complex by the fact that local velocity distributions are highly affected by the built environment, as well as the local roughness exposure.

Palyvos (2008) performed an extensive review of wind-driven CHTC correlations. He proposed two empirical correlations for windward and leeward surfaces by averaging the coefficients of the existing linear expressions correlating CHTC and free stream wind velocity at a reference height approximately 10 m above the collector. The author argued that the expressions from literature should be carefully selected depending on the similarities to the conditions they were developed for and that there is a lack of generality among them. He also argued that more full-scale studies are needed to address realistic conditions, as well as a standardization of measurement parameters (height above ground, distance from the wall/façade). The review of experimental investigations of PV/T systems in section 2 has shown that most researchers perform measurements during low (up to 1.5-2 m/s) or no wind conditions to avoid the calculation uncertainty imposed by wind-driven convection. This is less of an issue for studies involving glazed systems. From the monitoring of a full-scale roof BIPV/T system, it was reported that roughly for every 1 km/h (0.28 m/s) increase in wind speed, the outlet temperature drops by 2°C (Chen et al., 2010).

Some of the most common expressions for wind-driven CHTC, implemented in PV/T and BIPV/T modelling, are summarized in Table 2.5:

Table 2. 5: Wind-driven CHTC expressions used for PV/T

Author	Correlation	Conditions	Used by
(Test et al., 1981)	$h_{wind} = 8.55 + 2.56V_{wind}$	Rectangular plate exposed to varying wind directions	(Candanedo et al., 2011)
(Sharples & Charlesworth, 1998)	$h_{wind} = 11.9 + 2.2V_{wind}$ (-90° angle of attack)	Full scale measurements on roof mounted solar collector	(Candanedo et al., 2011)
(McAdams, 1954)	$h_{wind} = 5.7 + 3.8V_{wind}$	WTM, parallel flow on plate with smooth surface, V_w<5m/s (Includes radiative losses)	(Agathokleous et al., 2017; Y. B. Assoa & Ménézo, 2014; Ya Brigitte Assoa et al., 2017; Candanedo et al., 2011; Hussain et al., 2015; Kaiser et al., 2014)
(Duffie et al., 2003)	$h_{wind} = 2.8 + 3.0V_{wind}$	(Usually used for glazed collectors)	(Niccolò Aste et al., 2008; Kumar & Rosen, 2011b; Sarhaddi et al., 2010; Tonui & Tripanagnostopoulos, 2006, 2007)
(Palyvos, 2008)	$h_{wind} = 7.4 + 4.0V_{wind}$ (windward) $h_{wind} = 4.2 + 3.5V_{wind}$ (leeward)	Averaged coefficients from literature	(Chen et al., 2010)

2.7.2 Dimensional analysis

Balocco (2004) applied dimensional analysis to describe heat transfer through the wall of a ventilated façade and compare thermal energy performance of different façade systems like solar chimneys. The original 17 implicated variables were reduced to 14 non-dimensional numbers and their relation was established based on experimental measurements. This relation could then be used as a simple tool to evaluate the thermal performance of a façade system.

Nemati et al. (2016) introduced a new *Π* group in the evaluation of the Nu number. The new dimensionless quantity was the Stanton (St) number, as applied to the inter-channel radiative heat transfer, in addition to the Reynolds number, the aspect ratio and a dimensionless U-value for the channel air gap:

$$Nu = f(U, St_r, Re, \frac{L}{D}) \quad (2.10)$$

where:

$$U = \frac{k/D}{\rho u C_p} \quad (2.11)$$

and

$$St_r = \frac{h_{rad}}{\rho u C_p} \quad (2.12)$$

The adaptation of an early version of the methodology presented in Chapter 5 was showcased by Ioannidis et al. (2020), who introduced the effects of the boundary conditions in the evaluation of Nu for mechanically ventilated STPV-DSF applications. In said study a new dimensionless number was defined as:

$$\frac{(h_{c,out} \text{ or } U_{gl}) \cdot |T_{amb} - T_{room}|}{G} \quad (2.13)$$

where $h_{c,out}$ and U_{gl} the exterior heat transfer coefficient and the overall heat transfer coefficient of the inner layer of the DSF. The approach assumed a specific expression for the exterior heat transfer (Sharples & Charlesworth, 1998) and did not account for the effect of channel flow-driven convection on wind-driven convection.

2.7.3 Channel flow pressure drop and fan consumption

An important aspect of a BIPV/T system's modelling, also linked to its design optimization, is the system's pressure drop. The total pressure drop of a BIPV/T system determines the pumping power required by the fan to circulate the air and is a combination of the frictional pressure drop within the air channel, the pressure drop in the manifold that connects the outlets of the BIPV/T and the ducting which links the manifold to the HVAC system. The pressure drop of the manifold and the ducting is again a combination of frictional pressure drop from the straight parts of the ducts and minor pressure losses from contractions, expansions, elbows, converging streams etc.

The frictional pressure drop is calculated according to the Darcy-Weisbach equation:

$$\Delta P_f = f \frac{L}{D_h} \rho \frac{V_{avg}^2}{2} \quad (2.14)$$

The pressure drop due to minor losses is calculated as:

$$\Delta P_m = \sum K_i \, \rho \frac{V_{avg}^2}{2} \quad (2.15)$$

Where K_i denotes the loss coefficients for each type of minor loss.

For laminar flow, the friction factor, f, depends only on the Reynolds number and is calculated as follows [111]:

$$f = \frac{64}{Re} \tag{2.16}$$

For transitional and turbulent flow regimes the friction factor becomes also dependent on the absolute roughness, ε, of the duct wall and the hydraulic diameter, D_h, of the duct. An implicit form of the friction factor for the transitional and turbulent regime, developed through experimental studies data fitting is the Colebrook-White equation:

$$\frac{1}{\sqrt{f}} = -2\log\left(\frac{\varepsilon}{3.7D_h} + \frac{2.51}{Re\sqrt{f}}\right) \tag{2.17}$$

Table 2.6 presents several empirical approximations of the friction factor, which have been used in PV/T studies.

Table 2. 6: Friction factor correlations used in PV/T literature

Formula	**Comments**	**Conditions**
$f = \frac{64}{Re}$	Used for laminar flow.	Re < 2300
$f = 0.316Re^{0.25}$	Equation by Blasius, approximation for smooth surfaces	Re < $2x10^4$
$\frac{1}{\sqrt{f}} = -1.8\log\left(\left(\frac{\varepsilon}{3.7D_h}\right)^{1.11} + \frac{6.9}{Re}\right)$	Equation by Haaland which approximates the Colebrook-White equation	Re > 2300
$f = (0.79\ln(Re) - 1.64)^{0.25}$	Equation by Petukhov for transitional and turbulent flow in smooth ducts	3000 < Re < $5x10^6$

As far as the modelling of pressure drop is concerned, several aspects that require further investigation are the following:

- The pressure drop in the air channel of the PV/T depending on the internal geometry for different design configurations (frame protrusions, fins or other turbulence inducing media) should be further studied experimentally and pressure drop – flow correlations need to be developed to cover a wide range of PV/T and BIPV/T designs.
- Given that most of the pressure drop may occur in the ducting of the manifold, it is important to have studies exploring its optimal design and scalability for different BIPV/T system sizes and applications.

- When evaluating the overall system pressure drop and assessing the benefits of a BIPV/T, it is important to distinguish between the pressure drop that would anyway take place in the original HVAC system and that due to the BIPV/T, additional ducting and/or fan installation, which is dependent upon the specific thermal application.

Apart from the air channel, the pressure drop for different inlet types for roof and façade applications that may employ meshes/filters should be evaluated.

2.7.4 Discussion on PV/T and BIPV/T modelling

When talking about BIPV/T modelling, it is important to consider the different stages modelling can be applied and the purpose it is serving, as well as the fact that convective heat transfer, especially wind-driven, cannot be the same at all locations and for all system types.

1. Early design stage, feasibility study: At this stage, the modelling tool could provide the option to use different correlations for wind-driven and channel convection, which may give range for best and worst-case scenario performance.

2. System design: Valuable information could be provided by research on the effect of different convective correlations when optimizing the system's geometric features, (the net electrical benefit of PV production and HVAC enhanced performance minus the fan consumption). Simulation studies that perform such an optimization for case studies using different modelling approaches and comparing the optimal end result would provide valuable information. I.e., if the different modelling approaches give small range of optimal air channels or system aspect ratios.

3. When a control algorithm is used to modulate the fan and optimize the coupled BIPV/T-HVAC operation, the particular system features, as well as local environmental effects can be taken into consideration by a combination of on-site system monitoring with key sensors, physics-based modelling and calibration of the convective correlations based on the monitored data. This is similar to the thermal models by King et al. (2004) and Faiman (2008) for the evaluation of PV temperatures in PV plants.

2.8 Key performance indicators (KPI)

The establishment of KPI's is essential for the characterization and comparison of different PV/T and BIPV/T technologies. KPI's developed for this purpose should be distinguished from the ones relevant to the overall system performance as integrated with the building envelope and HVAC system, and should convey the necessary information for comparison, including the electrical and thermal yield, as well as temperatures of the various parts of the system, depending on a set (or given range) of reference conditions.

There have been several approaches for the establishment of a single overall performance metric that can be used for the comparison of different system configurations. However, given the different thermoelectric value of electricity and heat, the development of a meaningful combined metric is a difficult task. Some of the most common approaches are the following

Combined electrical and thermal performance

One of the most common single metrics used is the combined electrical and thermal efficiency, defined as the added electrical and thermal efficiencies of the system (N. Aste et al., 2017; Bombarda et al., 2016):

$$\eta_{tot} = \eta_{el} + \eta_{th} \tag{2.18}$$

This approach, however, assigns the same value for the electrical and thermal energy, which can be misleading regarding the actual usable energy delivered by the system.

Equivalent thermal energy and primary energy savings (PES) efficiency

Bambara et al. (2011) proposed the term "equivalent thermal efficiency" which converts the electrical output of a hybrid system based on the coefficient of performance (COP) of a conventional heat pump and adds it to the thermal output of the system:

$$\eta_{th\_equivallent} = {}^{\eta_{el}}/_{COP} + \eta_{th} \tag{2.19}$$

Similarly, other studies consider the efficiency of electrical generation of a conventional power plant (N. Aste et al., 2017; Farshchimonfared et al., 2015), η_{power}, to define the total system efficiency as:

$$\eta_{tot} = {}^{\eta_{el}}/_{\eta_{power}} + \eta_{th} \tag{2.20}$$

Both approaches, however, are highly case specific and cannot be generalized. The former depends upon the HVAC integration and the latter upon the power generation technology used on a national level, while none considers the usable thermal yield delivered by the system.

Another approach aiming to introduce qualitative criteria and take into account the coolant outlet temperature is the exergy method (N. Aste et al., 2017; Bombarda et al., 2016; Farshchimonfared et al., 2015). This method evaluates the overall exergetic output of the system as the amount of thermal output that can be converted to work in addition to the electrical generation and the exergetic efficiency defined as follows:

$$\varepsilon_{tot} = \frac{q\left(1 - {}^{T_{amb}}/_{T_{out}}\right) + P_{elec}}{G} \tag{2.21}$$

However, studies have argued that for PV/T and BIPV/T low temperature applications, conversion to work is an irrelevant process (Farshchimonfared et al., 2015).

It may, therefore, be more convenient to maintain the distinction between the electrical and thermal performance for the purpose of characterising and comparison of different PV/T and BIPV/T types since these can then be used to assess the overall system performance for a specific application. That being said, there is room for improvement of the already established metrics to provide more practical information.

As far as the electrical yield is concerned, by evaluating the flow/pressure drop correlation for a given system design and deducting the required fan power from the total power yield under the established reference conditions and flow rates (per collector area) that cover a range of potential BIPV/T applications, the net energy yield/efficiency can be evaluated.

As far as the thermal efficiency is concerned, Bombarda et al. (2016) proposed a modified definition by subtracting the PV generation from the available incident radiation, namely:

$$\eta_{th}^{*} = {}^{\eta_{th}}/_{(1-\eta_{el})} \tag{2.22}$$

This approach eliminates the effect of different PV module types and power outputs when comparing different PV/T and BIPV/T samples.

Furthermore, this paper suggests that these performance metrics, including channel convective coefficients should be provided as a function of the operating conditions (environmental conditions, flow rate) in order to be more useful from a system design perspective and operation, in addition to the system comparison. Such an approach was adopted for the evaluation of channel convective coefficients for a double-skin façade STPV thermal system, implementing the environmental conditions as a new dimensionless number when evaluating the Nusselt number (Ioannidis et al., 2020).

Finally, overall system performance and financial indicators should be studied in detail focusing on the state of the art of BIPV/T thermal applications. A review of existing performance metrics for overall system performance can be found in (Wang et al., 2017).

2.9 Research opportunities

The following are the major research needs that have been identified by the literature review and addressed in the present thesis:

- **BIPV/T system design and implementation of existing building practices.** As discussed previously, there is a lack of design standardization and/or best practice guides for BIPV/T systems. As a result, the majority of realized systems are custom designs with significant initial cost. Further research is required in the system design from the architectural, structural, and building envelope perspective and more specifically:
    - Investigation of design solutions for both new buildings and retrofits, which adhere to commonly used building practices (i.e., curtain wall, wood/masonry structures etc.), which can lead to design standardization and simplification of the construction process.
    - Incorporation of modularity, prefabrication and the plug-and-play concept that can further simplify the construction process and quality, facilitate easier system maintenance and bring down fabrication costs.

- **Modelling of wind effects and channel convection.** There is no consensus on which expression best describes either case of convective heat transfer. The choice of expressions both for wind-driven and channel convection highly depends on the similarity of the studied system and the operating conditions to the ones for which the expressions were originally developed, and the expert knowledge of the engineer. However, for the case of BIPV/T systems this can be a complex issue, since the studies on convective phenomena have primarily focused on the channel Nu, with limited investigation of the wind effects.

  The significant variance among expressions developed for the same system but tested under different conditions, indicates the importance of the boundary conditions of the system. These boundary conditions are in no form included in the evaluation of convective heat transfer coefficients in existing expressions; and

- **Development of BIPV/T characterization procedure.** Standardization of the experimental process and characterization for PV/T and BIPV/T systems, as well as modelling can lead to improved confidence in the systems performance. The models developed can be implemented in widely used building simulation programs, which can then be used for extensive studies of BIPV/T systems for different thermal applications, archetype buildings and climates.

Chapter 3: BIPV/T Curtain Wall Systems: Design, Development and Testing

3.1 Introduction

This chapter presents the design, development, and experimental testing of a BIPV/T curtain wall prototype. The purpose of this part of the thesis was to address the lack of design standardization in BIPV/T systems by proposing a BIPV/T prototype in a modular form with the prospect of prefabrication, taking into consideration architectural and building envelope requirements, but also with comparable electrical and thermal performance to that of stand-alone PV/T systems. This design concept was successfully implemented as a roof BIPV/T application for the 2018 Solar Decathlon competition in China.

Furthermore, thermal enhancement methods suitable for BIPV/T systems such as multiple-inlets and a flow deflector were implemented to enhance the thermal performance of the prototype. These were studied experimentally in an indoor solar simulator facility for different configurations including varying flow and PV transparency. Furthermore, the convective heat transfer phenomena have been evaluated and compared to other studies in literature.

Test results showed a thermal efficiency of up to 33%. A multiple-inlet configuration assisted by a flow deflector behind the PV panel was found to enhance the thermal performance by up to 16% and reduced the peak PV temperatures by 3.5°C, with a marginal increase in the electrical efficiency. The BIPV/T curtain wall prototype provides a foundation for air-based BIPV/T design standardization and incorporation of common building practices.

3.2 Methodology

The following section describes the BIPV/T curtain wall concept development, the design considerations and thermal enhancements, and finally the experimental procedure that was carried out at an indoor solar simulator facility. The experimental data were used to assess the overall electrical and thermal performance of the prototype and investigate the effectiveness of the implemented thermal enhancements. All testing configurations considered were compared in terms of thermal and electrical efficiency, and maximum PV temperatures. Finally, the Nusselt numbers (Nu) of the air gap or air channel at the PV interface, the insulation and the average channel Nu were evaluated. They were then compared to ones derived from expressions commonly used in PV/T and BIPV/T literature, based on the review study by Rounis et al., (2021) as well as from expressions developed specifically for BIPV/T systems for single inlet configurations (Candanedo et al., 2011) and for the multiple-inlet configurations (Yang & Athienitis, 2015b). The applicability of said expressions was subsequently discussed.

[2] Presented in: Rounis, E. D., Athienitis, A. K., & Stathopoulos, T. (2021). BIPV / T curtain wall systems: Design , development and testing. Journal of Building Engineering, 42(July), 103019.

3.2.1 Overall concept and design

Figure 3.1 presents the overall concept of a BIPV/T curtain wall, as well as a breakdown of its main components.

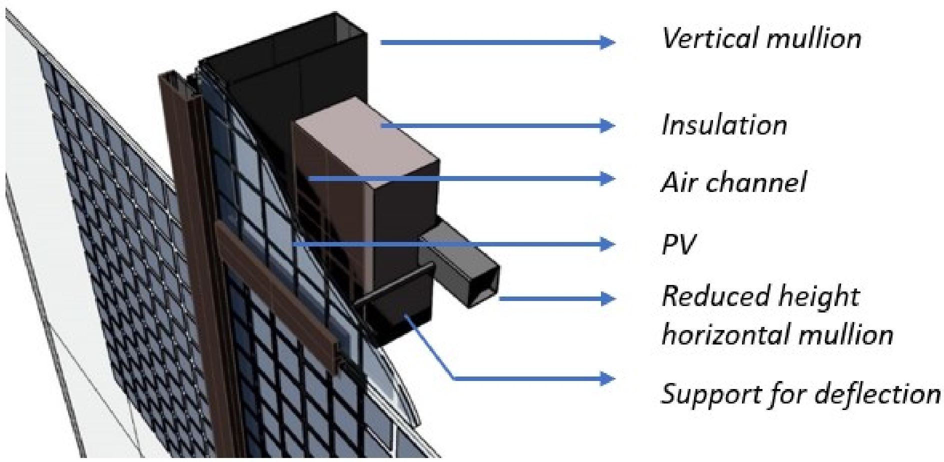

Figure 3. 1: Rendering of the BIPV/T curtain wall concept. The curtain wall design is modified to facilitate an air channel, while frameless PV modules replace the glazing section.

The experimental BIPV/T curtain wall prototype was conceived and developed as a part of a larger system (Fig. 3.2). Its purpose was to serve as a means of acquiring design insight for fully integrated, PV/T systems, as well as investigating and analyzing results for the modelling of the performance of different system configurations and thermal enhancements.

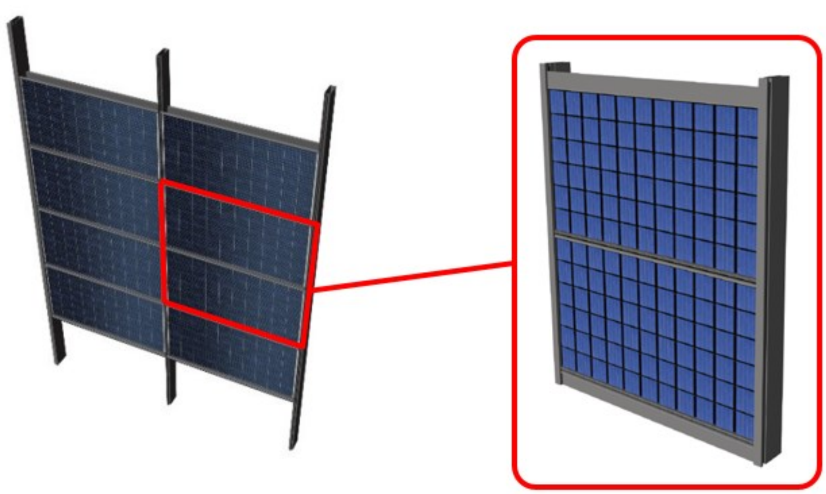

Figure 3. 2: Conceptual rendering of a BIPV/T curtain wall system (left) and rendering of the experimental prototype of the present study (right).

The design of the prototype was carried out within a frame of considerations, namely, architectural, structural and building envelope functions, while also aiming for the facilitation of a modular design. Modularity and the plug-and-play concept have been identified by the IEA Task 56 as key approaches for the wider implementation and cost reduction of active solar envelope systems (IEA SHC TASK 56, 2020).

In summary, the main design considerations were the following:

- Architectural/Structural: The goal was to adopt a common building technique and modify it accordingly in order to facilitate the BIPV/T concept. The final result would be a system that can be seamlessly integrated, with high aesthetic value and with the potential of modularization and prefabrication. The framing system was built with commercial mullion extrusions.

- Building envelope: The prototype had to fulfill building envelope function requirements in terms of air, moisture and heat transfer, including the necessary rainscreen, water shedding, air and vapor barrier, and insulation layers. This is further discussed in 3.2.1.2.

Electrical and thermal performance should be enhanced by means suitable for building integration, as discussed in 3.2.1.3.

3.2.1.1 Framing

The prototype's frame consists of two side vertical mullions, a middle vertical mullion, a bottom and a top transom. Fig. 3.3 demonstrates an elevation view including inlet and framing details of the prototype.

The cross-sectional area of the air channel is 0.19 m^2. A 45 mm x 45 mm middle structural framing member is installed along the channel in order to counter the PV modules deflection, which creates a blockage of almost 1% in the cross-sectional area. The depth of the air channel is 95 mm and its hydraulic diameter 0.18 m. The total length of the flow path is 2.09 m.

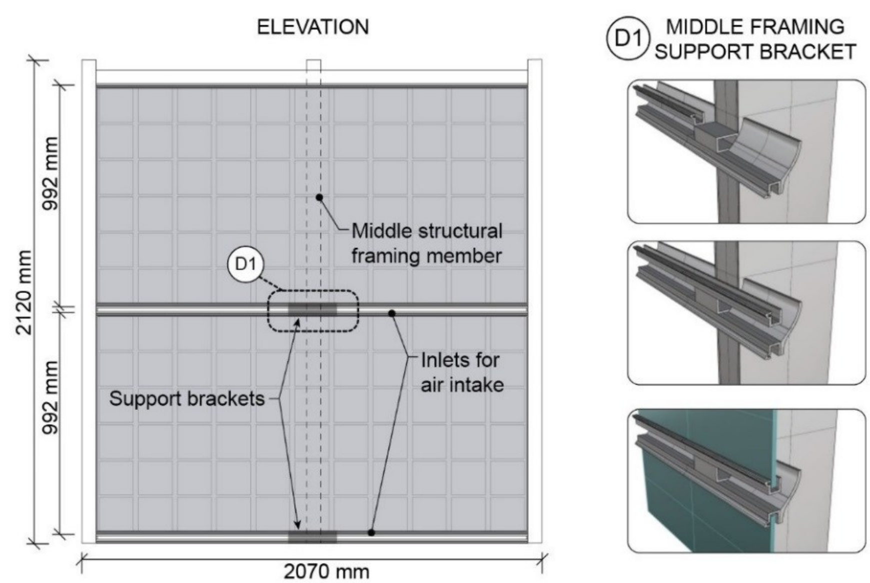

Figure 3. 3: BIPV/T curtain wall prototype elevation and details. D1 illustrates the facilitation of an additional air intake and the support of the frameless PV modules.

3.2.1.2 Building envelope considerations

Figure 3.4 presents a cross section of the prototype and demonstrates how it manages air, moisture and heat transfer, as well as water penetration. The frameless PV and the curtain wall frame form a rain-screen surface. At the level of the inlet, a flow deflector prevents rain penetration in the air channel. For the case of a single-inlet system, a shallow mullion would provide horizontal support for the top and bottom PV, while maintaining the continuity of the air channel.

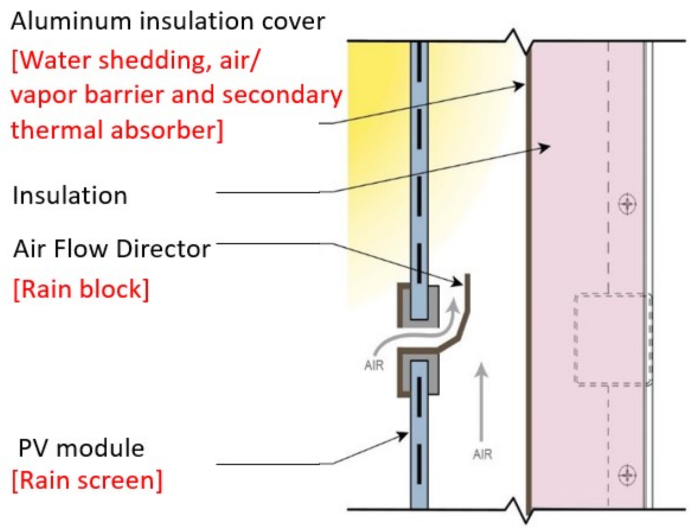

Figure 3. 4: Building envelope function of the BIPV/T curtain wall.

On the rear side, 51 mm (2 in) of extruded polystyrene (XPS) insulation was used, sandwiched between two aluminum sheets. These sheets have the role of air and moisture barrier, similar to the spandrel section back-pan of a curtain wall, as well as of the water resistive surface for any amount of water that penetrates the PV layer, especially for the multiple-inlet configuration. Additionally, the front aluminum sheet (interfacing with the air channel) acts as a secondary absorber for the part of solar irradiation that is transmitted through the semi-transparent PV. This sheet was painted black to increase its absorptance. Adhesive insulation (tape) was used at the side walls of the air channel, namely the mullion interior surface, in order to minimize lateral heat losses. Overall, a near adiabatic boundary was formed for the sides and rear of the air channel. Further details regarding the system's building envelope function can be found in Kruglov et al., (2017).

3.2.1.3 Thermal enhancements

Three main ways to enhance the thermal performance of the prototype were considered, namely the use of transparent versus opaque PV modules, multiple inlets and use of a flow deflector. These techniques were chosen based on their simplicity, efficiency - as reported in literature - and ease of application for building integrated systems.

Semi-transparent PV and secondary absorber

The use of semi-transparent PV (STPV) instead of opaque PV with the same packing factor (PF) has been found to increase both the electrical and thermal performance of PV/T systems, due to the reduced radiation absorbed on the spacing between the PV cells and therefore lower temperature at the PV layer, and the increased transmitted radiation to the rear surface (Guiavarch & Peuportier, 2006; Yang & Athienitis, 2015b). Increasing the PV module transparency by reducing the number of opaque cells diminishes the electrical output but increases the heat recovery from the surface opposite the PV (Sandnes & Rekstad, 2002; Vats et al., 2012).

Two sets of glass-on-glass STPV modules (Fig. 3.5) were custom fabricated, with transparencies of 20% (66 cells) and 12% (72 cells) and respective nominal module electrical efficiencies at standard testing conditions (STC) of 14.2 % and 15.5%. The dimensions of both PV module types are 1.968 m x 0.992 m x 0.0058 m. These were installed in a landscape orientation (see Fig. 3.3) to allow for the facilitation of a second air intake and take better advantage of the additional thermal entrance effects. The PV modules were fixed to the side and top mullions with pressure plates. The central longitudinal mullion (Fig. 3.3) provided support against deflection, as well as two extra point supports for the dead weight of the modules, essential for the vertical placement of the specimen.

The use of STPV was supplemented by the dark absorbing surface of the top insulation cover which interfaces with the air channel (see Fig. 3.4), allowing for better absorption of the transmitted radiation.

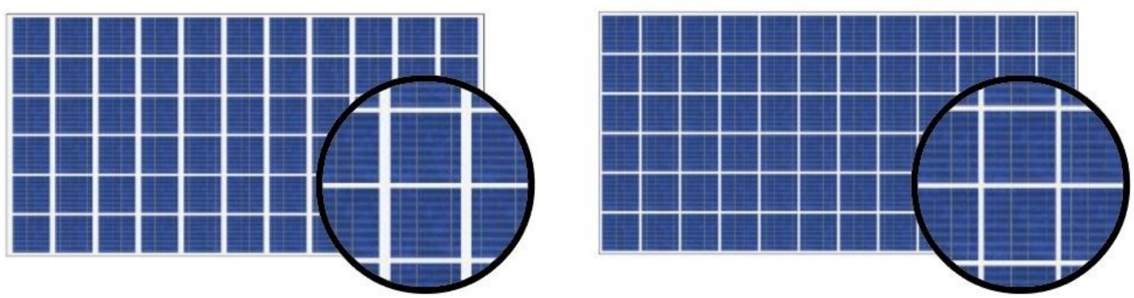

Figure 3. 5: Semi-transparent PV modules used for the prototype's testing with 20% transparency (left) and 12% transparency (right).

Multiple inlets and flow deflector

The introduction of additional air intakes on a BIPV/T system has been found to improve both its thermal and electrical performance by disrupting the thermal boundary layer formed on the PV surface and introducing additional entrance effects that increase heat extraction along the flow path (Athienitis et al., 2018; Rounis et al., 2016; Yang & Athienitis, 2015b). Such a technique has the potential to maintain near uniform PV temperatures throughout the BIPV/T channel by tuning the flow rates of the multiple inlets (Athienitis et al., 2018; Rounis et al., 2016).

For the BIPV/T curtain wall prototype this technique was facilitated by creating a 30 mm space between the PV modules which was maintained by a point support/separator between the modules. Additionally, a flow deflector extrusion was installed on the top part of the PV of the bottom section of the BIPV/T prototype (Fig. 3.6). Its purpose was to serve as a blockage to rain water penetration and as a means to direct the air entering from the second inlet towards the surface of the PV of the upper section of the prototype. The effect of this flow deflector was also investigated during the experimental procedure and it was found that it had a considerable impact on the thermal and electrical performance of the prototype, as compared to the double-inlet configuration without the flow deflector.

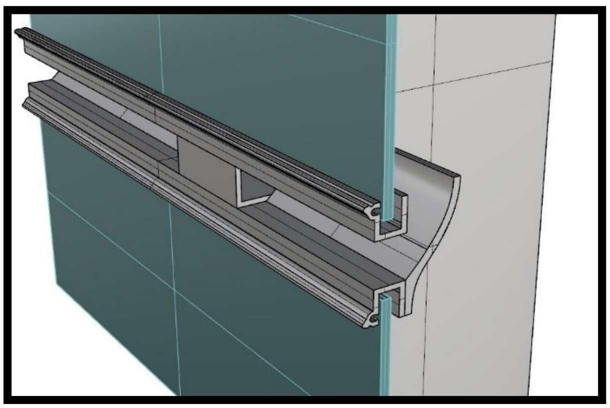

Figure 3. 6: Flow deflector extrusion placed on the additional inlet to prevent rain penetration and direct the cool air towards the PV surface.

As mentioned earlier, the prototype was not considered as stand-alone system, rather as part of a larger BIPV/T installation. As such, the channel depth was designed so that it could facilitate the addition of the flow deflector without creating severe blockage to the available cross-sectional area, with resulting high frictional pressure losses, considering a flow length for one to two storeys. A depth of 95 mm was selected as a compromise between imposing less than 70% blockage to the channel flow of the bottom section and achieving average channel velocities of up to 1 m/s, given the capacity of the air collector unit that was used for the experimental procedure.

3.2.1.4 Full-scale application

Although developed primarily for façade applications, the BIPV/T curtain wall concept was successfully incorporated for the BIPV/T roof of the DPD house by Team Montreal in the 2018 Solar Decathlon competition in China (Dumoulin et al., 2021; Rounis et al., 2018). Apart from the seamless integration, the curtain wall technique, allowed for the incorporation of an integrated skylight, as seen in Fig. 3.7. This extended the multi-functionality of the BIPV/T to the daylighting aspect as well.

Figure 3. 7: Roof BIPV/T of the Deep Performance Dwelling with integrated skylight (highlighted in yellow) (Dumoulin et al., 2021).

3.2.2 Experimental setup

The prototype was tested at the Paul Fazio Solar Simulator and Environmental Chamber facility of Concordia University in Montreal. The lamp field of the solar simulator consists of 8 metal halide lamps which can produce an irradiance intensity between 500 and 1200 W/m^2, with a uniformity of up to 97% (depending on the required coverage area and lamp placement). The position and intensity of each lamp can be individually adjusted in order to achieve the required uniformity. The lamps create a spectral distribution that complies with standards ISO 9806 and EN 12975 (Kapsis et al., 2016).

In front of the lamp field, a ventilated artificial sky maintains a surface temperature of 13ºC ±2ºC in order to remove the effect of the infrared radiation generated by the lamps, as well as simulate the sky temperature. This is an important component, as previous studies have shown that the blackbody temperature of the sky is not properly represented by hot lighting devices in indoors facilities (Mei et al., 2003).

The test platform is located beneath the lamp field, whereupon the specimens are placed. Both the platform and the lamp field can rotate between 0º (horizontal placement) and 90º (vertical placement) to simulate low-sloped and pitched roofs, as well as vertical facades. The room where the solar simulator is located is maintained at 21ºC ±1ºC (and 30% ±5% relative humidity). A cooling unit is used to remove the heat generated by the lamps from the room.

A linear, variable-speed fan is used to emulate wind-driven convection. The height of the fan relative to the platform can be adjusted according to the height of the specimen and it blows ambient air parallel to the specimen with up to 14 m/s maximum velocity. A pyranometer and an anemometer mounted on a traverse system above the testing area measure the irradiation and wind speed respectively, with a minimum measurement spacing of 15 cm. Figure 3.8 shows the solar simulator test setup of the prototype.

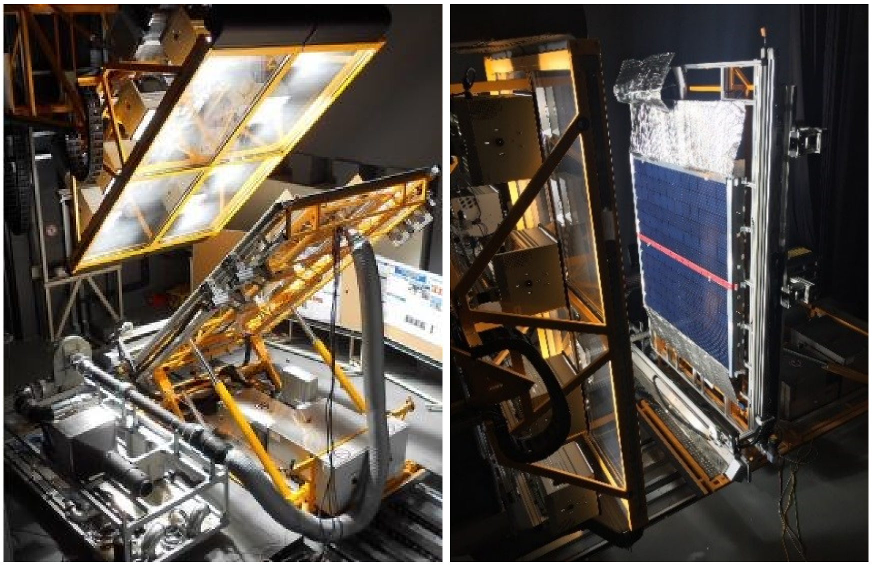

Figure 3. 8: The experimental setup of the prototype at the solar simulator facility.

3.2.2.1 Temperature measurements

A total of 85 T-type thermocouples and 3 RTD probes were used to monitor the temperature on the insulation/secondary absorber, in the air channel and on the top part of the PV modules where the highest temperatures were expected. The PV temperatures were also used to calibrate infra-red images taken during the measurements, which provided more detailed temperature distributions on the surface of PV modules. Additional thermocouples were used to monitor the inner and outer surface temperatures of the frame, as well as the air film temperatures over the PV surface to account for the effect of wind.

Two RTD sensors were placed on the main outlets of the manifold which collected the preheated air, and one was used for the room ambient temperature. Four measurement lines were formed along the flow path, as shown in Fig. 3.9, to evaluate the temperature distribution both along and across the flow path. On the upper half section of the prototype, more detailed measurements were taken, with thermocouples placed at different heights, in order to investigate the mixing of the two streams (from the bottom and top inlet).

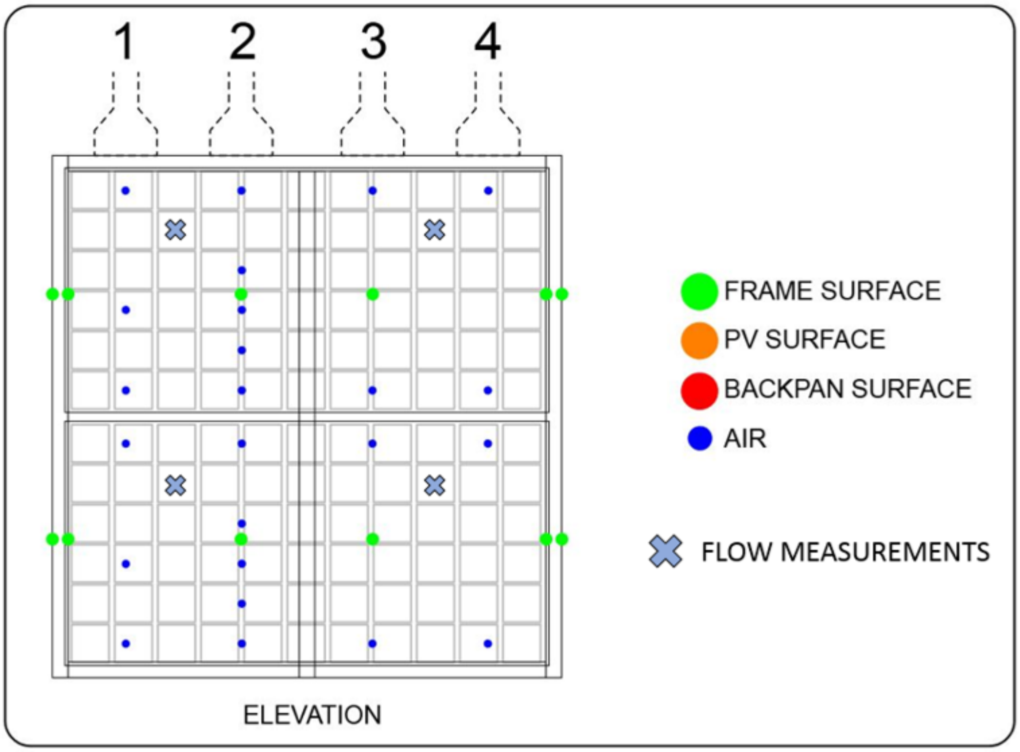

Figure 3. 9: Elevation and view of the thermocouple placement and location points for flow measurements.

3.2.2.2 Manifold and flow measurements

Due to the large width of the prototype and in order to ensure uniform flow within the air channel (and avoid flow convergence), four outlets of 25 cm x 5 cm were made by cutting out of the top mullion, upon which a custom manifold was attached. The manifold (Fig. 3.10) consisted of a central "T" split with two branches on each end, with four resulting branches funneling into the main outlet. Flow measurements were carried out at the locations indicated in Fig. 3.9 with a TSI hotwire handheld anemometer to verify the uniformity of the flow across the collector's channel. Measurements showed a variance of less than 10%, indicating a rather uniform flow. The manifold outlet was connected to the Air Collector Test Stand of the solar simulator, which allows the mass flow rate to be set manually and measured by an orifice flow meter which uses three differential pressure transducers of different ranges.

Figure 3. 10: The custom four-branch manifold used in the experiments. One quarter of the total flow rate was drawn from each outlet.

3.2.2.3 Cases studied

The prototype testing focused on the effect of the following on its electrical and thermal performance, and PV temperatures:

- The use of one or multiple inlets (one for each PV module) for the intake of fresh air
- The use of a flow deflector for the double-inlet configuration
- The effect of different transparency (with varying packing factor) of the PV modules

For each PV set (20% and 12% transparency), three configurations were tested, namely, single-inlet, double-inlet and double-inlet with use of a flow deflector. These will be referred to as system I, II and III for the remainder of this study and are summarized in Table 3.1. Each system was tested under varying irradiation (842 W/m^2, 989 W/m^2, 1109 W/m^2) and mass flow rates (0.028 kg/s.m^2, 0.034 kg/s.m^2 and 0.041 kg/s.m^2, and respective Reynolds number range between 5957-8816). All tests were carried out under ambient temperature between 21ºC to 22ºC and a constant average wind velocity of 1.1 m/s.

The thermal efficiency of the collector was calculated as follows:

$$\eta_{th} = \frac{q}{A_c G} \tag{3.1}$$

where Q_{air} is the heat recovered, defined as:

$$q = \dot{m} C_p \Delta T \tag{3.2}$$

G is the irradiance (W/m^2) and A_c the gross surface area of the collector (PV modules and frame), equal to 4.39 m^2.

The electrical efficiency of the assembly was calculated as the summation of the power output of the two PV modules (P_{PV_1} and P_{PV_2}) over the irradiance on the gross collector area.

$$\eta_{PV} = \frac{P_{PV\_1} + P_{PV\_2}}{A_c G} \tag{3.3}$$

Table 3. 1: BIPV/T testing configurations (red color indicates the inlets and purple the flow deflector)

20% transparency (66-cell) STPV modules		
System I (Single-inlet):	*System II (Double-inlet):*	*System III (Double-inlet, air deflector):*
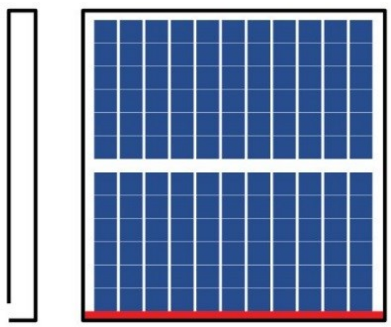	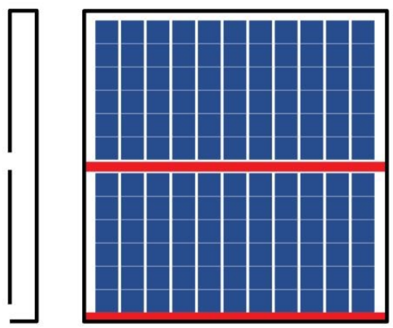	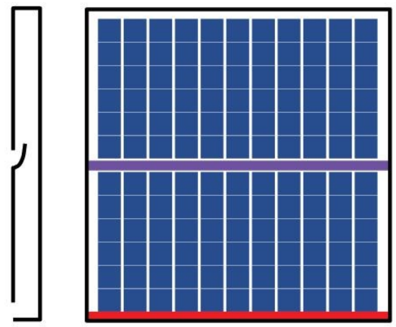
12% transparency (72-cell) STPV modules		
Single-inlet:	Double-inlet:	Double-inlet, air deflector:
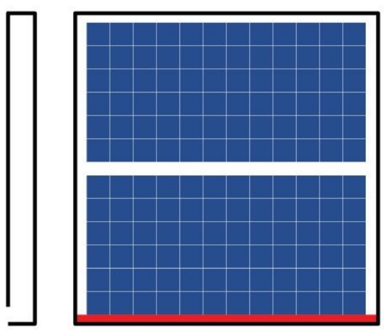	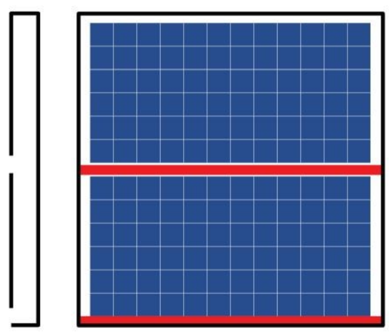	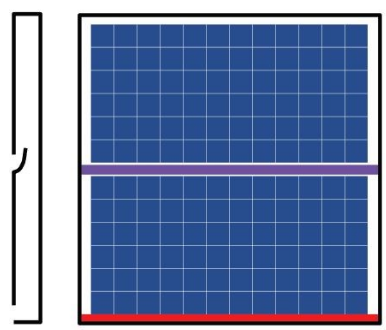

3.2.3 Recorded Nu and comparison to commonly used expressions

The channel convective heat transfer coefficient (CHTC) and respective Nusselt number (Nu) were evaluated for the bottom and top section of each system configuration from Table 3.1, as shown in Figure 3.11, as well as for the whole collector, by performing an energy balance for each respective section (see Appendix B). The CHTC and Nu calculations were performed for the following:

- The interface between the PV and the air-channel (PV side)
- The interface between the insulation and the air-channel (insulation side)

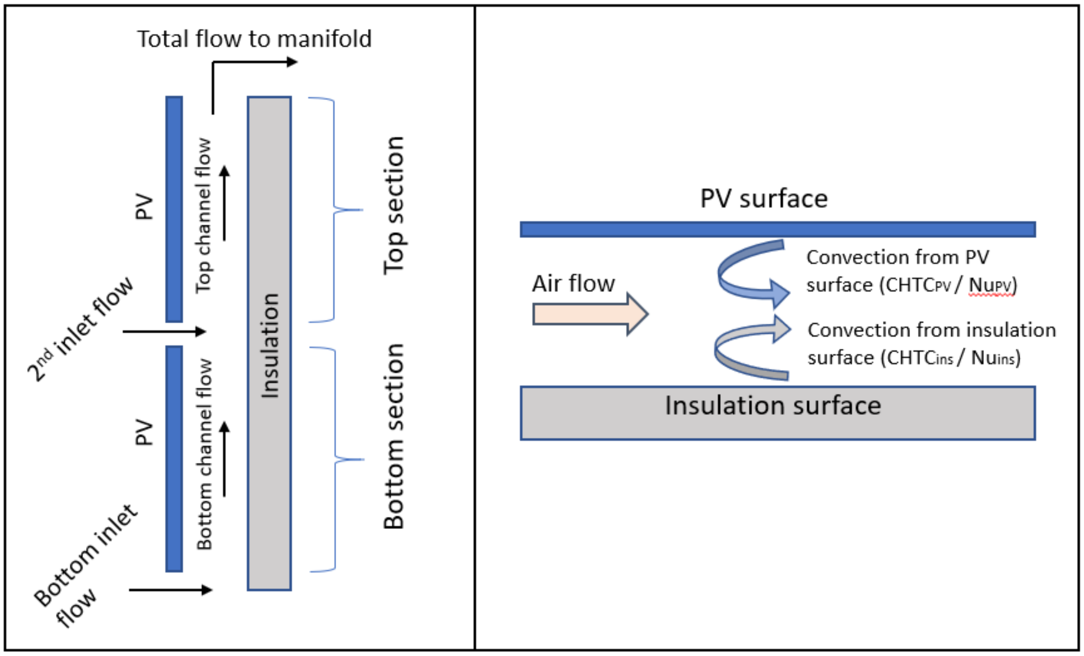

Figure 3. 11: Schematic of inlet and channel flows for the bottom and top section and of the CHTC and Nu for the PV and insulation surface.

Additionally, an overall (combined) CHTC and Nu was evaluated for each system type and section. This was done to compare with other Nu expressions from the literature, which have been extensively used in PV/T modelling, and which are used interchangeably for both interfaces. The overall CHTC and respective Nu were calculated according to equations 3.4 and 3.5.

$$\dot{m}C_p\Delta T = CHTC \cdot (T_{PV} + T_{ins} - 2\overline{T_{air}}) \cdot A \tag{3.4}$$

$$Nu = CHTC \cdot D_h/k \tag{3.5}$$

where CHTC is the overall (combined) convective heat transfer coefficient for the PV and insulation side, T_{PV}, T_{ins} and T_{air}, the average temperature of the PV, insulation and air of the respective section, D_h is the hydraulic diameter of the air channel and k the conductivity of air (evaluated based on the average air temperature of the respective section).

The recorded Nu were then compared to ones derived from expressions that have been developed for heat transfer in duct flow (Dittus, 1985; Tan & Charters, 1969, 1970) and have been extensively used in PV/T and BIPV/T modelling literature, for a wide range of PV/T system types. Additionally, expressions developed specifically for BIPV/T systems by Candanedo et al. (2011) for single inlet configurations and (Yang & Athienitis, 2015a) for the multiple-inlet configurations were also investigated. The agreement of the considered expressions with the experimental findings and their conditional applicability are discussed in section 3.3.3.

3.3 Results

The following results demonstrate the air temperature rise, maximum PV temperatures as well as electrical and thermal efficiency values for the prototype tested under 842 W/m^2 solar irradiation on the cell surface with an approximate uniformity of 94%, an ambient air temperature of 21°C ±1°C, and an average exterior wind speed of 1.1 m/s. This set of conditions is similar to the nominal operating cell temperature (NOCT) conditions, used to evaluate PV cell temperatures. The prototype showed similar behavior for the other two solar irradiation values (989 W/m^2, and 1109 W/m^2, respectively), which were used for model verification purposes that will be part of a future study. Tables 3.2 through 3.5 demonstrate the results for thermal and electrical efficiency, air temperature rise and maximum PV temperatures, for the two types of STPV modules used.

Table 3. 2: Thermal efficiency of the prototype for the different configurations

Configuration	**66-cell (20% transparency)**			**72-cell (12% transparency)**		
Flow rates (kg/s.m^2)	*0.028*	*0.034*	*0.041*	*0.028*	*0.034*	*0.041*
Single inlet (System I)	23.6%	24.7%	27.3%	21.4%	23.6%	26.1%
M-inlet (System II)	23.4%	28.4%	31.9%	22.6%	26.3%	29.8%
M-inlet, air deflector (System III)	25.7%	29.2%	32.3%	24.5%	27.8%	30.3%

Table 3. 3: Electrical efficiency of the prototype for the different configurations

Configuration	**66-cell (20% transparency)**			**72-cell (12% transparency)**		
Flow rates (kg/s.m^2)	*0.028*	*0.034*	*0.041*	*0.028*	*0.034*	*0.041*
Single inlet (System I)	11.2 %	11.4 %	11.4 %	12.6 %	12.7 %	12.7 %
M-inlet (System II)	11.3 %	11.4 %	11.5 %	12.6 %	12.7 %	12.7 %
M-inlet, air deflector (System III)	11.4 %	11.4 %	11.5 %	12.7 %	12.7 %	12.8 %

Table 3. 4: Air temperature rise in the air channel of the prototype for the different configurations

Configuration	66-cell (20% transparency)			72-cell (12% transparency)		
Flow rates (kg/s.m²)	*0.028*	*0.034*	*0.041*	*0.028*	*0.034*	*0.041*
Single inlet (System I)	6.9°C	6.6°C	6.0°C	7.1°C	6.3°C	5.8°C
M-inlet (System II)	7.8°C	7.6°C	7.1°C	7.5°C	7.0°C	6.6°C
M-inlet, air deflector (System III)	8.5°C	7.8°C	7.2°C	8.2°C	7.4°C	6.7°C

Table 3. 5: Maximum PV temperatures for the different configurations

Configuration	66-cell (20% transparency)			72-cell (12% transparency)		
Flow rates (kg/s.m²)	*0.028*	*0.034*	*0.041*	*0.028*	*0.034*	*0.041*
Single inlet (System I)	59.4°C	57.1°C	55.3°C	56.8°C	56.0°C	54.7°C
M-inlet (System II)	58.1°C	56.1°C	53.4°C	56.6°C	55.6°C	53.7°C
M-inlet, air deflector (System III)	55.6°C	54.3°C	52.1°C	55.4°C	54.2°C	53.0°C

3.3.1 Effect of multiple inlets and flow deflector

3.3.1.1 Thermal efficiency and air temperature rise

System III showed the highest thermal efficiency for all test configurations, followed by systems II and I. The double inlet system had 1.2% to 3.7% higher thermal efficiency (or 5.5% to 14% relative increase) compared to the reference single-inlet (System I) and when a flow deflector was added the thermal efficiency was 3.1% to 4.2% higher (or 14.6% to 16% relative increase). The latter can be attributed to the fact that the flow from the second air intake is directed towards the surface of the PV, which is subjected to a cooler air stream and thus the heat exchange with the hot PV surface is increased.

The temperature rise inside the air channel (or temperature difference between inlet and outlet) followed the same pattern as the thermal efficiency, in that the highest temperature rise was achieved by the system III (6.7°C to 8.2°C, highest to lowest mass flow rate, 12% transparency), followed by system II (6.6°C to 7.5°C) and the lowest by system I (5.8°C to 7.1°C). With increasing irradiation levels, the temperature rise increased and was about 1 to 1.3°C higher for system III vs system I.

3.3.1.2 Maximum PV temperatures and electrical efficiency

System I had the highest peak PV temperatures, namely for the top row of cells of the top section PV module. System II had slightly lower peak PV temperatures and system III had the lowest. The PV of the first section for the single inlet configurations had slightly lower temperature than for the double-inlet, on average around 0.8ºC, due to the higher flow rate entering solely from the bottom opening. However, the peak PV temperature of the top section for the double-inlet was on average lower by 3˚C to 3.5˚C, indicating an important cooling effect introduced by the second inlet and the flow deflector, with only a small part of the total flow entering from the second inlet. Figure 3.12 shows an infra-red image of the PV surface temperatures for systems I and III. For system III, the temperatures of the top PV are considerably lower than for the single-inlet configuration.

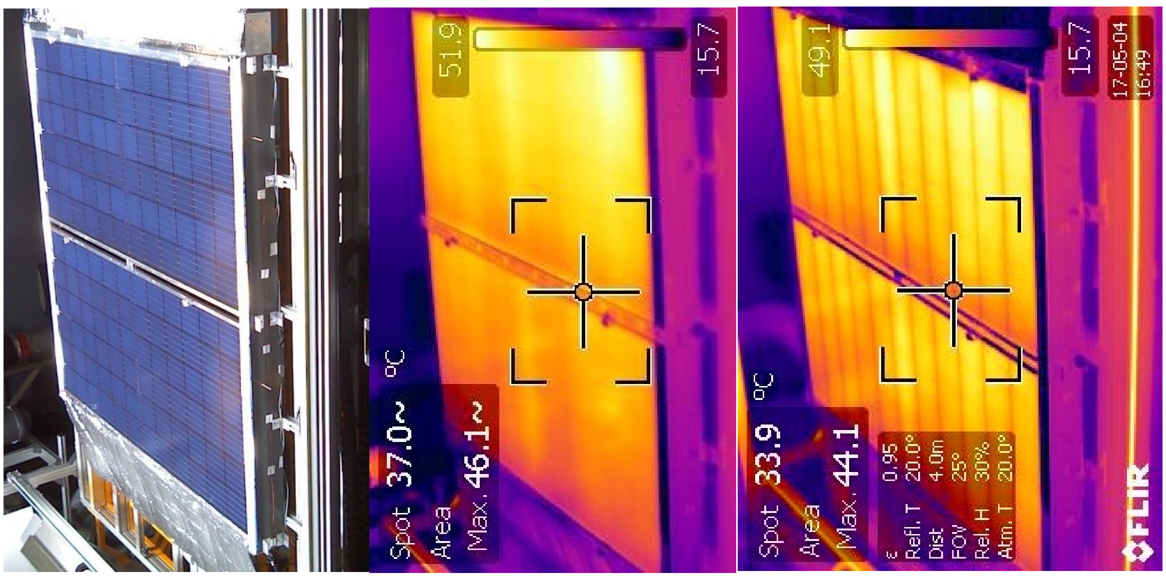

Figure 3. 12: IR imagery of the surface PV temperatures for system I (middle) and system III (right).

The aforementioned differences in PV temperatures were reflected in the electrical performance of the three systems with system III performing the best, although marginally. Figure 3.13 summarizes the electrical and thermal efficiencies and the peak PV temperatures for the three configurations (12% transparency, 0.041 kg/s.m^2).

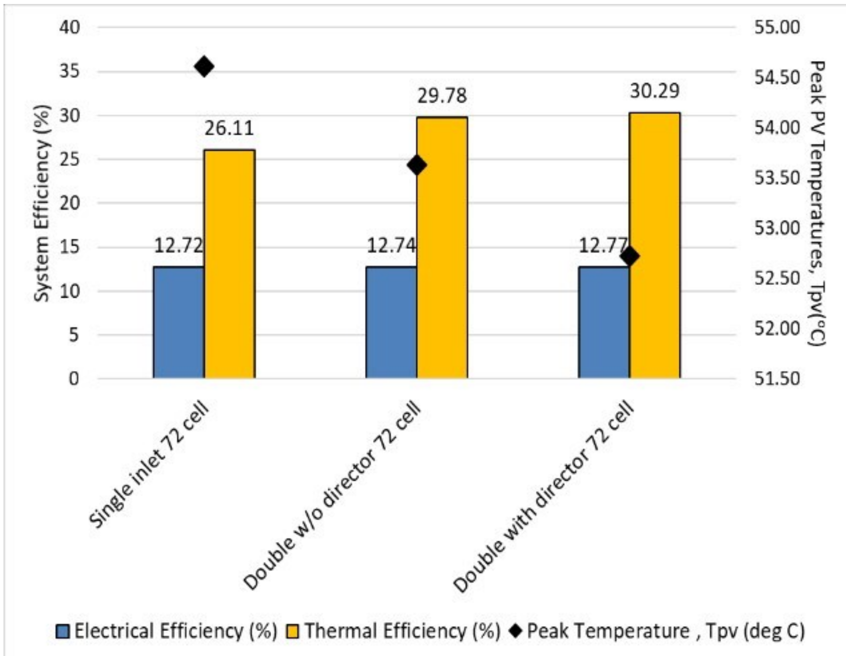

Figure 3. 13: Electrical efficiency, thermal efficiency and peak PV temperature for the three configurations of the 72-cell set, at 0.041 kg/s.m² total mass flow rate.

3.3.2 Effect of STPV transparency

The higher transparency PV modules (66-cell set) had 10% to 11% lower electrical output versus the 72-cell set, which was consistent in all tested configurations and flow rates, reflecting the corresponding difference of PV cell coverage (or packing factor). The higher amount of radiation transmitted to the back absorber resulted in a 5% to 10% higher thermal output and slightly higher outlet air temperature (up to 0.7ºC). The peak PV temperatures for the 72-cell set were higher by 0.6ºC to 3.6ºC, due to the higher radiation absorbed by a larger PV cell area. These results agree with previous investigations (Yang & Athienitis, 2014b, 2015a). The choice of packing factor in a real application would depend on the desired electrical and thermal output. Indicatively, Figure 3.14 demonstrates the electrical and thermal efficiencies of the two sets for all configurations at an air collection rate of 600 kg/hr (0.041 kg/s.m²).

The highest recorded $\Delta T_{inlet-outlet}$ for system III equipped with the modules of 20% transparency was between 9.2ºC to 11.1ºC (for higher to lower mass flow rate respectively, irradiation of 1109 W/m²) – channel length of 2.09 m.

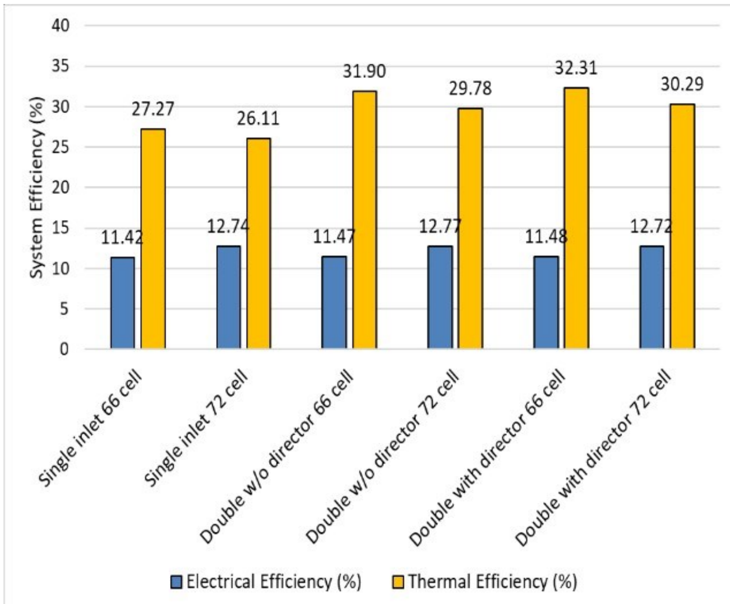

Figure 3. 14: Electrical and thermal efficiency for the single-inlet, double-inlet and double-inlet with installed flow deflector, for the 66-cell and 72-cell PV module sets.

It should be mentioned that other thermal enhancements such as the use of fins and a more conductive substrate for the PV modules could be employed to further increase the amount of recovered heat. Furthermore, the geometric features of the air channel, such as the channel height and/or the distance between the inlet and outlet, should be optimized accordingly given a specific thermal application (coupling with the HVAC) and flow rate range, taking into consideration the fan consumption.

3.3.3 Convective heat transfer and Nusselt number

3.3.3.1 Entire collector

Figures 3.15 through 3.17 demonstrate the collector average Nu of the PV side, the insulation side and the combined, plotted against the Reynolds number, for the three system configurations and compared to Nu expressions that have been widely used in PV/T and BIPV/T literature. The three lines on the lower section of each graph correspond to average Nu (for either side of the channel) that have been developed for heat transfer in duct flow (Dittus, 1985; Tan & Charters, 1969, 1970). The top lines are Nu expressions specifically developed for BIPV/T for the PV and the insulation side separately (Candanedo et al., 2011).

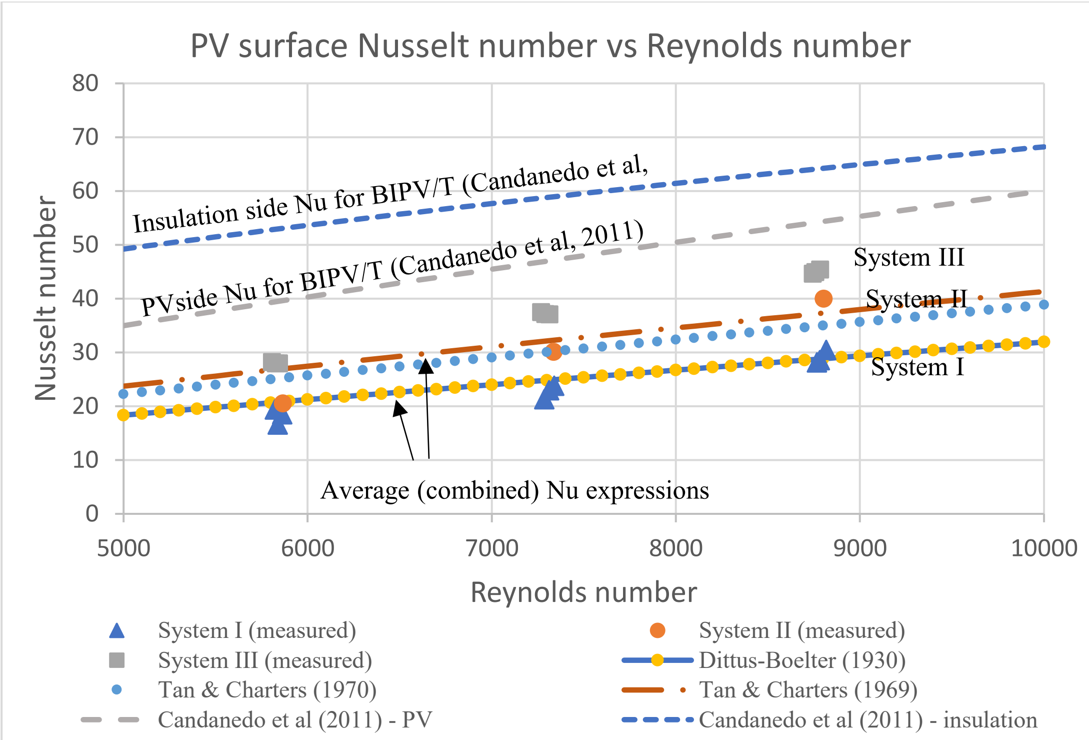

Figure 3. 15: PV side Nu plotted against the Re and compared with Nu expressions from literature.

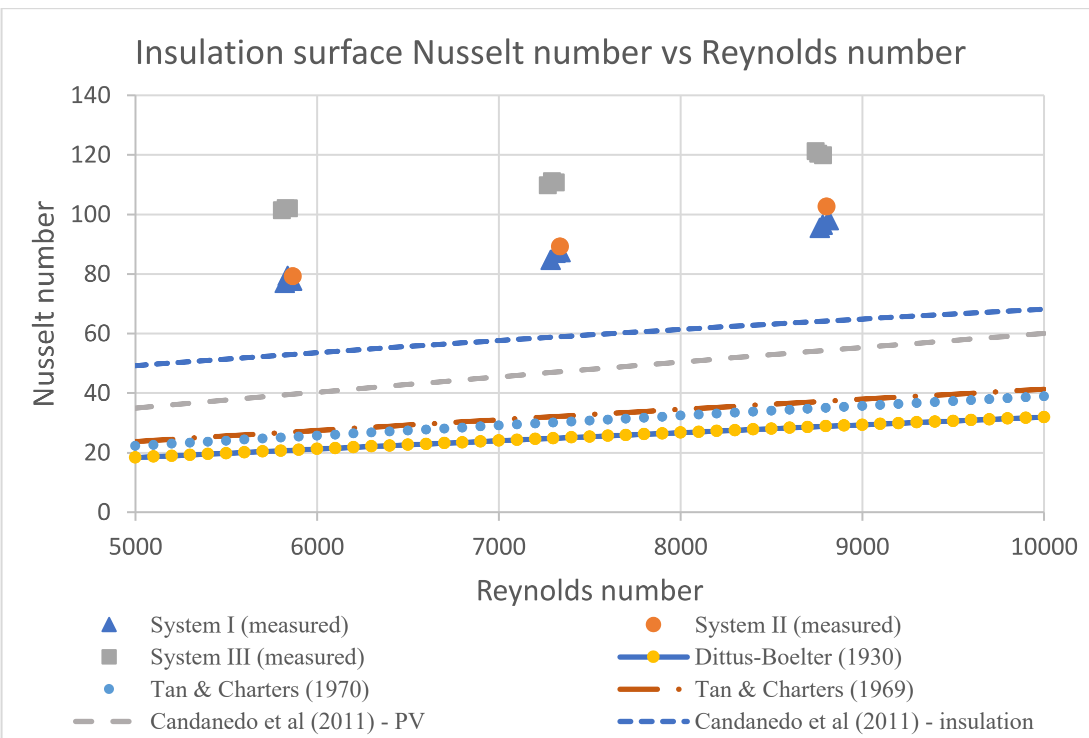

Figure 3. 16: Insulation side Nu plotted against the Re and compared with Nu expressions from literature.

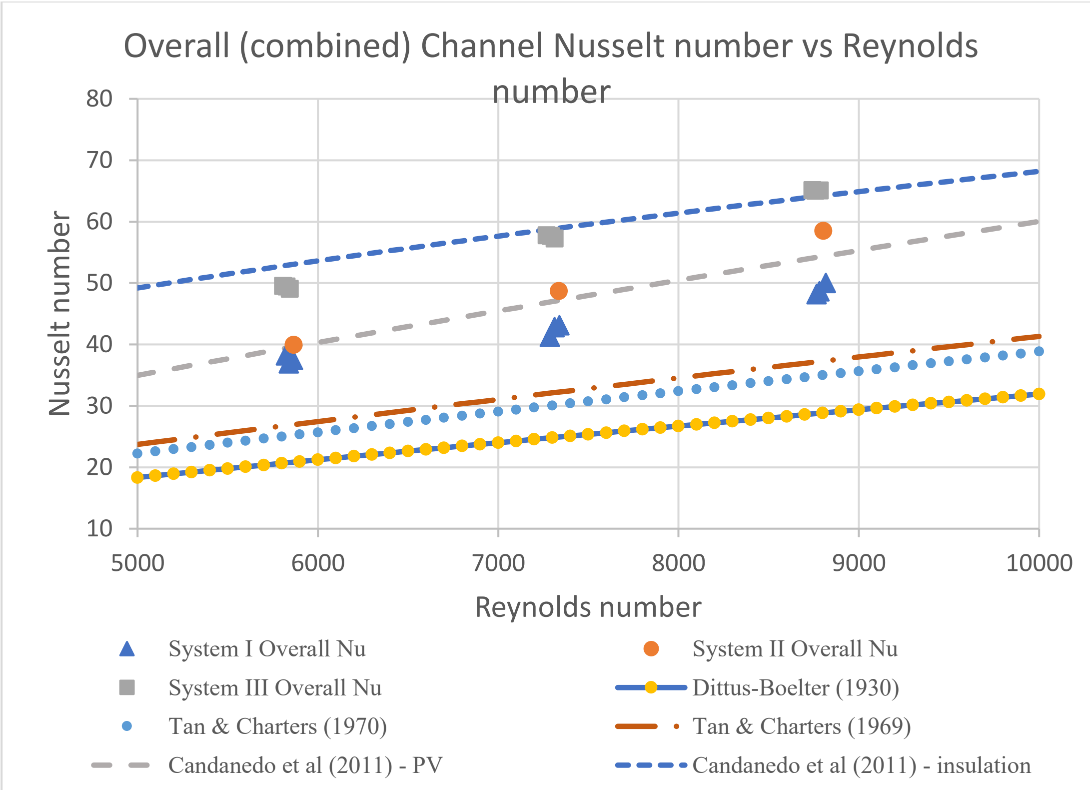

Figure 3. 17: Average Nu for the PV and insulation side of the air channel plotted against the Re and compared with Nu expressions from literature.

Some important observations can be summarized as follows:

- There is a significant asymmetry in the CHTC of the PV and the insulation side, with the latter being considerably higher. This asymmetry can be attributed to the different boundary conditions and the fact that the PV side is directly exposed to the environmental conditions. This further hints to the importance of the wind-driven convection and thermal losses.

- This asymmetry for the studied system is far greater than what is proposed by Candanedo et al. (2011).

- The Nu for the PV side seems to be in line with the average Nu expressions by Dittus, (19850 and Tan & Charters (1969, 1970). However, the monitored Nu for the insulation side far exceeds the predictions of all Nu expressions.

- In terms of combined Nu, the ones recorded for the double-inlet configurations were found closer to the predictions of the expressions developed for BIPV/T systems (Candanedo et al., 2011).

Table 3.6 summarizes the respective average convective heat transfer coefficient ranges (CHTC for the entire collector) for the PV side, the insulation side, as well as the combined CHTC for both sides, for the three studied system types.

Table 3. 6: Average CHTC for the three system types

	System I (single inlet)	System II (double inlet)	System III (double inlet with flow deflector)
PV	2.37-4.32	2.92-5.67	3.98-6.46
Insulation	11.01-13.89	11.24-14.56	14.54-17.32
Overall (Combined CHTC for PV and insulation side)	**5.27-7.09**	**5.67-8.30**	**7.00-9.31**

3.3.3.2 Bottom and top section

The same procedure was repeated for the double inlet configurations (Systems II and III), this time focusing on the bottom and top section of the collector. The Nu of the PV side of the two sections was compared to Nu numbers for the PV side by Yang & Athienitis (2015) which is the only known instance of Nu developed specifically for a double-inlet system (different for each section of the double-inlet system.

Figures 3.18 and 3.19 demonstrate the monitored values of Nu for the PV side for the bottom and top section respectively, compared to the predicted Nu according to the Nu expression by Yang & Athienitis (2015) for each respective section.

The measured Nu confirm two of the findings of the study by Young & Athienitis (2015):

- The Nu for the top (second) section of the double inlet system is enhanced compared to the bottom section

- The Nu for the bottom (first) section of both the single and double inlet systems lie within the same trendline. This is with the exception of System III which demonstrates an increased Nu for the Bottom section as well, which can be attributed to local acceleration phenomena instigated by the presence of the flow deflector.

Otherwise, the suggested expressions seem to overpredict the Nu and there is generally poor agreement with the measured values. It should be noted that the systems studied by Candanedo et al. (2011) and Yang & Athienitis (2015) and for which the correlations were developed had drastic differences in comparison to the present study's setup. Said test subjects were scaled versions of a wood-frame roof BIPV/T system (Chen et al., 2010), with channel cross section dimensions of 400 mm x 39 mm and with organic flexible PV pasted on metal roofing. The variations in the Nu, at least for the subjects tested in a solar simulator, can be attributed to a great extent to the different testing conditions (irradiance and wind velocity), material and surface properties, and setup geometric features.

As a general comment, there is overall poor or conditional agreement between the measured Nu and the predictions from commonly used expressions. Even expressions developed specifically for BIPV/T systems or systems with multiple-inlets seem to be case specific and this is the main reason that an explicit Nu formulation was not developed in the present study. This signifies the need for a generalized approach on convective heat transfer for BIPV/T systems with special focus on the boundary conditions, especially the effect of wind and irradiance, as well as the specific features of the system (aspect ratio, PV transparency, thermal enhancements etc.) and other factors that may affect the performance of a BIPV/T. Such an approach will be introduced in a future study including a modular BIPV/T setup, which allows for great flexibility in terms of geometric features (adjustable air channel height), thermal enhancements, PV transparency and module types.

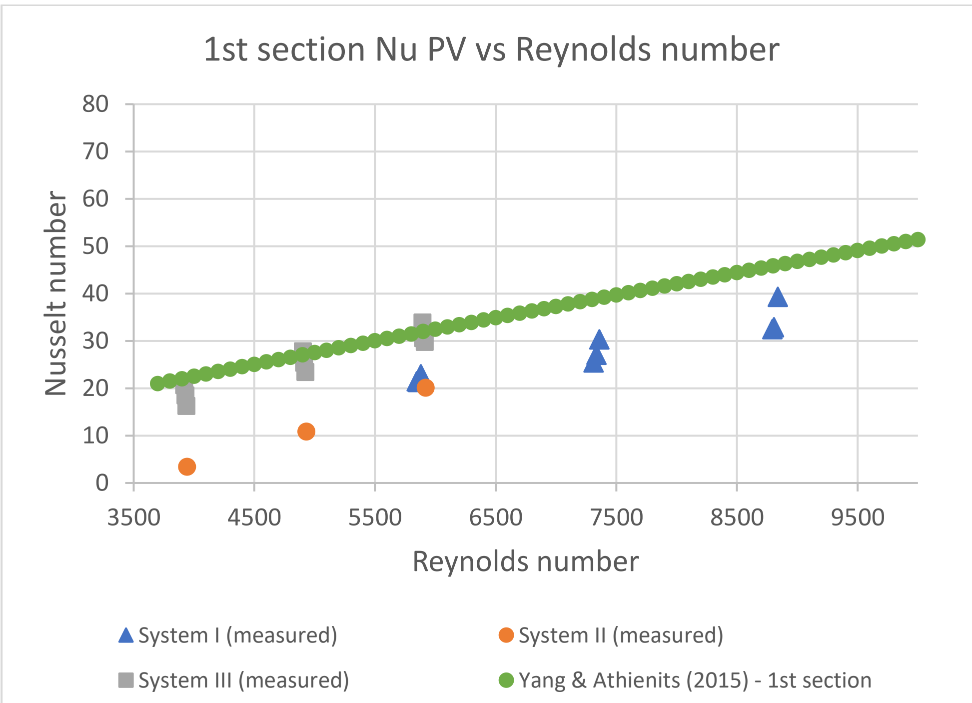

Figure 3. 18: Measured Nu PV of the bottom section for each of the three systems, compared to the Nu suggested by Yang & Athienitis [30] for the respective section.

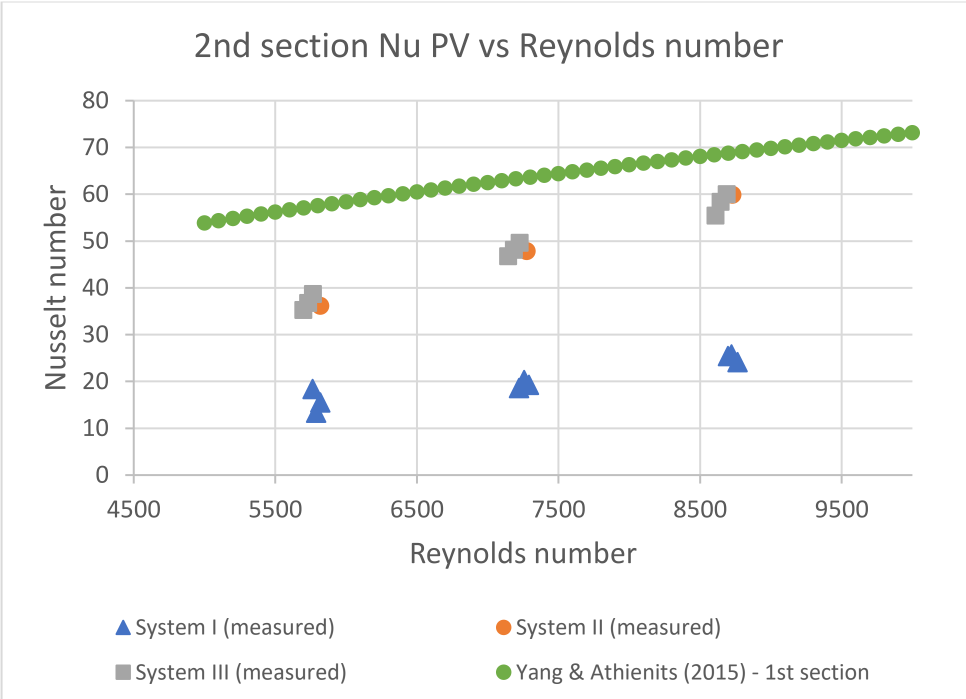

Figure 3. 19: Measured Nu PV of the top section for each of the three systems, compared to the Nu suggested by Yang & Athienitis [30] for the respective section.

3.3.4 Discussion

As mentioned previously, the performance of the prototype was not optimized as a stand-alone collector. The prototype itself served as a platform to implement the curtain wall design approach and investigate inexpensive and easy to implement thermal enhancements, suitable for building integrated systems. The flow rates used (normalized by the area of the assembly) were selected based on existing full-scale BIPV/T applications (Bambara et al., 2011; Chen et al., 2010).

It should be noted that with proper geometric optimization (channel height, inlet opening areas), the performance of a fully-integrated system can be further enhanced to fit the particular thermal application and connection to the HVAC. The flow rate or a range of flow rates may be imposed by the HVAC application, while the channel height may have constraints as for façade applications it may take up usable space. A follow-up investigation, involving a modular BIPV/T with variable channel depth, PV modules transparency and number of inlets will serve as a means for a sensitivity study of the main parameters that affect a BIPV/T curtain wall performance.

The PV modules used employed common junction boxes and wiring, not designed for the purpose of building integration. Facilitation of wiring, optimal junction box design and position, as well as facilitation of easy connectivity and replacement of PV modules for BIPV and BIPV/T systems requires further research.

Similarly, new approaches in PV module design such as use of more thermally conductive substrates (Koech et al., 2012; Zondag, 2008), potentially integrated with fins acting as heat sinks, could further enhance the thermal performance and allow for more flexibility when using PV as a building material

3.4. Conclusion

This chapter presented the design, development and testing of a novel BIPV/T curtain wall prototype. The developed system has the potential for prefabrication and modularization, and it is intended as a complete building envelope solution. The design of the prototype was based on structural, architectural and building envelope requirements. The main objective was to propose a standardized design approach and provide the basis for adaptation of common building techniques in the design of BIPV/T. Additionally, this study proposed thermal enhancements suitable for building integrated systems, such as the use of multiple-inlets, semi-transparent PV and a newly introduced flow deflector. Finally, issues relevant to the modelling of the air-channel convective phenomena were addressed This was done through the comparison of the recorded Nu to commonly used expressions in BIPV/T literature, as well as expressions specifically developed for BIPV/T systems (with one or multiple air intakes).

As far as thermal enhancements are concerned, the use of multiple inlets and a flow deflector unit were found to significantly improve the thermal performance by up to 16%, marginally improve the electrical performance and decrease the maximum PV temperatures by up to almost 4ºC. Furthermore, the use of semi-transparent PV increased the heat recovery from the rear surface of the air channel. Increasing PV transparency was found to increase the thermal performance but at the cost of the electrical performance.

Regarding the modelling of the air-channel convective phenomena, the convective coefficients and respective Nusselt numbers for all studied system types were found to have with poor or conditional agreement with the ones suggested in the relevant literature, indicating that most suggested expressions are case specific and there is a need for a more generalized approach for the modelling of convective phenomena in BIPV/T systems. It is important to study channel convection as a function of the boundary conditions, which are governed primarily by the effect of wind and solar irradiance, as well as the materials and the specific geometry of the system.

The curtain wall technology shows significant potential for standardized, easy to construct BIPV/T systems which also allows for design flexibility (incorporation of skylights and daylight elements). The authors have laid the groundwork for technology adoption using components and techniques familiar to building design professionals.

Chapter 4: Effect of convective heat transfer coefficients in PV/T and BIPV/T modelling[3]

4.1 Introduction

This section presents the comparison between simulated results in MATLAB against measured data from a solar simulator experimental setup and from a full-scale BIPV/T roof system. A reference simulation case was created for both systems that provided the best fit with the experimental data in terms of temperature rise in the air channel (or outlet air temperature). Following, simulations were performed to investigate the effect of using different wind-driven CHTC expressions by maintaining the internal convective coefficient that gave the best fit and altering the wind-driven expression. The same procedure was then repeated by maintaining the wind-driven coefficient and varying the Nu expression for channel convection to assess the effect of the latter.

4.2 Solar Simulator experimental setup

The first case study was based upon the solar simulator investigation of Yang & Athienitis (2014). The 2.89 x 0.038 BIPV/T sample, with a channel depth of 0.04 m (Fig. 4.1a) was tested under steady state conditions, namely 1080 W/m^2 solar irradiation, ambient temperature of 21ºC and 1.6 m/s wind velocity. The authors developed detailed PV, air and insulation temperature profiles, based on which local convective correlations for the interior and exterior were developed (Fig. 4.1b).

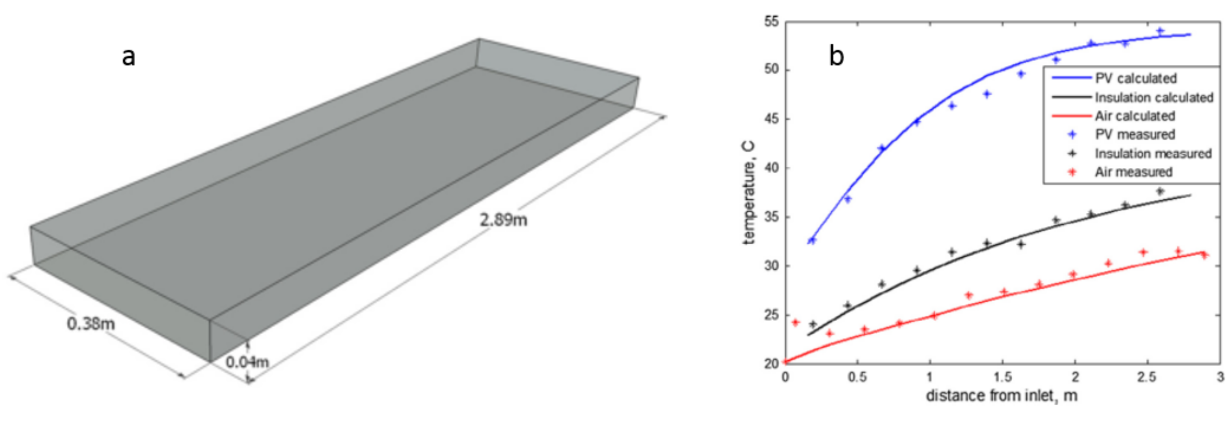

Figure 4. 1: a. BIPV/T sample dimensions, b. PV, air and insulation temperature profiles [70].

Table 4.1 presents the simulated results with different Nu expressions used in PV/T modelling (average PV, air and insulation temperatures, and average top and bottom convective heat transfer coefficients), while maintaining the wind-driven expression from the reference case. The last column shows the difference of each simulation from the reference case in terms of air temperature

[3] Presented in: Rounis, E. D., Athienitis, A., & Stathopoulos, T. (2021). Review of air-based PV/T and BIPV/T systems - Performance and modelling. Renewable Energy, 163, 1729–1753.

rise. Similarly, Table 4.2 presents the respective results in terms of temperature rise when the Nu expression from the reference case is maintained, while wind-driven expressions are varied.

The results of Table 4.1 demonstrate that there are significant differences in the evaluation of the channel CHTC when using different Nu expressions, which in turn reflect upon the calculation of the air temperature rise. The minimum (7.73 W/m^2.K) and maximum (20.83 W/m^2.K) CHTC value varied by more than 60% from the channel CHTC of the reference case (13.06 W/m^2.K) and more than 160% between them. This translated in a ΔT difference of up to 18.2% from the reference (13.5ºC versus 11.46ºC) and a difference of 30% (almost 4ºC) between the extreme cases.

Table 4.2 demonstrates that the different wind-driven CHTC expressions could create even more significant difference in the calculation of the air temperature rise. Indicatively, the combined radiative/CHTC calculated according to the commonly used formula by (McAdams, 1954) (11.67 W/m^2.K) varied by almost 160% from the reference case with a respective difference in the calculated ΔT of more than 57% (6.5ºC). It should be noted that with varying environmental and operating conditions, as well as system dimensions, these differences are expected to be greater. Such discrepancies could cause significant uncertainty when evaluating the performance of a coupled BIPV/T-HVAC system, as well as its optimal design.

Table 4. 1: Simulated results: changing Nu expression

Wind effect as evaluated experimentally / Varying Nu expressions							
Nu expression	**T_{PVavg}**	**T_{air_avg}**	**T_{ins_avg}**	**h_{PV_avg}**	**h_{ins_avg}**	**ΔT**	**Difference from reference (%)**
Yang & Athienitis (2014b)	47.62	26.15	29.54	13.06	17.92	11.46	Reference
Candanedo et al. (2011)	45.60	26.38	29.5	15.75	15.75	12.87	12.3
Chen et al. (2010)	43.63	27.31	29.29	20.83	20.82	13.54	18.2
Dittus & Boelter (1985)	48.67	24.76	31.41	8.38	8.38	9.86	13.9
Tan & Charters (1969)	49.05	24.56	31.83	7.73	7.73	9.48	17.3
Petukhov (1976)	48.57	24.81	31.31	8.56	8.56	9.95	13.2

Table 4. 2: Simulated results: changing wind-driven CHTC expression

Experimental Nu / Varying CHCT$_{wind}$ expression							
CHTC$_{wind}$ expression	**T$_{PVavg}$**	**T$_{air_avg}$**	**T$_{ins_avg}$**	**CHTC$_{wind}$**	**h$_{rad}$**	**ΔT**	**Difference from reference (%)**
Yang & Athienitis (2014)	47.62	26.15	29.54	22.17	5.17	11.46	Reference
Sharples & Charlesworth (1998)	50.95	27.60	31.57	15.42	5.26	13.12	14.5
McAdams (1954)	62.36	30.08	35.97	Combined: 11.67		18.00	57.1
Duffie et al. (2003)	59.92	29.566	35.02	7.6	5.51	16.95	47.9
Palyvos (2008)	52.44	29.92	32.14	13.80	5.30	13.75	20.0

4.3 Full-scale roof BIPV/T

The second case study is a BIPV/T roof system installed in one of the first net-zero institutional buildings in Quebec, Canada (Fig. 4.2). The featured BIPV/T system is 6 m long, 18.5 m wide, with a 7 cm air gap. The heated air from the BIPV/T is used as pre-heated ventilation air, boosting the performance of an energy recovery unit. When the solar-heated air is at a higher temperature than about 22°C, it provides free additional space heating.

Figure 4. 2: Roof BIPV/T system of the Varennes Library in Quebec, Canada.

For this case, monitored PV outlet temperatures of five consecutive days were used and the same procedure as for the previous case study was followed. The climatic conditions are shown in Fig. 4.3. The fan is producing an average channel air velocity of 0.9 m/s. Figures 4.4 and 4.5 demonstrate the simulated results against the measured outlet air temperature (black dashed line) when varying the Nu and wind CHTC expressions respectively.

The best fit between simulated and measured results was found when using the channel convective correlation by Chen et al. (2010) and the wind-driven convective correlation by Palyvos (2008). These expressions formulated the reference simulation case. Nu expressions developed for PV/T system (Candanedo et al., 2011; Yang & Athienitis, 2014) also provided quite good fit.

It was found that by changing wind CHTC expressions, simulated results could vary by up to 20ºC, while when changing Nu expressions, the difference was about 10ºC.

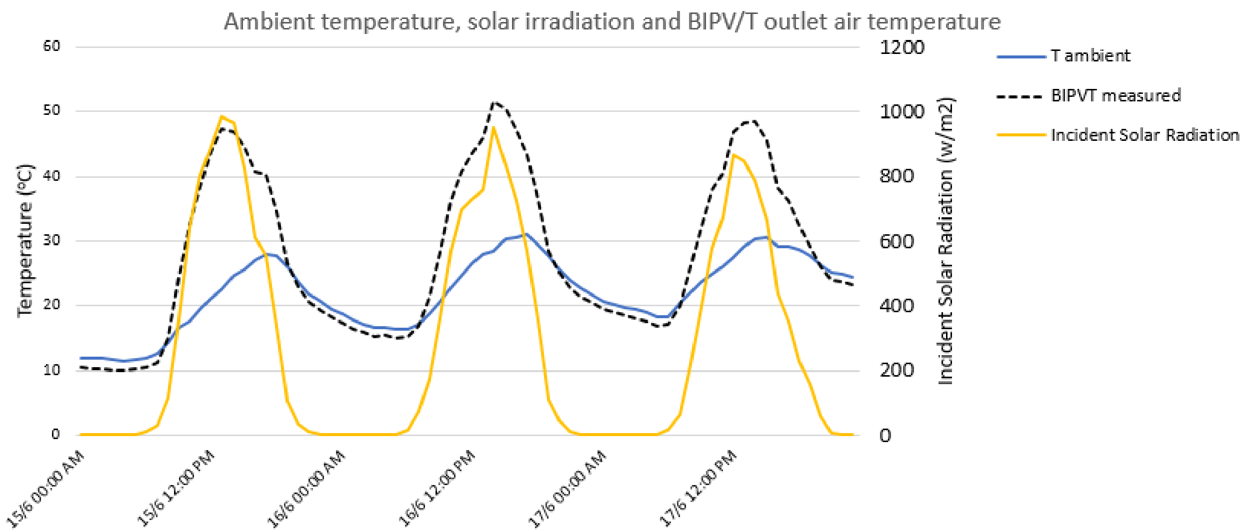

Figure 4. 3: Ambient conditions, channel velocity and outlet air temperature for the roof BIPV/T during the 5 days of testing.

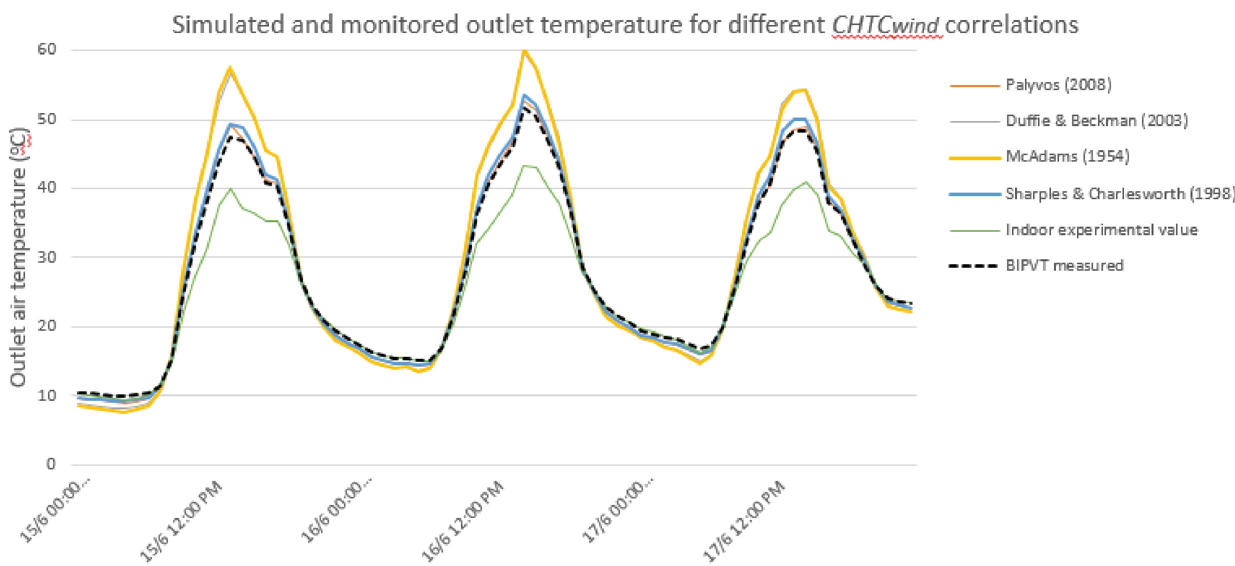

Figure 4. 4: Simulated vs measured outlet air temperature for different wind-driven CHTC expressions (maintaining reference Nu correlation).

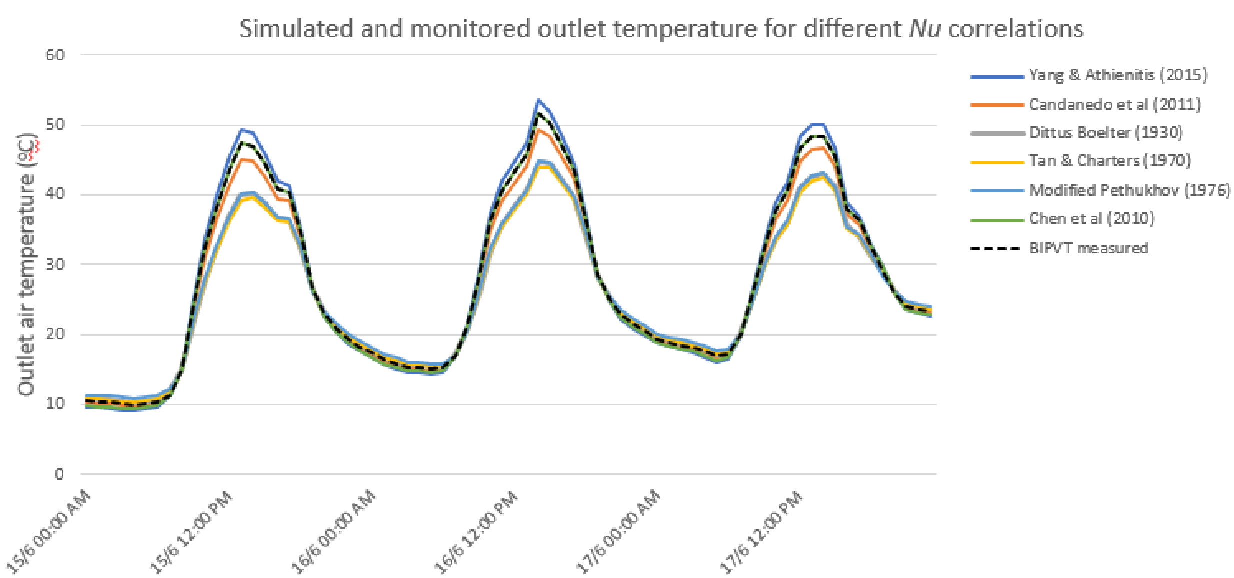

Figure 4. 5: Simulated vs measured outlet air temperature for different Nu expressions (maintaining reference wind-CHTC correlation).

4.4 Discussion

It is evident that using different expressions for wind-driven and internal convection from the available literature can cause great discrepancies in the predicted thermal performance of a BIPV/T system.

As far as internal convection is concerned, existing correlations generally under-predict the thermal performance, primarily due to the assumption of smooth duct and the neglection of entrance effects. Correlations developed specifically for PV/T systems generally provide more accurate predictions, but they have significant differences with each other. This may signify the need for a different approach in the development of channel convection expressions, one that apart from the flow conditions and channel geometry, will take into account the boundary conditions as well.

Wind effects were found to have the greatest impact, and this is attributed to the fact that the PV/absorber surface for a BIPV/T system is in direct contact with the ambient environment. The suitability of a wind-driven convection correlation highly depends on the local conditions, orientation and size of the systems, while it may be important to investigate the local effects from the wind velocity distributions over a large BIPV/T installation area.

Chapter 5: A novel approach for the modelling of convective phenomena for BIPV/T systems[4]

5.1 Introduction

This chapter introduces a novel approach for the modelling of convective phenomena for air-based building integrated photovoltaic thermal (BIPV/T) systems, which takes into consideration the interlinked nature of wind-driven and channel flow-driven convective phenomena. In chapters 3 and 4 it was shown that expressions for wind-driven and channel convection used BIPV/T systems modelling tend to be case specific, and their accuracy is highly dependent on the system type and specific environmental conditions. Predictions for air temperature rise have been found to differ by more than 10°C from monitored values, resulting in poor thermal utilization and cooling of the PV panels.

In the proposed approach, the key parameters affecting the thermal performance of a BIPV/T system, as discussed in section 2.3, have been formulated into dimensionless groups and correlated to the ratio of wind-driven convective heat transfer to the system heat recovery. This correlation was verified experimentally through testing in a full-scale solar simulator of a modular BIPV/T system under varying environmental conditions, flow rate, channel aspect ratio and PV module opacity.

Air temperatures rise predictions from the proposed modelling approach showed good agreement with the experimental results, with an R^2 of 0.93. The proposed methodology can be tailored to individual systems and climates via calibration through key temperatures monitoring and can be instrumental in the optimal control and heat utilization for a coupled BIPV/T-HVAC system. In addition, it can yield increased durability and performance of the PV installation through incorporation of more efficient cooling strategies, through accurate outlet air temperature and PV temperature predictions, respectively.

5.2 Methodology

This section presents the proposed methodology and the supporting experimental procedure. In this methodology, wind-driven (or combined wind-driven and radiative) heat transfer and channel heat recovery are combined together in the form of a ratio and not being treated as independent phenomena. This ratio of exterior heat transfer over the heat recovery is correlated to the various parameters that have been found to affect the thermal performance of BIPV/T systems, formulated in dimensionless groups. An experimental process involving specifically designed BIPV/T modules was carried out in the controlled environment of a solar simulator facility to verify the validity of the proposed methodology, by varying several of the identified key parameters, namely irradiance, wind velocity, channel geometry and PV module optical properties.

5.2.1 Dimensionless groups

[4] Presented in: Rounis, E. D., Ioannidis, Z., Sigounis A.M., Athienitis, A., & Stathopoulos, T. (2021). A Novel Approach for the Modelling of Convective Phenomena for Building Integrated Photovoltaic Thermal (BIPV/T) Systems. Solar Energy (submitted).

In the literature so far, the air channel has been treated as a closed system and the heat transfer from the air-channel boundaries, or walls, is considered a function of the average channel flow velocity, the temperature difference between the walls and the fluid (assuming constant wall temperature), the fluid thermal properties (conductivity, heat capacitance, density), the diameter, or hydraulic diameter of the duct/pipe, and on occasion the length and roughness of the duct, as summarized in eq. 5.1:

$$q_c = f(u, \Delta T, D, \mu, \rho, c_p, k, L, \varepsilon) \tag{5.1}$$

The dimensionless form of equation 5.1 is that of the Nu as function of the Re and the Pr, (and occasionally the aspect ratio, D/L and the friction factor f):

$$\overline{Nu} = f\left(Re, \mathrm{Pr}, \frac{\mathrm{L}}{\mathrm{D}}, \mathrm{f}\right) \tag{5.2}$$

However, for BIPV/T systems, the boundary conditions are not constant due to heat transfer occurring on either side of the PV module, which interfaces with both the air channel and the ambient environment. These two processes of heat transfer can affect one another. In the proposed methodology, a new quantity is defined as the ratio of exterior heat transfer (from the PV surface to the environment) over the heat that is recovered (channel convection):

$$Q_{ratio} = \frac{q_{exterior}}{q_{recovered}} = \frac{exterior\ heat\ transfer}{heat\ recovery} \tag{5.3}$$

In addition to the coolant fluid properties (specific heat capacity, conductivity and viscosity), this ratio depends upon the parameters discussed in Section 2.3, namely:

- The environmental parameters (irradiance, wind velocity and ambient temperature)
- The operational conditions (flow rate or average fluid velocity)
- The unique design features of the system/boundary properties which may include:
    - The geometric features (length, hydraulic diameter)
    - The optical properties (PV and rear surface emissivity, PV transparency, rear surface absorptivity
    - The material properties (roughness, thermal conductivity of above-cell layer, thermal conductivity of below-cell layer, PV efficiency)
- The coolant properties (thermal conductivity, viscosity, specific heat capacity)

The ratio of exterior heat transfer over the heat recovery can then be expressed as:

$$Q_{ratio} = f(G, T_{ambient}, V_{wind}, u, D_h, L, \eta_{PV}, \tau_{PV}, \alpha_{PV}, \alpha_{ins}, \varepsilon, \varepsilon_{PV}, \varepsilon_{ins}, U_{top}, U_{bot}, \rho, \mu, c_p) \tag{5.4}$$

The wind velocity, V_{wind}, could be considered a direct indicator of the wind *CHTC*, h_{wind}, given their majorly linear correlation. For the present study, V_{wind} and h_{wind} are used interchangeably.

Equation 5.4 can be simplified with the definition of a different metric for the solar irradiance, the available solar irradiance, or $G_{available}$. This quantity expresses the amount of solar radiation that is available for thermal conversion and is defined as the total amount of absorbed radiation by the PV, minus the electricity generation and adding to that the amount of radiation that may be transmitted through the transparent part of the PV module (if applicable) and then absorbed by the rear (insulation) surface:

$$G_{available} = (\alpha_{PV} + \tau_{PV} \cdot \alpha_{ins} - \eta_{PV}) \cdot G \tag{5.5}$$

This is in line with the modified thermal efficiency proposed by Bombarda et al. (2016), in which PV generation is subtracted from the incident radiation, and further introduces the optical features of the system to extend to STPV configurations.

Taking into consideration equation (*5.5*), equation 5.4 can be simplified to the following:

$$Q_{ratio} = f(G_{available}, T_{ambient}, h_{wind}, u, D_h, L, \varepsilon, \varepsilon_{PV}, \varepsilon_{ins}, U_{top}, U_{bot}, \rho, \mu, c_p, k) \tag{5.6}$$

By inspection, the variables of equation 5.6 can be transformed into the following dimensionless groups:

$$G_1 = Q_{ratio} = \frac{q_{exterior}}{q_{recovered}} \tag{5.7}$$

$$G_2 = \frac{h_{wind} \cdot T_{ambient}}{G_{available}} \tag{5.8}$$

$$G_3 = \frac{\rho \cdot u \cdot D_h}{\mu} = Re \tag{5.9}$$

$$G_4 = \frac{c_p \cdot \mu}{k} \tag{5.10}$$

$$G_5 = \frac{D_h}{L} \tag{5.11}$$

$$G_6 = \frac{\varepsilon}{D_h} \tag{5.12}$$

$$G_7 = \frac{U_{top}}{U_{bot}} \tag{5.13}$$

G_1 is already dimensionless and is the dependent variable of the analysis. G_2 is a newly defined dimensionless number that combines the environmental effect at the interface between the environment and the air channel. The denominator combines the effect of the available solar radiation, as defined in equation 5.5, and the nominator expresses the combined convective/radiative loss as a function of the ambient temperature. G_3 is the Reynolds number which characterizes the flow regime of the air channel and G_4 is the Prandtl number which incorporates the fluid properties. Groups G_5 through G_6 summarize the unique features of the system (aspect ratio, relative roughness and ratio of encapsulation conductance above and below the PV cell).

This set of dimensionless numbers fully describes the ratio of heat recovery over the exterior heat transfer - see eq. 5.7 - as a function of the various groups of affecting parameters, discussed in section 2.1. Using the set of dimensionless numbers, equation 5.7 can be rewritten in the following form:

$$Q_{ratio} = f(\frac{h_{wind} \cdot T_{ambient}}{G_{available}}, Re, Pr, \frac{D_h}{L}, \frac{\varepsilon}{D_h}, \frac{U_{top}}{U_{bot}}) \tag{5.14}$$

The significance of the above relationship can be better understood when considering the simplified energy balance presented in Fig. 5.1. The incident radiation available for thermal conversion (total radiation absorbed by the PV and rear surface minus the PV generation) is equal to the exterior heat transfer and the heat recovered by the system.

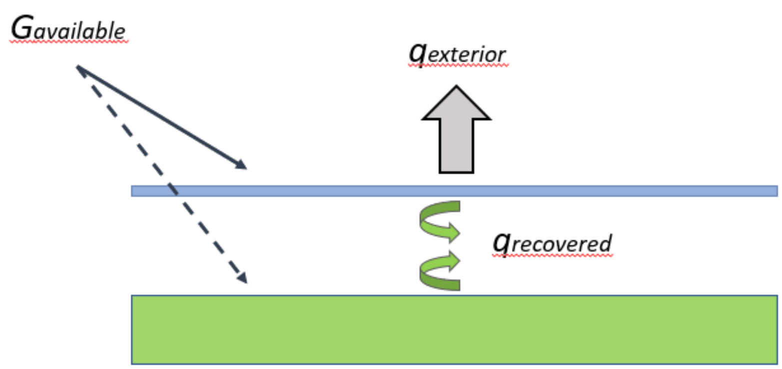

Figure 5. 1: Simplified BIPV/T energy balance.

It should be noted that the heat conduction through the insulation to the adjacent zone is considered negligible, based on the findings of Candanedo et al. (2011) and Yang & Athienitis (2014) as well as the experimental findings of the present research, for which this mode of heat transfer accounts for less than 1% of the overall energy balance.

The simplified energy balance can be then described by a single equation:

$$G_{available} = q_{recovered} + q_{exterior} \tag{5.15}$$

Or, when combined with equation 5.7:

$$q_{recovered} = G_{available}/(1 + Q_{ratio}) \tag{5.16}$$

5.2.2 Experimental procedure

The proposed approach was investigated through an extensive experimental procedure, carried out at the Solar Simulator and Environmental Chamber facility of Concordia University in Montreal, Canada. This process involved a modular BIPV/T prototype, which offered flexibility of testing configurations, with a variable air channel height and interchangeable PV modules of varying transparency.

The indoor solar simulator facility of Concordia University (Figure 5.2a) consists of a lamp field featuring 8 metal halide lamps, and a test platform where test subjects can be mounted. The lamp field can produce irradiance intensity between 500-1200 W/m^2, with a uniformity up to 97%. The spectral distribution of the lamps meets the specifications of standards ISO 9806 and EN 12975 (Kapsis et al., 2016). A ventilated artificial sky placed in front of the lamp field removes the infra-red interference caused by the heat produced by the lamps (Mei et al., 2003) and simulates the effect of the sky temperature with a surface temperature of 13ºC ±2ºC. Both the platform and the lamp field can rotate between 0º (horizontal) and 90º (vertical) to simulate different building envelope slopes.

Wind-driven convection is emulated by a linear fan set over the rear end of the platform (Fig. 4a). It can produce air velocities of up to 14 m/s, while its height can be adjusted to match that of the specimen (flow parallel to the specimen surface). An air collector test stand can be attached to the specimen to produce air flow within the air channel (Fig. 5.2b). The mass flow rate is measured by an orifice flow meter featuring three differential pressure transducers and can be manually adjusted.

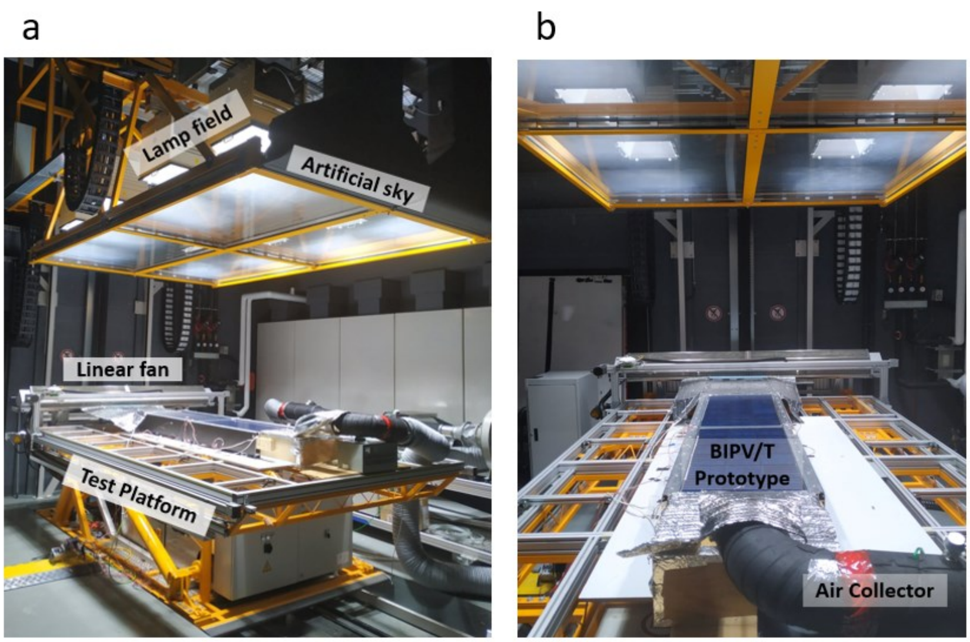

Figure 5. 2: a. Components of the solar simulator and b. the mounted prototype, connected to the air collector test stand.

The prototype used in the experimental process features a curtain wall design approach (Kruglov et al., 2017; Rounis et al., 2017, 2021a), and was designed to allow for different testing configurations with an adjustable height for the rear section (insulation) and interchangeable PV modules of different transparency (Fig. 5.3). It further features a modular form which allows for an expanding setup that allows for future testing of different arrangements with up to 4 inlets.

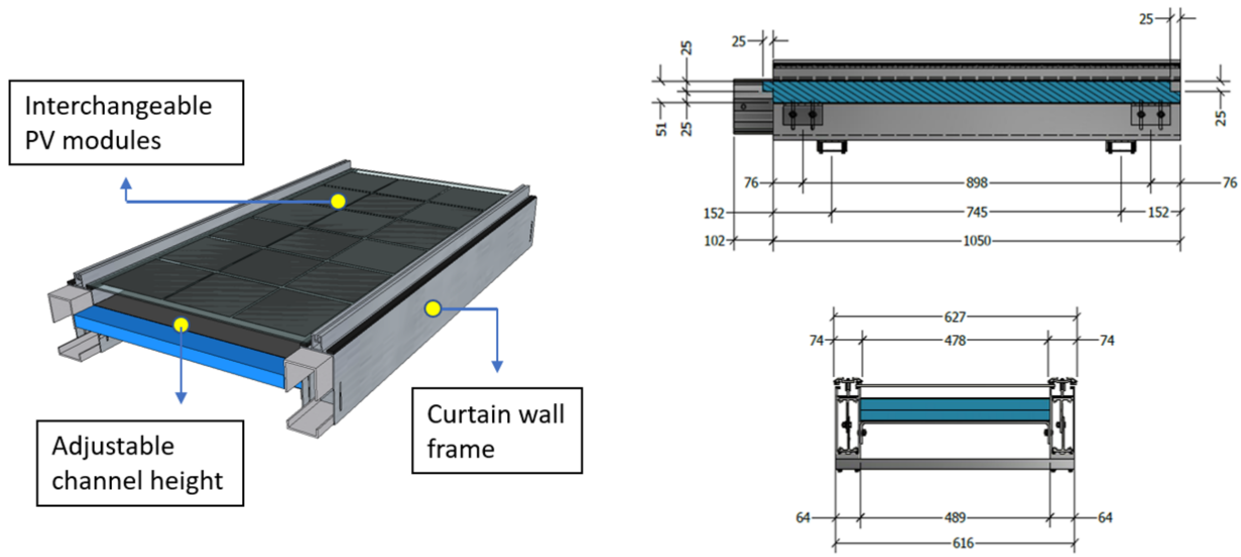

Figure 5. 3: Experimental BIPV/T modules with varying channel height and interchangeable PV modules.

The frame of each module consists of two 1.05 m long mullions connected by transoms to form a rigid frame. Aluminum sleeves are placed at the front end of each mullion for the connection of two or more modules. The insulated rear side consists of 51 mm extruded polystyrene, sandwiched between two aluminum sheets. The cover interfacing with the air channel was painted black to absorb more of the transmitted radiation, for the cases involving semi-transparent PV modules. The side walls of the channel were covered by adhesive insulation to minimize conductive heat transfer from the sides of the system.

Two of these BIPV/T modules were linked to form a 2.09 m by 0.48 m specimen (net channel dimensions). The channel depth was set at two distinct heights, namely 0.03 m and 0.06 m, with respective hydraulic diameters of 0.057 m and 0.107 m, channel cross sectional areas of 0.029 m^2 and 0.015 m^2, and two resulting channel aspect ratios (L/D_h) of 19.55 and 36.96.

Two sets of custom-made 1.04 m x 0.515 m PV modules were used, each featuring 18 p-Si PV cells, with a peak power output of 80W (η_{STC}=12.7%) and a packing factor (*PF*) of 85.94%.

The optical properties at the PV level were averaged over the whole specimen aperture. For the absorptance, reflectance and transmittance of each material, the values provided by the manufacturer were assumed. The emissivity of the front and back surface of each PV, as well as the insulation surface were measured by a TIR 100-2 emissivity meter. For the average values, the net projection of the PV to the air channel was assumed.

5.2.3 Measurements

The instrumentation of the setup involved 36 T-type thermocouples, 12 for each layer of interest, namely the rear PV surface (interfacing with the air channel), the middle of the air channel and the insulation surface (Fig. 5.4). These were placed along the centerline of the flow path (Fig. 5.5). Each PV sensor was placed at the center of each cell and the corresponding air and insulation sensors were accordingly aligned. Two thermocouples were used to monitor the inlet and outlet air temperature and six thermocouples were used to monitor the inner and outer wall surface temperature, as well as the back of the insulation in order to evaluate the conductive heat losses. Finally, three surface sensors were used to monitor the temperature the outer air film.

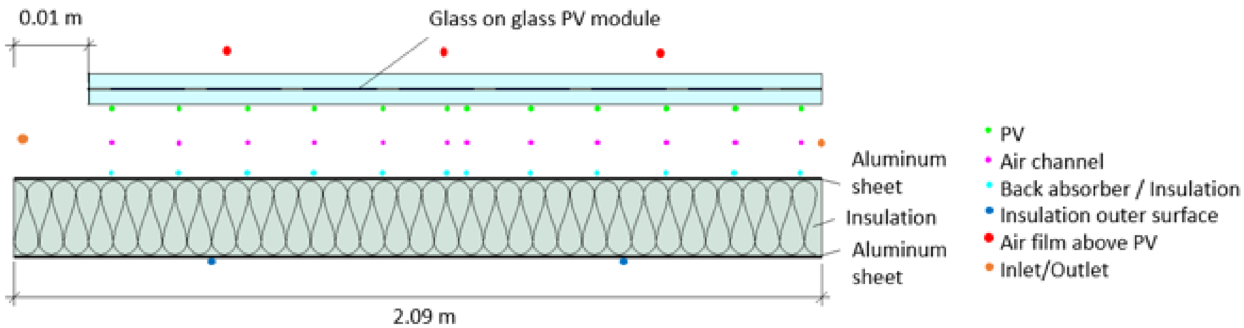

Figure 5. 4: Location of the temperature and wind velocity measurements.

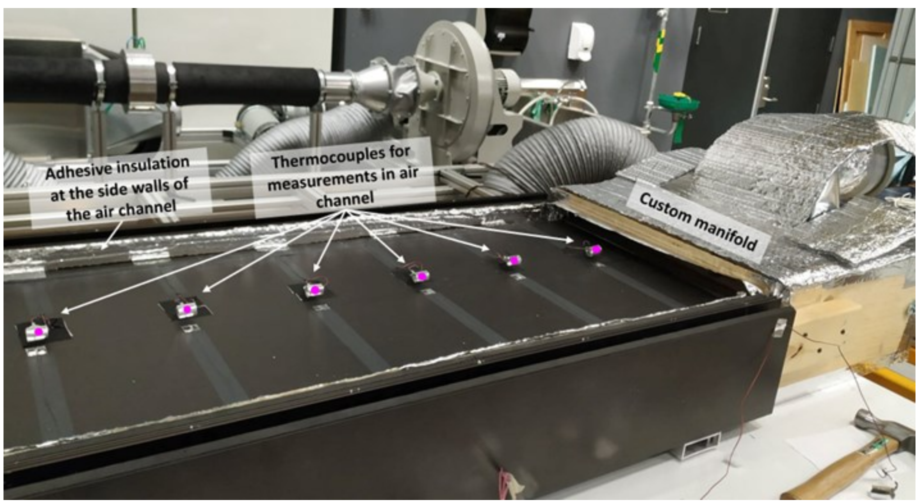

Figure 5. 5: Thermocouple placement on the insulation and air channel, and the custom manifold used to connect to the air collector test stand.

The air flow rate inside the air channel was determined by the orifice plate of the Air Collector Test Stand, which was attached to the specimen via a custom manifold (Fig. 5.5). The wind velocity profile over the BIPV/T module was measured above the edges and middle of each PV panel locations with a TSI hot-wire anemometer (measuring precision) and averaged over the collector's length. This was done for three distinct settings of the linear fan and each measurement was repeated three times.

5.3. Experimental results and discussion

A detailed energy balance for each case was initially performed as a reference and to provide detailed information regarding the convective and radiative heat transfer coefficient of the involved surfaces.

The recorded temperatures, solar radiation, PV power generation, channel mass flow and wind velocity measurements were used to establish the relationship between the tested system against the dimensionless groups G_2, G_3 and G_5 (environmental/boundary effects, Re and aspect ratio respectively), as defined in section 3.

5.3.1 Cases studied

Two sets of experiments were carried out, one implementing transparent PV modules and one opaque. For each set of experiments, two channel depths were considered, namely 0.06 m and 0.03 m. Each configuration was tested under varying irradiations (807 W/m^2, 928 W/m^2, 1058 W/m^2), mass flow rates (120 kg/s.m^2, 180 kg/s.m^2 and 240 kg/s.m^2) and wind speeds (1.53 m/s, 2.32 m/s, 3.18 m/s). All tests were carried out under room temperature of 21ºC ±1ºC. For each test, measurements were taken for 15 minutes after steady state was reached and the 15-minute averaged values were then used to deduce the respective coefficients for each mode of heat transfer involved.

Figure 5.6 summarizes the various cases considered throughout the experimental procedure.

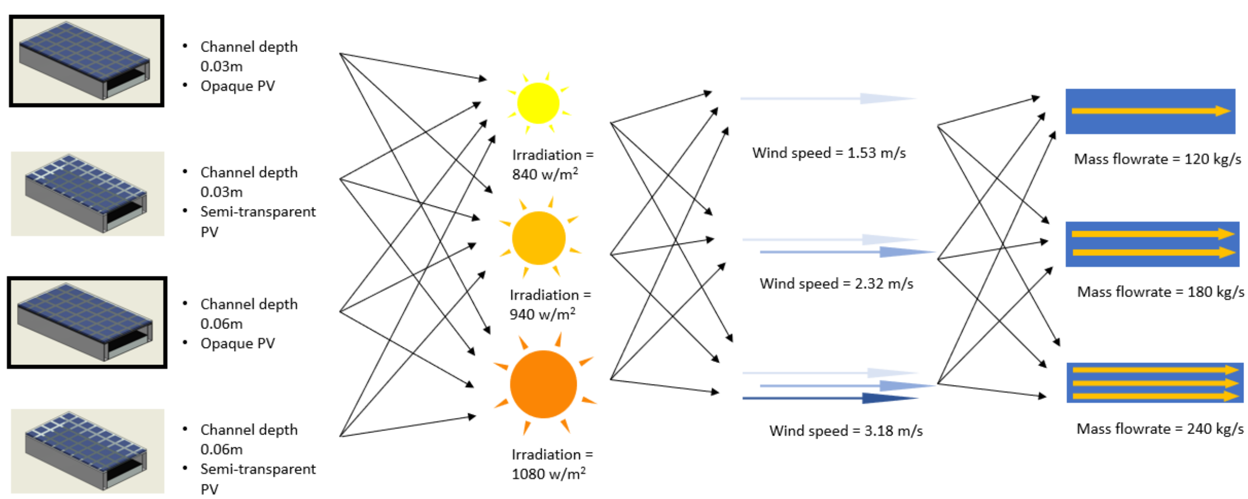

Figure 5. 6: Channel configurations and operating conditions used in the measurements.

5.3.2 Convective heat transfer coefficients

Figure 5.7 demonstrates the PV side Nusselt number plotted against the Reynolds number for all cases considered. A high variance of the Nusselt number is noticed, even for the cases with same *Re* and aspect ratio. This signifies that the evaluation of the Nusselt number as a function of the *Re*, the *Pr* (which for air temperatures involved can be considered constant, ranging from 0.69 to 0.72) and the aspect ratio, can result in high uncertainty.

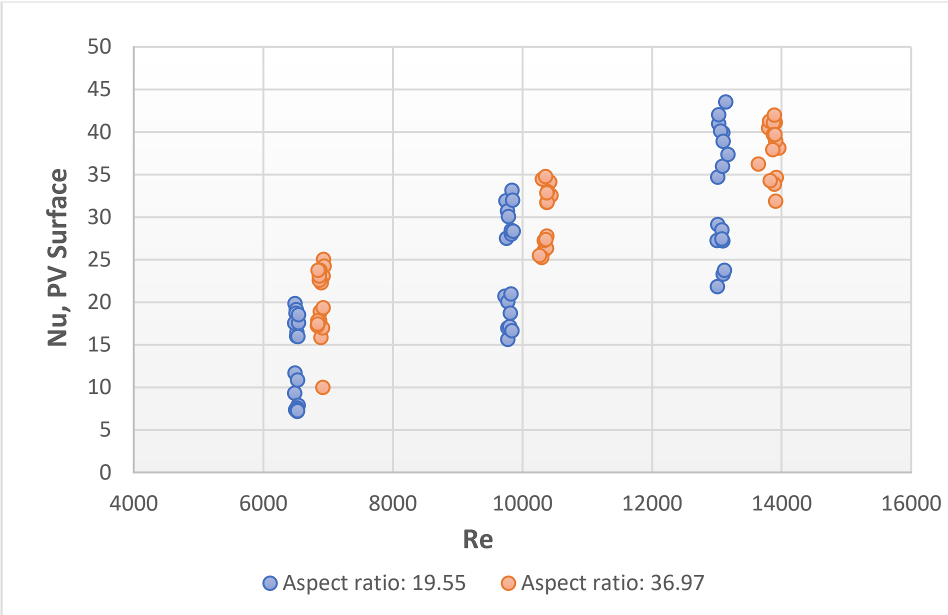

Figure 5. 7: Nusselt number of the PV side interfacing with the air channel plotted against the Re of the flow, for the two setup aspect ratios involved in the experiments.

Similarly, Figure 5.8 shows the wind driven *CHTC* plotted against the wind velocity, for all cases considered. Again, a significant variance is observed for the wind-driven *CHTC* at the same wind velocities, which indicates that for the case of air-based BIPV/T systems, assuming a linear correlation can lead to significant prediction inaccuracies.

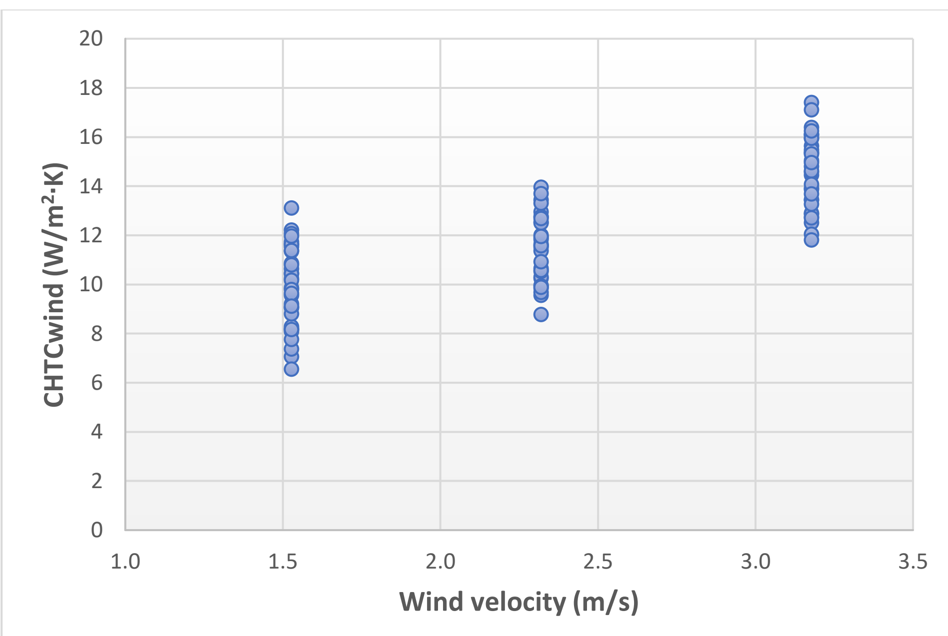

Figure 5. 8: Wind-driven convective heat transfer coefficient plotted against the average wind velocity over the BIPV/T surface.

5.3.3 Correlation of Q_{ratio} to the dimensionless groups

Figure 5.9 demonstrates the correlation of the ratio of exterior heat transfer over the heat recovered by the system, Q_{ratio}, plotted against the product of the dimensionless group G_2, which combines the effect of the environmental conditions, the aspect ratio, D_h/L, and the inverse of the Re, which characterizes the flow regime.

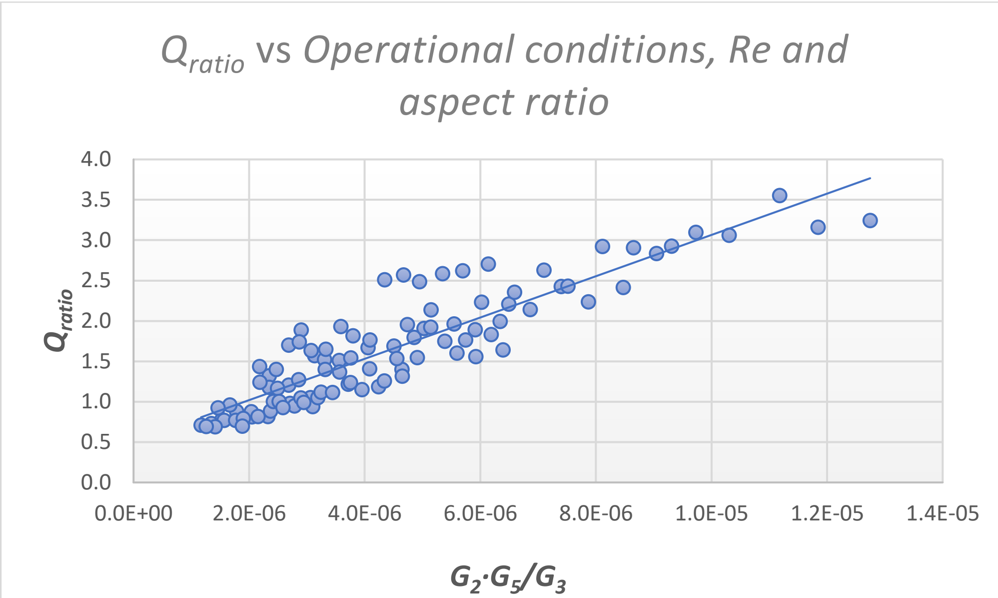

Figure 5. 9: Q_{ratio} plotted against the product of G_2 (environmental parameters), G_5 (aspect ratio) and the inverse of G_3 (Reynolds number).

The seemingly linear trend of the plot indicates a strong correlation between the ratio of exterior heat transfer over the heat recovered to the environmental conditions, the operating conditions (flow rate) and the system geometry. It should be noted that this plot includes the data points from tests using both the transparent and the opaque set of PV modules which shows that $G_{available}$, included in the dimensionless group G_2, can adequately help in the generalization of the effect of incident radiation, accounting for the optical properties of the system.

Finally, it should be noted that the data points showing the highest scattering correspond to the cases with the lowest wind velocity settings, where natural convection and radiative phenomena are expected to have a more major role in the energy balance.

The linear regression of the data from Figure 5.9 indicates a R^2=0.81. The correlation that corresponds to this specific system and operating conditions is the following:

$$Q_{ratio} = 255656 \cdot \frac{G_2 \cdot G_5}{G_3} + 0.5083 \tag{5.17}$$

This, however will be different for different system types (geometry, materials) and operating conditions (local climate). It can be determined during a commissioning stage of the system. However, it will not be expected to significantly change for a given location and system design. It will form an excellent basis for optimal model-predictive control of the system, in which an optimal flow rate of a variable speed fan is automatically selected to achieve a certain outlet air temperature based on the application needs and the weather variables.

5.3.4 Relation between the ratio of wind-driven and channel *CHTC* to Q_{ratio}

A noteworthy result was the virtually linear relationship between the Q_{ratio} and the ratio of wind-driven and channel flow convective heat transfer coefficients, as shown in Fig. 5.10. This could establish the expected convective coefficients for a given system, to be used for a control algorithm. This would however require additional monitoring of the average air temperature inside the air channel.

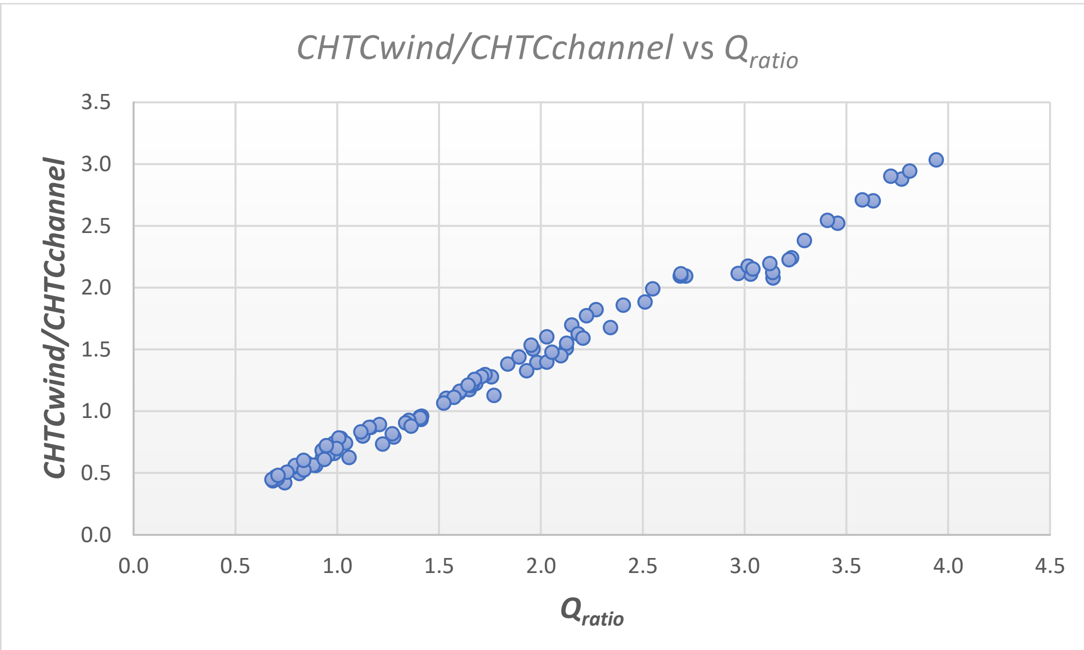

Figure 5. 10: Variation of ratio of wind-driven CHTC over the air channel CHTC with Q_{ratio}.

5.3.5 Predicted outlet temperature

The least-squares fit of the data presented in Figure 11 was used in conjunction with equation 25 to predict the air temperature rise in the air channel for all studied cases.

Figure 5.11 presents a scatterplot of the predicted and corresponding measured values of ΔT. The modelled results show high level of accuracy, with a coefficient of determination (R^2) of 0.93, a mean absolute error (MAE) of 0.37°C and a root mean square error (RMSE) of 0.49°C.

The accuracy of the proposed method was further evaluated against commonly used modelling approaches in PV/T and BIPV/T literature. These approaches involved a fundamental BIPV/T energy balance (eq. 2-6) with a finite control volume scheme, and different combinations of the most commonly used wind-driven *CHTC* and channel *Nu* expressions in PV/T and BIPV/T literature, according to the review study by Rounis et al (2021). These expressions included four wind-driven *CHTC* correlations (Duffie et al., 2003; McAdams, 1954; Palyvos, 2008; Sharples & Charlesworth, 1998), two *Nu* expressions from heat transfer in pipe/duct flow (Dittus, 1985; Tan & Charters, 1969), and two expressions specifically developed for BIPV/T systems (Candanedo et al., 2011; Yang & Athienitis, 2014a).

All considered models were compared in terms of the coefficient of determination (R^2), the mean absolute error (MAE) the and a root mean square error (RMSE). Table 5.1 summarizes the considered cases (expression combinations and proposed methodology) and the respective indicators for each model.

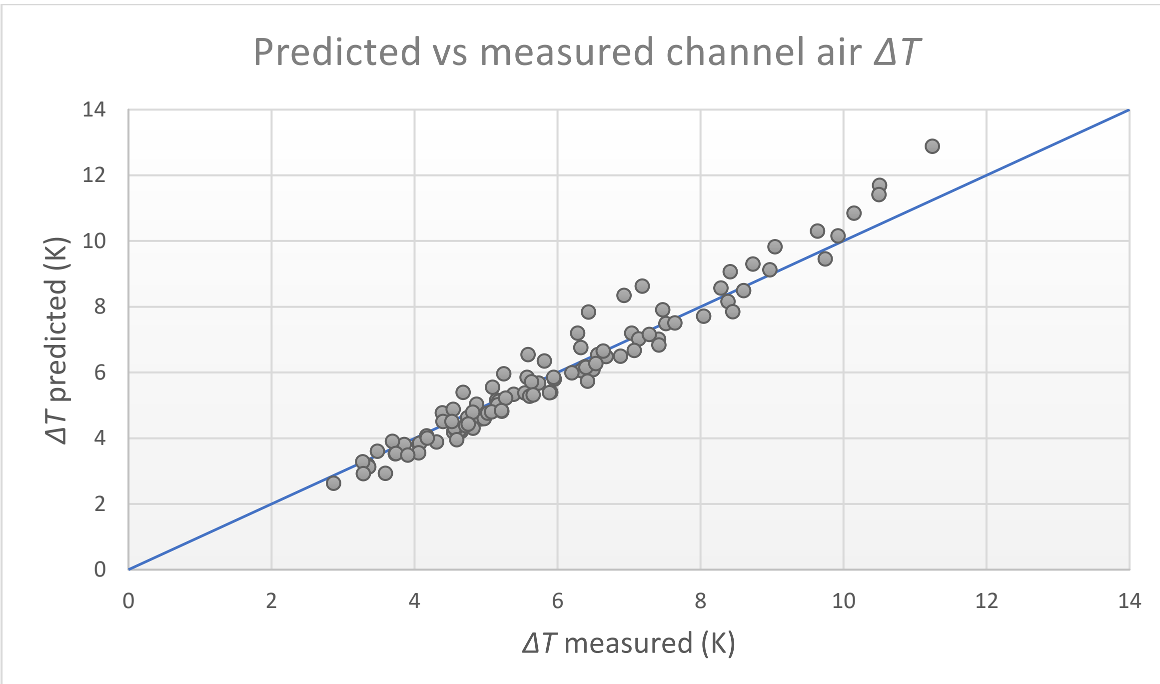

Figure 5. 11: Scatterplot of the predicted values of air temperature rise (ΔT) based on the proposed method and the monitored experimental values.

Table 5. 1: R^2, MAE and RMSE of different modelling approaches

Case	Model description	R^2	MAE (°C)	RMSE (°C)
1	Proposed methodology	0.93	0.37	0.49
2	*Nu*: Dittus-Boelter, $CHTC_{wind}$: Sharples & Charlseworth	-0.02	1.69	1.88
3	*Nu*: Dittus-Boelter, $CHTC_{wind}$: McAdams	0.34	1.32	1.50
4	*Nu*: Dittus-Boelter, $CHTC_{wind}$: Duffie & Beckman	0.77	0.68	0.88
5	*Nu*: Dittus-Boelter, $CHTC_{wind}$: Palyvos	0.06	1.63	1.80
6	*Nu*: Yang & Athienitis, $CHTC_{wind}$: Sharples & Charlseworth	-0.50	2.07	2.27
7	*Nu*: Yang & Athienitis, $CHTC_{wind}$: McAdams	-0.53	2.09	2.29
8	*Nu*: Yang & Athienitis, $CHTC_{wind}$: Duffie & Beckman	-1.03	2.16	2.65
9	*Nu*: Yang & Athienitis, $CHTC_{wind}$: Palyvos	-0.48	2.06	2.26

10	*Nu*: Candanedo et al, $CHTC_{wind}$: Sharples & Charlseworth	-1.56	2.78	2.97
11	*Nu*: Candanedo et al, $CHTC_{wind}$: McAdams	-1.00	2.44	2.62
12	*Nu*: Candanedo et al, $CHTC_{wind}$: Duffie & Beckman	-0.02	1.67	1.87
13	*Nu*: Candanedo et al, $CHTC_{wind}$: Palyvos	-1.44	2.72	2.90
14	*Nu*: Tan & Charters, $CHTC_{wind}$: Sharples & Charlseworth	-0.03	1.64	1.88
15	*Nu*: Tan & Charters, $CHTC_{wind}$: McAdams	0.33	1.29	1.52
16	*Nu*: Tan & Charters, $CHTC_{wind}$: Duffie & Beckman	0.74	0.75	0.95
17	*Nu*: Tan & Charters, $CHTC_{wind}$: Palyvos	0.05	1.58	1.81

Table 5.1 indicates that the predictions based on the proposed methodology show the highest accuracy and the smallest spread. These results are consistent with the findings of Rounis et al. (2021b) regarding the spread of predictions when using different combinations of convective heat transfer expressions.

5.4 Applications and limitations

Applications and limitations of the proposed methodology are addressed in this section.

The proposed methodology can be applied as follows:

1. System control: Firstly, the ratio of exterior heat transfer to the heat recovery can be established for a particular BIPV/T system (or well insulated PV/T collector) through use of equation 23 and monitoring of the environmental parameters, channel flow rate, PV generation, inlet/outlet temperature and PV temperature. If the PV temperature cannot be directly monitored, it can be deduced from the measured electrical generation and equation 2.1 (temperature dependence of PV efficiency). Having established that, equation 25 can then be used to predict the heat recovery and resulting outlet temperature given the environmental conditions and system flow rate. These predictions can be utilized to optimize the BIPV/T flow rate, or HVAC operation.

2. Development of BIPV/T case studies library and system comparison:

Given its dimensionless nature, this methodology could be used for the development of a library of BIPV/T and PV/T system case studies that can allow for easier comparison of the thermal performance of different system types operating under varying conditions. This could potentially provide valuable feedback for engineers when deciding upon the system type for a particular building or climate, as well as help refine convective modelling in the long run.

Proposed methodology limitations:

As mentioned earlier, the proposed methodology is not intended for initial design optimization, given that it requires monitored data to produce the relationship between the involved dimensionless quantities. Furthermore, this methodology is currently based on indoor experimental measurements, where the radiative phenomena had limited effect over the energy balance. Radiative heat transfer could be accounted for as a separate term in the energy balance, with known PV, sky and surrounding temperature. Clearly, it would be interesting and beneficial to carry out measurements on a full-scale BIPV/T system, monitored under real conditions.

5.6 Conclusions

This paper presents a novel approach which accounts for the combined effect of wind-driven and channel flow-driven convection, in the modelling of convective phenomena for BIPV/T systems. This was done by correlating the ratio of exterior heat transfer (wind-driven convection) over the recovered heat to the various parameters that have been identified to affect the thermal performance of hybrid systems, formed in dimensionless groups. Indeed, a dimensionless group which combines the effect of the boundary conditions (irradiance, wind-driven convection and ambient temperature) was introduced.

The proposed modelling methodology provides a generalized approach for different system types and climates. This involves a calibration stage where the correlation between the ratio of exterior heat transfer over the heat recovery and the dimensionless groups of the affecting parameters is established. The methodology is primarily intended for the control stage of a BIPV/T system, for which accurate predictions of the supply air temperature are required with optimal flow rate. However, it also provides a foundation for the comparison of the performance of different BIPV/T and PV/T systems, due to its generalized form.

The experimental investigation of a modular BIPV/T specimen in an indoor solar simulator facility, under varying irradiance and wind velocity, mass flow rate, as well as air channel aspect ratio and PV module transparency, showed that wind-driven and channel convective phenomena are closely linked and one can significantly affect the other. Thus, the use of *Nu* and *CHTC* expressions that do not account for this effect can result in significant uncertainties in the modelling of a BIPV/T system and the prediction of the outlet air temperature.

The results also indicate a strong correlation between the ratio of exterior heat transfer over the heat recovered to the environmental conditions, the operating conditions (flow rate) and the system geometry. Conversely, the channel Nu and the wind-driven *CHTC* can vary significantly while maintaining the same flow conditions and velocity respectively, but changing the rest of the test parameters.

The proposed methodology was used to predict the outlet temperature of the specimen and showed good agreement with the experimental findings. Additionally, it showed superior performance to models implementing different combinations of commonly used *CHTC* and *Nu* expressions from literature.

This methodology can be tailored to individual systems via calibration through key temperatures monitoring and can be instrumental in the optimal control and heat utilization for a coupled BIPV/T-HVAC system, as well as increased durability and performance of the PV system through incorporation of more efficient cooling strategies, through accurate supply (outlet) air temperature and PV temperature predictions, respectively.

Chapter 6: Conclusions

This thesis addressed two of the main issues that have been identified to hinder the widespread adoption of BIPV/T system by the mainstream market, namely the lack of design standardization and of best practice guides, and the inconsistency in modelling, especially of the convective phenomena. The first part of the thesis presented the design, development and testing of a BIPV/T prototype which served as a design platform for the incorporation of the well-established curtain wall building practice, with the prospect of modularization and prefabrication, as well as for the implementation of thermal enhancing techniques easily adoptable by building integrated systems. The system was studied at an indoor solar simulator facility at Concordia University and the results were used to investigate the performance of the prototype and the implemented thermal enhancement techniques, as well as study the applicability of commonly used expressions in BIPV/T modelling. The main objective was to set a foundation for air-based BIPV/T design standardization and incorporation of common building practices, and highlight issues regarding convective heat transfer modelling.

The second part of the thesis presented a novel approach which accounts for the combined effect of wind-driven and channel flow-driven convection, in the modelling of convective phenomena for BIPV/T systems. In the proposed methodology, wind-driven heat transfer and heat recovery by the BIPV/T were combined in the form of a ratio and related to dimensionless groups incorporating the main parameters that affect the thermal behaviour of BIPV/T. The correlation was verified through solar simulator testing of a modular BIPV/T system under varying environmental conditions, flow rate, geometry and PV transparency. The proposed modelling methodology provides a generalized approach for different system types and climates and is primarily intended for the control stage of a BIPV/T system, for which accurate predictions of the supply air temperature are required with optimal flow rate. However, it also provides a foundation for the comparison of the performance of different BIPV/T and PV/T systems, due to its generalized form. This methodology can be tailored to individual systems via calibration through key temperatures monitoring and can be instrumental in the optimal control and heat utilization for a coupled BIPV/T-HVAC system, as well as increased durability and performance of the PV system through incorporation of more efficient cooling strategies, through accurate supply (outlet) air temperature and PV temperature predictions, respectively.

The main conclusions of the work presented in this thesis can be summarized as follows:

Regarding BIPV/T design:

- The curtain wall design concept presented can be readily implemented as a standardized design method for BIPV/T systems for the opaque and spandrel parts of the façade, maintaining the main function of the building envelope in terms of heat, air, and moisture transfer.

- Building-integrated systems can benefit from easily implemented thermal enhancements such as the use of multiple inlets and, as introduced in the present work, a flow deflector unit. These enhancements were found to significantly improve the thermal performance of an experimental BIPV/T curtain wall prototype by up to 16%, marginally improve the electrical performance and decrease the maximum PV temperatures by up to almost 4ºC. Furthermore, the use of semi-transparent PV increased the heat recovery from the rear surface of the air channel. Increasing PV transparency was found to increase the thermal performance but at the cost of the electrical performance.

Regarding BIPV/T modelling:

- Air-based BIPV/T modelling is highly inconsistent, especially with regards to wind-driven and air channel convective heat transfer. The use of relevant expressions, commonly used in the respective literature, is case specific and can have different degree of modelling accuracy among different system types and testing conditions. This was showcased through the analysis of multiple case studies, including previous and present experimental work and comparison of monitored data to modelled results using different combinations of the most commonly used convective heat transfer expressions.

- The investigation of Nu correlations presented in previous studies referring to the exact same BIPV/T design but tested under different conditions (solar simulator testing, outdoor testing, and full-scale installation) showed that these expressions can vary considerably. This signifies the importance of operating/boundary conditions on the evaluation of the Nu number. The same was true for wind-driven convection, indicating a strong link between the convective phenomena on either side of the PV panel in a BIPV/T system.

- A strong correlation between the ratio of exterior heat transfer over the heat recovered to the environmental conditions, the flow rate, and the geometry of the system was established though the experimental investigation of a modular BIPV/T setup. The proposed methodology was used to predict the outlet temperature of the specimen and showed very good agreement with experimental findings, as well as superior performance to models implementing different combinations of commonly used CHTC and Nu expressions from literature.

6.1 Contributions:

This intent of this thesis has been to address issues pertinent to the lack of design standardization for air-based BIPV/T systems, and the inconsistency testing and modelling of said systems. The main contributions can be summarized as follows:

- Introduction of the curtain wall concept in BIPV/T design as a complete building envelope solution. A BIPV/T curtain wall prototype was designed and developed within a frame of architectural, structural and building envelope considerations, and provided a foundation for the implementation of common building techniques in BIPV/T design. The proposed system has been implemented in two research buildings as a façade and roof applications (Deep Performance Dwelling – Solar Decathlon, 2018; CFI Research Facility, Concordia University).

- Thermal enhancements suitable for and easily incorporated in building integrated systems, including the use of STPV, multiple inlets and a newly introduced flow deflector have been studied experimentally.
- A thorough investigation in the applicability of commonly used expressions for convective heat transfer has been carried out, through the analysis of multiple case studies from existing and present experimental work. This analysis indicated that use of said correlations can be highly case-specific, while correlations developed for the same system could vary considerably under different operating conditions.
- Introduction of a novel approach for the modelling of convective phenomena, in which wind-driven and channel convection are treated as interlinked and not as independent phenomena. This involved the introduction of a new dimensionless number that incorporates the effect of the boundary conditions (irradiance, wind and ambient temperature). The irradiance term has been modified in order to account for the PV efficiency and the optical properties of the system, thus being independent of the system type.
- The development of a methodology, based on the proposed modelling approach that can be easily implemented in the controls of a BIPV/T system, for which accurate predictions of the supply air temperature are required. The proposed modelling methodology involves a calibration stage where the correlation between the ratio of exterior heat transfer over the heat recovery and the dimensionless groups of the affecting parameters is established. Then a simple energy balance can be solved to evaluate the outlet air temperature. This methodology also provides a foundation for the comparison of the performance of different BIPV/T and PV/T systems, due to its generalized form, and the creation of a library of BIPV/T case studies for engineering reference.
- The design and early control approaches presented in this thesis have been implemented in the study of:
    - A coupled BIPV/T - air-source heat pump - thermal energy storage system for a residential building in a cold climate.
    - A coupled BIPV/T - desiccant cooling system for a warm and humid climate (India-Canada Centre for Innovative Multidisciplinary Partnerships to Accelerate Community Transformation and Sustainability – IC IMPACTS)

6.2 List of publications

The work presented in this thesis has produced several journal and conference publications, which are summarized as follows:

Journal publications:

Rounis, E. D., Athienitis, A. K., & Stathopoulos, T. (2021a). BIPV / T curtain wall systems : Design , development and testing. Journal of Building Engineering, 42(July), 103019.

Rounis, E. D., Athienitis, A., & Stathopoulos, T. (2021b). Review of air-based PV/T and BIPV/T systems - Performance and modelling. Renewable Energy, 163, 1729–1753.

Rounis, E.D., Ioannidis Z., Sigounis, A.M., Athienitis, A., & Stathopoulos, T. A Novel Approach for the Modelling of Convective Phenomena for Building Integrated Photovoltaic Thermal (BIPV/T) Systems - Submitted to the Journal of Solar Energy.

Ioannidis, Z., Rounis, E., Athienitis, A., & Stathopoulos, T. (2020). Double skin façade integrating semi-transparent photovoltaics: Experimental study on forced convection and heat recovery. Applied Energy, 278.

Dumoulin, R., Rounis, E. D., & Athienitis, A. (2021). Operation and grid interaction modeling of a house with a building integrated photovoltaic thermal (BIPV/T) system coupled to an air-source heat pump. Science and Technology for the Built Environment, 0(0), 1–19.

Conference publications

Rounis, E. D., Ioannidis, Z., Dumoulin, R., Kruglov, O., Athienitis, A. K., & Stathopoulos, T. (2018). Design and performance assessment of a prefabricated BIPV/T roof system coupled with a heat pump. Proceedings of the 12th EuroSun Conference.

Rounis, E. D., Kruglov, O., Ioannidis, Z., Athienitis, A. K., & Stathopoulos, T. (2017). Experimental investigation of BIPV/T envelope system with thermal enhancements for roof and curtain wall applications. Proceedings of the 34th European PV Solar Energy Conference (EU PVSEC).

Kruglov, O., Rounis, E. D., Athienitis, A. K., & Ge, H. (2017). Experimental investigation and implementation of a multiple-inlet BIPV/T system in a curtain wall. Proceedings of the 15th Canadian Conference on Building Science and Technology (CCBST).

Nibandhe, A., Bonvadi, N., Rounis, E. D., Lee, B., Athienitis, A. K., & Bagchi, A. (2019). Design of a coupled BIPV/T - Solid desiccant cooling system for a warm and humid climate. Proceedings of the ISES Solar World Congress 2019 and IEA SHC International Conference on Solar Heating and Cooling for Buildings and Industry.

6.3 Outlook and future research needs

In order to achieve wider adoption of BIPV/T in the built environment, the following research needs have been identified in terms of design, testing and characterization, and modelling and control optimization:

- Building integration:
    - Investigation of design solutions for both new buildings and retrofits, which adhere to commonly used building practices (i.e., curtain wall, wood/masonry structures etc.), which can lead to design standardization and simplification of the construction process.
    - Incorporation of modularity, prefabrication and the plug-and-play concept that can further simplify the construction process and quality, facilitate easier system maintenance and bring down fabrication costs.
    - Investigation of details such as the facilitation of hidden wiring and junction boxes, building envelope continuity, as well as manifold design and ducting for the connection to the HVAC system.
    - Micro-inverters or inverters with optimizers can be considered as potential options for PV connectivity, which can help reduce the effects of partial shading from nearby structures/obstacles as well as allow for easier module replacement.
    - Integration of smart local controllers to control the air flow so as to obtain a desired outlet temperature that matches the application (i.e. fresh air heating versus source for a heat pump).
- Testing and characterization standardization:

  Before developing a framework for standardized PV/T and BIPV/T system testing, it is important to consider the following challenges:

    - Indoor testing can provide repeatable conditions, however, access to a solar simulator with an artificial sky may be a limiting factor, while there can be considerable differences from simulator to simulator (irradiance range, AM spectrum, ability to simulate wind etc.). Furthermore, as was seen from the studies of Candanedo et al (2011) and Yang & Athienitis (2014), indoors and outdoors study of the same BIPV/T prototype resulted in the development of different Nu correlations, therefore indoors conditions may not always reflect the actual conditions, even with the inclusion of an artificial sky.
    - Outdoor testing allows for testing of the system’s performance under realistic conditions, which are however very difficult to repeat and/or maintain.

- There is no single PV/T or BIPV/T design. This makes a direct comparison between different design types very difficult and very dependent on wind conditions.

According to these considerations, a methodology involving indoor and outdoor testing of a reference PV/T system could be developed. The reference system can serve as a benchmark against which developed PV/T and BIPV/T prototypes will be compared. Indoor testing under specified reference conditions similar to the standard testing conditions for PV, but with an artificial sky, will provide the nominal performance metrics for the system. The reference system's performance under realistic conditions can be carried out with outdoor testing and corrective factors ban be established to correlate the indoor and outdoor performance. When a new PV/T or BIPV/T system is being developed its nominal performance metrics can be deduced by side-by-side testing against a recreated reference system and with use of the appropriate corrective factors. The basic steps of such a method could be summarized as follows:

- Establishment of the necessary metrics for the characterization of and comparison between different PV/T and BIPV/T technologies (different configurations, thermal enhancements, etc.).
- Establishment of a reference system that is easy to reconstruct and will provide a benchmark for the performance of other prototypes.
- Establishment of a set of reference testing conditions for indoors testing (environmental conditions and flow rate) which will be used for the characterization of the nominal performance of the reference system and test subjects.
- Additional testing under a range of different operating conditions (environmental conditions, flow rate) to develop performance curves for the system. The performance curves should ideally be provided in dimensionless form (with use of dimensional analysis) in order to provide a higher degree of generalization and independence from the explicit conditions themselves.
- Outdoor testing of the reference system and development of correction factors correlating to the indoor performance.
- The characterization of a new PV/T and BIPV/T prototype can then take place with side-by-side testing against a reference system and using the respective correction factors.

- Coupled performance with the HVAC:

  BIPV/T is only part of the overall system. Simple and efficient thermal applications such as ventilation air preheating and boosting of an air-source heat pump seem to be promising solutions. BIPV/T coupling with the HVAC has to be optimized accordingly depending on the intended thermal application (i.e. building energy flexibility involves the air-source heat pump, thermal energy storage etc.).

It is important to create a library of case studies that can be informative to engineers and potential clients. Lack of case studies can be alleviated in two possible ways:

- With extensive numerical studies on archetype buildings and different climates, to evaluate the contribution of BIPV/T for different thermal applications, optimize/investigate required BIPV/T coverage etc.
- With incentives for research and development in the industry to develop standardized products and full-scale demonstration projects that can highlight the performance of such systems, as well as their architectural value within the building context.

Eventually studies need to extend from the building to the district level where strategic placement of BIPV/T systems within a densely built environment, optimal district planning, as well as district electrical and thermal storage can be investigated.

References

Adeli, M. M., Sobhnamayan, F., Farahat, S., Alavi, M. A., & Sarhaddi, F. (2012). Experimental performance evaluation of a photovoltaic thermal (PV/T) air collector and its optimization. *Strojniski Vestnik/Journal of Mechanical Engineering*, *58*(5), 309–318. https://doi.org/10.5545/sv-jme.2010.007

Agathokleous, R. A., Kalogirou, S. A., & Karellas, S. (2017). Exergy analysis of a naturally ventilated Building Integrated Photovoltaic/Thermal (BIPV/T) system. *Renewable Energy*, 1–12. https://doi.org/10.1016/j.renene.2017.06.085

Agrawal, B., & Tiwari, G. N. (2010). Optimizing the energy and exergy of building integrated photovoltaic thermal (BIPVT) systems under cold climatic conditions. *Applied Energy*, *87*(2), 417–426. https://doi.org/10.1016/j.apenergy.2009.06.011

Agrawal, S., & Tiwari, A. (2011). Experimental validation of glazed hybrid micro-channel solar cell thermal tile. *Solar Energy*, *85*(11), 3046–3056. https://doi.org/10.1016/j.solener.2011.09.003

Ahn, J. G., Kim, J. H., & Kim, J. T. (2015). A study on experimental performance of air-type PV/T collector with HRV. *Energy Procedia*, *78*, 3007–3012. https://doi.org/10.1016/j.egypro.2015.11.705

Al-Waeli, A. H. A., Sopian, K., Kazem, H. A., & Chaichan, M. T. (2017). Photovoltaic/Thermal (PV/T) systems: Status and future prospects. *Renewable and Sustainable Energy Reviews*, *77*(April), 109–130. https://doi.org/10.1016/j.rser.2017.03.126

Amori, K. E., & Abd-AlRaheem, M. A. (2014). Field study of various air based photovoltaic/thermal hybrid solar collectors. *Renewable Energy*, *63*, 402–414. https://doi.org/10.1016/j.renene.2013.09.047

Assoa, Y. B., & Ménézo, C. (2014). Dynamic study of a new concept of photovoltaic-thermal hybrid collector. *Solar Energy*, *107*, 637–652. https://doi.org/10.1016/j.solener.2014.05.035

Assoa, Ya Brigitte, Mongibello, L., Carr, A., Kubicek, B., Machado, M., Merten, J., Misara, S., Roca, F., Sprenger, W., Wagner, M., Zamini, S., Baenas, T., & Malbranche, P. (2017). Thermal analysis of a BIPV system by various modelling approaches. *Solar Energy*, *155*, 1289–1299. https://doi.org/10.1016/j.solener.2017.07.066

Aste, N., Del Pero, C., & Leonforte, F. (2017). Water PVT Collectors Performance Comparison.

Energy Procedia, *105*, 961–966.

Aste, Niccolò, Chiesa, G., & Verri, F. (2008). Design, development and performance monitoring of a photovoltaic-thermal (PVT) air collector. *Renewable Energy*, *33*(5), 914–927. https://doi.org/10.1016/j.renene.2007.06.022

Athienitis, A. K., Barone, G., Buonomano, A., & Palombo, A. (2018). Assessing active and passive effects of façade building integrated photovoltaics/thermal systems: Dynamic modelling and simulation. *Applied Energy*, *209*(August 2017), 355–382. https://doi.org/10.1016/j.apenergy.2017.09.039

Badescu, V. (2002). Model of a space heating system integrating a heat pump, photothermal collectors and solar cells. *Renewable Energy*, *27*(4), 489–505. https://doi.org/10.1016/S0960-1481(01)00191-4

Badescu, V. (2003). Model of a thermal energy storage device integrated into a solar assisted heat pump system for space heating. *Energy Conversion and Management*, *44*(10), 1589–1604. https://doi.org/10.1016/S0196-8904(02)00184-X

Bakar, M. N. ., Othman, M., Din, M. H., Manaf, N. A., & Jarimi, H. (2014). Design concept and mathematical model of a bi-fluid photovoltaic/thermal (PV/T) solar collector. *Renewable Energy*, *67*, 153–164.

Bakari, R., Minja, R. J. A., & Njau, K. N. (2014). Effect of Glass Thickness on Performance of Flat Plate Solar Collectors for Fruits Drying. *Journal of Energy*, *2014*(August 2015), 1–8. https://doi.org/10.1155/2014/247287

Bakirci, K., & Yuksel, B. (2011). Experimental thermal performance of a solar source heat-pump system for residential heating in cold climate region. *Applied Thermal Engineering*, *31*(8–9), 1508–1518. https://doi.org/10.1016/j.applthermaleng.2011.01.039

Bakker, M., Zondag, H. A., Elswijk, M. J., Strootman, K. J., & Jong, M. J. M. (2005). Performance and costs of a roof-sized PV/thermal array combined with a ground coupled heat pump. *Solar Energy*, *78*(2), 331–339. https://doi.org/10.1016/j.solener.2004.09.019

Balocco, C. (2004). A non-dimensional analysis of a ventilated double fa??ade energy performance. *Energy and Buildings*, *36*(1), 35–40. https://doi.org/10.1016/S0378-7788(03)00086-0

Bambara, J., Athienitis, A. K., & O'Neill, B. (2011). Design and performance of a photovoltaic/thermal system integrated with transpired collector. *ASHRAE Transactions*, *117*(PART 2), 403–410. https://doi.org/10.1016/j.solener.2010.10.008

Bambrook, S. M., & Sproul, A. B. (2012). Maximising the energy output of a PVT air system. *Solar Energy*, *86*(6), 1857–1871. https://doi.org/10.1016/j.solener.2012.02.038

Bazilian, M. D., & Prasad, D. (2002). Modelling of a photovoltaic heat recovery system and its role in a design decision support tool for building professionals. *Renewable Energy*, *27*(1), 57–68. https://doi.org/10.1016/S0960-1481(01)00165-3

Beccali, M., Finocchiaro, P., & Nocke, B. (2009). Energy and economic assessment of desiccant cooling systems coupled with single glazed air and hybrid PV/thermal solar collectors for applications in hot and humid climate. *Solar Energy*, *83*(10), 1828–1846. https://doi.org/10.1016/j.solener.2009.06.015

Bergene, T., & Løvvik, O. M. (1995). Model calculations on a flat-plate solar heat collector with integrated solar cells. *Solar Energy*, *55*(6), 453–462. https://doi.org/10.1016/0038-092X(95)00072-Y

Bigaila, E., & Athienitis, A. K. (2017). Modeling and simulation of a photovoltaic/thermal air collector assisting a façade integrated small scale heat pump with radiant PCM panel. *Energy and Buildings*, *149*, 298–309. https://doi.org/10.1016/j.enbuild.2017.05.045

Bigorajski, J., & Chwieduk, D. (2018). Analysis of a micro photovoltaic/thermal - PV/T system operation in moderate climate. *Renewable Energy*, 1–10. https://doi.org/10.1016/j.renene.2018.01.116

Biyik, E., Araz, M., Hepbasli, A., Shahrestani, M., Yao, R., Shao, L., Essah, E., Oliveira, A. C., del Caño, T., Rico, E., Lechón, J. L., Andrade, L., Mendes, A., & Atlı, Y. B. (2017). A key review of building integrated photovoltaic (BIPV) systems. *Engineering Science and Technology, an International Journal*, *20*(3), 833–858. https://doi.org/10.1016/j.jestch.2017.01.009

Bombarda, P., Marcoberardino, G. Di, Lucchini, A., Leva, S., Manzolini, G., Molinaroli, L., Pedranzini, F., & Simonetti, R. (2016). *Thermal and electric performances of roll-bond flat plate applied to conventional PV modules for heat recovery*. *105*, 304–313. https://doi.org/10.1016/j.applthermaleng.2016.05.172

Brahim, T., & Jemni, A. (2017). Economical assessment and applications of photovoltaic/thermal hybrid solar technology: A review. *Solar Energy*, *153*, 540–561. https://doi.org/10.1016/j.solener.2017.05.081

Brideau, S. A., & Collins, M. R. (2012). Experimental model validation of a hybrid PV/thermal air based collector with impinging jets. *Energy Procedia*, *30*, 44–54. https://doi.org/10.1016/j.egypro.2012.11.007

Candanedo, L. M., Athienitis, A. K., Candanedo, J., O'Brien, W., & Chen, Y. (2010). Transient-and-steady-state-models-for-open-loop-air-based-BIPV-T-systems.pdf. *ASHRAE Transactions*, *116*, 600–612.

Candanedo, L. M., Athienitis, A., & Park, K.-W. (2011). Convective Heat Transfer Coefficients in a Building-Integrated Photovoltaic/Thermal System. *Journal of Solar Energy Engineering*, *133*(2), 021002. https://doi.org/10.1115/1.4003145

Candanedo, L. M., O'Brien, W., & Athienitis, A. K. (2009). Development of an Air-Based Open Loop Building-Integrated Photovoltaic/Thermal System Model. *Proceedings of the Building Simulation*.

Charron, R., & Athienitis, A. K. (2006). Optimization of the performance of double-façades with integrated photovoltaic panels and motorized blinds. *Solar Energy*, *80*(5), 482–491. https://doi.org/10.1016/j.solener.2005.05.004

Chen, Y., Athienitis, A. K., & Galal, K. (2010). Modeling, design and thermal performance of a BIPV/T system thermally coupled with a ventilated concrete slab in a low energy solar house: Part 1, BIPV/T system and house energy concept. *Solar Energy*, *84*(11), 1892–1907. https://doi.org/10.1016/j.solener.2010.06.013

Chow, T. T., He, W., & Ji, J. (2006). Hybrid photovoltaic-thermosyphon water heating system for residential application. *Solar Energy*, *80*(3), 298–306. https://doi.org/10.1016/j.solener.2005.02.003

Debbarma, M., Sudhakar, K., & Baredar, P. (2017). Thermal modeling, exergy analysis, performance of BIPV and BIPVT: A review. *Renewable and Sustainable Energy Reviews*, *73*(August 2015), 1276–1288. https://doi.org/10.1016/j.rser.2017.02.035

Delisle, V., & Kummert, M. (2016). Cost-benefit analysis of integrating BIPV-T air systems into energy-efficient homes. *Solar Energy*, *136*, 385–400. https://doi.org/10.1016/j.solener.2016.07.005

Dermadiros, V., Athienitis, A. K., & Bucking, S. (2019). Energy Performance, Comfort, and Lessons Learned from an Institutional Building Designed for Net Zero Energy. *ASHRAE Transactions*, *125*, 682+.

Dittus. (1985). *Heat Transfer in Automobile Radiators*. *12*, 3–22.

Dubey, S., Solanki, S. C., & Tiwari, A. (2009). Energy and exergy analysis of PV/T air collectors connected in series. *Energy and Buildings*, *41*(8), 863–870. https://doi.org/10.1016/j.enbuild.2009.03.010

Duffie, J. a., Beckman, W. a., & Worek, W. M. (2003). Solar Engineering of Thermal Processes, 4nd ed. In *Journal of Solar Energy Engineering* (Vol. 116). https://doi.org/10.1115/1.2930068

Dumoulin, R., Rounis, E. D., & Athienitis, A. (2021). Operation and grid interaction modeling of a house with a building integrated photovoltaic thermal (BIPV/T) system coupled to an air-source heat pump. *Science and Technology for the Built Environment*, *0*(0), 1–19. https://doi.org/10.1080/23744731.2021.1941247

Elbreki, A. M., Alghoul, M. A., Al-Shamani, A. N., Ammar, A. A., Yegani, B., Aboghrara, A. M., Rusaln, M. H., & Sopian, K. (2016). The role of climatic-design-operational parameters on combined PV/T collector performance: A critical review. *Renewable and Sustainable Energy Reviews*, *57*, 602–647. https://doi.org/10.1016/j.rser.2015.11.077

Faiman, D. (2008). Assessing the outdoor operating temperature of photovoltaic modules. In *Progress in Photovoltaics: Research and Applications* (Vol. 16, Issue 4, pp. 307–315). https://doi.org/10.1002/pip.813

Farshchimonfared, M., Bilbao, J. I., & Sproul, A. B. (2015). Channel depth, air mass flow rate and air distribution duct diameter optimization of photovoltaic thermal (PV/T) air collectors linked to residential buildings. *Renewable Energy*, *76*, 27–35. https://doi.org/10.1016/j.renene.2014.10.044

Florschuetz, L. W. (1979). Extension of the Hottel-Whillier model to the analysis of combined photovoltaic/thermal flat plate collectors. *Solar Energy*, *22*(4), 361–366. https://doi.org/10.1016/0038-092X(79)90190-7

Fong, K. F., Chow, T. T., Lee, C. K., Lin, Z., & Chan, L. S. (2010). Comparative study of different solar cooling systems for buildings in subtropical city. *Solar Energy*, *84*(2), 227–244. https://doi.org/10.1016/j.solener.2009.11.002

Gaillard, L., Giroux-Julien, S., Ménézo, C., & Pabiou, H. (2014). Experimental evaluation of a naturally ventilated PV double-skin building envelope in real operating conditions. *Solar Energy*, *103*, 223–241. https://doi.org/10.1016/j.solener.2014.02.018

Gang, P., Jie, J., Wei, H., Keliang, L., & Hanfeng, H. (2007). Performance of Photovoltaic Solar Assisted Heat Pump System in Typical Climate Zone. *Energy*, *6*(May), 1–9.

Garg, H. P., & Adhikari, R. S. (1997). Conventional hybrid photovoltaic/thermal (PV/T) air heating collectors: steady-state simulation. *Renewable Energy*, *11*(3), 363–385. https://doi.org/10.1016/S0960-1481(97)00007-4

Ghani, F., Duke, M., & Carson, J. K. (2012). Effect of flow distribution on the photovoltaic performance of a building integrated photovoltaic/thermal (BIPV/T) collector. *Solar Energy*, *86*(5), 1518–1530. https://doi.org/10.1016/j.solener.2012.02.013

Gnielinski, V. (1983). *Forced convection in ducts, heat exchanger design handbook*. Hemisphere.

Gommed, K., & Grossman, G. (2007). Experimental investigation of a liquid desiccant system for solar cooling and dehumidification. *Solar Energy*, *81*(1), 131–138. https://doi.org/10.1016/j.solener.2006.05.006

Guiavarch, A., & Peuportier, B. (2006). Photovoltaic collectors efficiency according to their integration in buildings. *Solar Energy*, *80*(1), 65–77. https://doi.org/10.1016/j.solener.2005.07.004

Guo, J., Lin, S., Bilbao, J. I., White, S. D., & Sproul, A. B. (2017). A review of photovoltaic thermal (PV/T) heat utilisation with low temperature desiccant cooling and dehumidification. *Renewable and Sustainable Energy Reviews*, *67*, 1–14. https://doi.org/10.1016/j.rser.2016.08.056

Hamrouni, N., Jraidi, M., & Chérif, A. (2008). Solar radiation and ambient temperature effects on the performances of a PV pumping system. *Revue Des Energies Renouvelables*, *11*(1), 95–106. https://www.cder.dz/spip.php?article287

Hegazy, A. A. (2000). Comparative study of the performances of four photovoltaic / thermal solar air collectors. *Energy Conversion and Management*, *41*.

Hussain, F., Othman, M. Y. H., Sopian, K., Yatim, B., Ruslan, H., & Othman, H. (2013). Design development and performance evaluation of photovoltaic/thermal (PV/T) air base solar collector. *Renewable and Sustainable Energy Reviews*, *25*, 431–441. https://doi.org/10.1016/j.rser.2013.04.014

Hussain, F., Othman, M. Y. H., Yatim, B., Ruslan, H., Sopian, K., Anuar, Z., & Khairuddin, S. (2015). An improved design of photovoltaic/thermal solar collector. *Solar Energy*, *122*, 885–891. https://doi.org/10.1016/j.solener.2015.10.008

IEA SHC TASK 56. (2020). *Report on test methods and recommendations Report on test methods and recommendations*. https://doi.org/10.18777/ieashc-task56-2020-0003

IEC 61730-1. (2020). *Photovoltaics in buildings – Part 1*.

IEC 61730-2. (2020). *Photovoltaics in buildings – Part 2*.

Infield, D., Eicker, U., Fux, V., Mei, L., & Schumacher, J. (2006). A simplified approach to thermal performance calculation for building integrated mechanically ventilated PV facades. *Building and Environment*, *41*(7), 893–901. https://doi.org/10.1016/j.buildenv.2005.04.010

International Energy Agency. (2014). *Technology Roadmap – Solar Photovoltaic Energy*.

International Energy Agency. (2017). *World energy outlook*.

International Energy Agency Photovoltaic Power Systems Programme. (2018). *Snapshot of global photovoltaic markets*.

International Energy Agency Photovoltaic Power Systems Programme. (2019a). *Annual Report*.

International Energy Agency Photovoltaic Power Systems Programme. (2019b). *Trends in Photovoltaic Applications*.

International Renewable Energy Agency. (2019). IRENA (2019), Global Energy Transformation: A Roadmap to 2050. In *Global Energy Transformation. A Roadmap to 2050*. https://www.irena.org/publications/2019/Apr/Global-energy-transformation-A-roadmap-to-2050-2019Edition

Ioannidis, Z., Rounis, E., Athienitis, A., & Stathopoulos, T. (2020). Double skin façade integrating semi-transparent photovoltaics : Experimental study on forced convection and heat recovery. *Applied Energy*, *278*(March), 115647. https://doi.org/10.1016/j.apenergy.2020.115647

Jelle, B. P., & Breivik, C. (2012). State-of-the-art building integrated photovoltaics. *Energy Procedia*, *20*(1876), 68–77. https://doi.org/10.1016/j.egypro.2012.03.009

Jin, G. L., Ibrahim, A., Chean, Y. K., Daghigh, R., Ruslan, H., Mat, S., Othman, M. Y., & Sopian, K. (2010). Evaluation of single-pass photovoltaic-thermal air collector with rectangle tunnel absorber. *American Journal of Applied Sciences*, *7*(2), 277–282. https://doi.org/10.3844/ajassp.2010.277.282

Joshi, A. S., Tiwari, A., Tiwari, G. N., Dincer, I., & Reddy, B. V. (2009). Performance evaluation of a hybrid photovoltaic thermal (PV/T) (glass-to-glass) system. *International Journal of Thermal Sciences*, *48*(1), 154–164. https://doi.org/10.1016/j.ijthermalsci.2008.05.001

Joshi, S. S., & Dhoble, A. S. (2018). Photovoltaic -Thermal systems (PVT): Technology review and future trends. *Renewable and Sustainable Energy Reviews*, *92*(June 2017), 848–882. https://doi.org/10.1016/j.rser.2018.04.067

Kaiser, A. S., Zamora, B., Mazo´n, R., Garci´a, J. R., & Vera, F. (2014). Experimental study of cooling BIPV modules by forced convection in the air channel. *Applied Energy*, *135*, 88–97. https://doi.org/10.1016/j.apenergy.2014.08.079

Kamel, R. S., & Fung, A. S. (2014a). Modeling, simulation and Feasibility analysis of Residential bipv/t+ashp System in cold climate-Canada. *Energy and Buildings*, *82*, 758–770. https://doi.org/10.1016/j.enbuild.2014.07.081

Kamel, R. S., & Fung, A. S. (2014b). Modeling, simulation and feasibility analysis of residential BIPV/T+ASHP system in cold climate - Canada. *Energy and Buildings*, *82*, 758–770. https://doi.org/10.1016/j.enbuild.2014.07.081

Kamel, R. S., Fung, A. S., & Dash, P. R. H. (2015). Solar systems and their integration with heat pumps: A review. *Energy and Buildings*, *87*, 395–412. https://doi.org/10.1016/j.enbuild.2014.11.030

Kapsis, K., Athienitis, A. K., & Harrison, S. J. (2016). Determination of solar heat gain coefficient for semi-transparent photovoltaic windows: an experimental study. *ASHRAE Transactions*, *125*.

Karava, P., Mohammad Jubayer, C., Savory, E., & Li, S. (2012). Effect of incident flow conditions on convective heat transfer from the inclined windward roof of a low-rise building with application to photovoltaic-thermal systems. *Journal of Wind Engineering and Industrial Aerodynamics*, *104–106*(11–12), 428–438. https://doi.org/10.1016/j.jweia.2012.03.026

Karim, M. A., & Hawlader, M. N. A. (2006). Performance evaluation of a v-groove solar air collector for drying applications. *Applied Thermal Engineering*, *26*(1), 121–130. https://doi.org/10.1016/j.applthermaleng.2005.03.017

Kays, W. M. (1996). *Convective heat and mass transfer. Hemisphere Publishing*. Hemisphere Publishing Corporation.

Kim, J. H., Park, S. H., & Kim, J. T. (2014). Experimental performance of a photovoltaic-thermal air collector. *Energy Procedia*, *48*, 888–894. https://doi.org/10.1016/j.egypro.2014.02.102

King, D. L., Boyson, W. E., & Kratochvil, J. A. (2004). Photovoltaic array performance model. *Sandia Report No. 2004-3535*, *8*(December), 1–19. https://doi.org/10.2172/919131

Koech, R., Ondieki, H., Tonui, J., & Rotich, S. (2012). A Steady State Thermal Model For Photovoltaic/Thermal (PV/T) System Under Various Conditions. *Ijstr.Org*, *1*(11), 1–5. http://www.ijstr.org/final-print/dec2012/A-Steady-State-Thermal-Model-For-Photovoltaicthermal-Pvt-System-Under-Various-Conditions.pdf

Kruglov, O., Rounis, E. D., Athienitis, A. K., & Ge, H. (2017). Experimental investigation and implementation of a multiple-inlet BIPV/T system in a curtain wall. *Proceedings of the 15th Canadian Conference on Building Science and Technology (CCBST)*.

Kuang, Y. H., Wang, R. Z., & Yu, L. Q. (2003). Experimental study on solar assisted heat pump system for heat supply. *Energy Conversion and Management*, *44*(7), 1089–1098. https://doi.org/10.1016/S0196-8904(02)00110-3

Kumar, R., & Rosen, M. A. (2011a). A critical review of photovoltaic-thermal solar collectors for air heating. *Applied Energy*, *88*(11), 3603–3614. https://doi.org/10.1016/j.apenergy.2011.04.044

Kumar, R., & Rosen, M. A. (2011b). Performance evaluation of a double pass PV/T solar air heater with and without fins. *Applied Thermal Engineering*, *31*(8–9), 1402–1410. https://doi.org/10.1016/j.applthermaleng.2010.12.037

Ladas, D. I., Stathopoulos, T., & Rounis, E. D. (2017). Wind effects on the performance of solar collectors on rectangular flat roofs: A wind tunnel study. *Journal of Wind Engineering and Industrial Aerodynamics*, *161*(November 2016), 27–41. https://doi.org/10.1016/j.jweia.2016.12.008

Lamnatou, C., & Chemisana, D. (2017). Photovoltaic/thermal (PVT) systems: A review with emphasis on environmental issues. *Renewable Energy*, *105*, 270–287. https://doi.org/10.1016/j.renene.2016.12.009

Li, H., Dai, Y. J., Li, Y., La, D., & Wang, R. Z. (2011). Experimental investigation on a one-rotor two-stage desiccant cooling/heating system driven by solar air collectors. *Applied Thermal Engineering*, *31*(17–18), 3677–3683.

https://doi.org/10.1016/j.applthermaleng.2011.01.018

Li, Huixing, Cao, C., Feng, G., Zhang, R., & Huang, K. (2015). A BIPV/T System Design Based on Simulation and its Application in Integrated Heating System. *Procedia Engineering*, *121*, 1590–1596. https://doi.org/10.1016/j.proeng.2015.09.184

Liang, C. H., Zhang, X. S., Li, X. W., & Zhu, X. (2011). Study on the performance of a solar assisted air source heat pump system for building heating. *Energy and Buildings*, *43*(9), 2188–2196. https://doi.org/10.1016/j.enbuild.2011.04.028

Liao, L., Athienitis, A. K., Candanedo, L. M., Park, K.-W., Poissant, Y., & Collins, M. R. (2007). Numerical and experimental study of heat transfer in a BIPV/T system. *ASME J Sol Energy Eng*, *116*, 423–430.

Malik, M. A. S., & Buelow, F. H. (1973). Heat Transfer Characteristics of a Solar Drier. *Proceedings of the Sun Service Mankind, UNESCO Congress*.

Malvi, C. S., Dixon Hardy, D. W., & Crook, R. (2011). Energy balance model of combined photovoltaic solar-thermal system incorporating phase change material. *Solar Energy*, *85*, 1440–1446.

McAdams, W. H. (1954). *Heat Transmission Series in Chemical Engineering*. McGraw-Hill.

Mei, L., Infield, D., Eicker, U., & Fux, V. (2003). Thermal modelling of a building with an integrated ventilated PV fa??ade. *Energy and Buildings*, *35*(6), 605–617. https://doi.org/10.1016/S0378-7788(02)00168-8

Mekhilef, S., Saidur, R., & Kamalisarvestani, M. (2012). Effect of dust, humidity and air velocity on efficiency of photovoltaic cells. *Renewable and Sustainable Energy Reviews*, *16*(5), 2920–2925. https://doi.org/10.1016/j.rser.2012.02.012

Mercer, W. E., Pearce, W. M., & Hitchcock, J. E. (1967). Laminar Forced Convection in the Entrance Region Between Parallel Flat Plates. *Journal of Heat Transfer*, *89*(3), 251. https://doi.org/10.1115/1.3614373

Michael, J. J., S, I., & Goic, R. (2015). Flat plate solar photovoltaic-thermal (PV/T) systems: A reference guide. *Renewable and Sustainable Energy Reviews*, *51*, 62–88. https://doi.org/10.1016/j.rser.2015.06.022

Mills, A. F. (1999). *Heat Transfer* (2nd ed.). University of California.

Mirzaei, P. A., Paterna, E., & Carmeliet, J. (2014). Investigation of the role of cavity airflow on the performance of building-integrated photovoltaic panels. *Solar Energy*, *107*, 510–522.

https://doi.org/10.1016/j.solener.2014.05.003

Mojumder, J. C., Chong, W. T., Ong, H. C., Leong, K. Y., & Abdullah-Al-Mamoon. (2016). An experimental investigation on performance analysis of air type photovoltaic thermal collector system integrated with cooling fins design. *Energy and Buildings*, *130*, 272–285. https://doi.org/10.1016/j.enbuild.2016.08.040

Nahar, A., Hasanuzzaman, N., & Rahim, N. A. (2017). Numerical and experimental investigation on the performance of a photovoltaic thermal collector with parallel plate flow channel under different operating conditions in Malaysia. *Solar Energy*, *144*, 517–528.

Nemati, O., Ibarra, L. M. C., & Fung, A. S. (2016a). Review of computer models of air-based, curtainwall-integrated PV/T collectors. *Renewable and Sustainable Energy Reviews*, *63*, 102–117. https://doi.org/10.1016/j.rser.2016.04.026

Nemati, O., Ibarra, L. M. C., & Fung, A. S. (2016b). Review of computer models of air-based, curtainwall-integrated PV/T collectors. *Renewable and Sustainable Energy Reviews*, *63*, 102–117. https://doi.org/10.1016/j.rser.2016.04.026

Nibandhe, A., Bonvadi, N., Rounis, E. D., Lee, B., Athienitis, A. K., & Bagchi, A. (2019). Design of a coupled BIPV/T - Solid desiccant cooling system for a warm and humid climate. *Proceedings of the ISES Solar World Congress 2019 and IEA SHC International Conference on Solar Heating and Cooling for Buildings and Industry*.

Othman, M. Y. H., Hussain, F., Sopian, K., Yatim, B., & Ruslan, H. (2013). Performance study of air-based photovoltaic-thermal (PV/T) collector with different designs of heat exchanger. *Sains Malaysiana*, *42*(9), 1319–1325.

Othman, M. Y. H. J., Ruslan, H., Sopian, K., & Jin, G. L. (2009). Performance study of photovoltaic-thermal (PV/T) solar collector with ∇-grooved absorber plate | Kajian prestasi pengumpul suria fotovoltan-terma (PV/T) dengan plat penyerap lengkuk-∇. *Sains Malaysiana*, *38*(4).

Othman, M. Y. H., Yatim, B., Sopian, K., & Abu Bakar, M. N. (2005). Performance analysis of a double-pass photovoltaic/thermal (PV/T) solar collector with CPC and fins. *Renewable Energy*, *30*(13), 2005–2017. https://doi.org/10.1016/j.renene.2004.10.007

Othman, M. Y., Yatim, B., Sopian, K., & Abu Bakar, M. N. (2007). Performance studies on a finned double-pass photovoltaic-thermal (PV/T) solar collector. *Desalination*, *209*(1-3 SPEC. ISS.), 43–49. https://doi.org/10.1016/j.desal.2007.04.007

Palyvos, J. A. (2008). A survey of wind convection coefficient correlations for building envelope energy systems' modeling. *Applied Thermal Engineering*, *28*(8–9), 801–808. https://doi.org/10.1016/j.applthermaleng.2007.12.005

Pantic, S., Candanedo, L., & Athienitis, A. K. (2010). Modeling of energy performance of a house with three configurations of building-integrated photovoltaic/thermal systems. *Energy and Buildings*, *42*(10), 1779–1789. https://doi.org/10.1016/j.enbuild.2010.05.014

Pei, G., Ji, J., Chow, T. T., He, H., Liu, K., & Yi, H. (2008). Performance of the photovoltaic solar-assisted heat pump system with and without glass cover in winter: a comparative analysis. *Proceedings of the Institution of Mechanical Engineers, Part A: Journal of Power and Energy*, *222*(2), 179–187. https://doi.org/10.1243/09576509JPE431

Petukhov, B. S. (1976). *Turbulent Flow and Heat Transfer in Pipes Under Considerable Effect of Thermogravitational Forces*. Hemisphere Publishing Corporation.

Rajoria, C. S., Agrawal, S., Chandra, S., Tiwari, G. N., & Chauhan, D. S. (2016). A Novel investigation of building integrated photovoltaic thermal (BiPVT) system: A comparative study. *Solar Energy*, *131*, 107–118. https://doi.org/10.1016/j.solener.2016.02.037

Rounis, E. D., Athienitis, A. K., & Stathopoulos, T. (2016). Multiple-inlet Building Integrated Photovoltaic/Thermal system modelling under varying wind and temperature conditions. *Solar Energy*, *139*, 157–170. https://doi.org/10.1016/j.solener.2016.09.023

Rounis, E. D., Athienitis, A. K., & Stathopoulos, T. (2021a). BIPV / T curtain wall systems : Design , development and testing. *Journal of Building Engineering*, *42*(July), 103019. https://doi.org/10.1016/j.jobe.2021.103019

Rounis, E. D., Athienitis, A., & Stathopoulos, T. (2021b). Review of air-based PV/T and BIPV/T systems - Performance and modelling. *Renewable Energy*, *163*, 1729–1753. https://doi.org/10.1016/j.renene.2020.10.085

Rounis, E. D., Ioannidis, Z., Dumoulin, R., Kruglov, O., Athienitis, A. K., & Stathopoulos, T. (2018). Design and performance assessment of a prefabricated BIPV/T roof system coupled with a heat pump. *Proceedings of the 12th EuroSun Conference*.

Rounis, E. D., Kruglov, O., Ioannidis, Z., Athienitis, A. K., & Stathopoulos, T. (2017). Experimental investigation of BIPV/T envelope system with thermal enhancements for roof and curtain wall applications. *Proceedings of the 34th European PV Solar Energy Conference (EU PVSEC)*.

Sandnes, B., & Rekstad, J. (2002). A photovoltaic/thermal (PV/T) collector with a polymer absorber plate. Experimental study and analytical model. *Solar Energy*, *72*(1), 63–73. https://doi.org/10.1016/S0038-092X(01)00091-3

Sarhaddi, F., Farahat, S., Ajam, H., Behzadmehr, A., & Mahdavi Adeli, M. (2010). An improved thermal and electrical model for a solar photovoltaic thermal (PV/T) air collector. *Applied Energy*, *87*(7), 2328–2339. https://doi.org/10.1016/j.apenergy.2010.01.001

Saygin, H., Nowzari, R., Mirzaei, N., & Aldabbagh, L. B. Y. (2017). Performance evaluation of a modified PV/T solar collector: A case study in design and analysis of experiment. *Solar Energy*, *141*, 210–221. https://doi.org/10.1016/j.solener.2016.11.048

Shahsavar, A., & Ameri, M. (2010). Experimental investigation and modeling of a direct-coupled PV/T air collector. *Solar Energy*, *84*(11), 1938–1958. https://doi.org/10.1016/j.solener.2010.07.010

Sharples, S., & Charlesworth, P. S. (1998). Full-scale measurements of wind-induced convective heat transfer from a roof-mounted flat plate solar collector. *Solar Energy*, *62*(2), 69–77. https://doi.org/10.1016/S0038-092X(97)00119-9

Sohel, M. I., Ma, Z., Cooper, P., Adams, J., & Scott, R. (2014). A dynamic model for air-based photovoltaic thermal systems working under real operating conditions. *Applied Energy*, *132*, 216–225. https://doi.org/10.1016/j.apenergy.2014.07.010

Sopian, K., Alghoul, M. A., Alfegi, E. M., Sulaiman, M. Y., & Musa, E. A. (2009). Evaluation of thermal efficiency of double-pass solar collector with porous-nonporous media. *Renewable Energy*, *34*(3), 640–645. https://doi.org/10.1016/j.renene.2008.05.027

Sopian, K., Liu, H. T., Kakac, S., & Veziroglu, T. N. (2000). Performance of a double pass photovoltaic thermal solar collector suitable for solar drying systems. *Energy Conversion and Management*, *41*(4), 353–365. https://doi.org/10.1016/S0196-8904(99)00115-6

Tan, H. M., & Charters, W. W. S. (1969). Effect of Thermal Entrance Region on Turbulent Forced Convective Heat Transfer for an Asymmetrically Heated Rectangular Duct With Uniform Heat Flux. *Solar Energy*, *12*, 513–516.

Tan, H. M., & Charters, W. W. S. (1970). An Experimental Investigation of Forced Convective Heat Transfer for Fully Developed Turbulent Flow in a Rectangular Duct with Asymmetric Heating. *Solar Energy*, *13*, 121–125.

Teo, H. G., Lee, P. S., & Hawlader, M. N. A. (2012). An active cooling system for photovoltaic modules. *Applied Energy*, *90*(1), 309–315. https://doi.org/10.1016/j.apenergy.2011.01.017

TESSLibs 17. (2017). *Component libraries for the TRNSYS simulation environment. Vol. 3, Electrical library mathematical reference*.

Test, F. L., Lessmann, R. C., & Johary, A. (1981). Heat Transfer During Wind Flow ower Rectangular Bodies in the Natural Environment. *Transactions of the ASME*, *103*(May 1981), 262–267. https://doi.org/10.1115/1.3244451

Tiwari, A., & Sodha, M. S. (2007). Parametric study of various configurations of hybrid PV/thermal air collector: Experimental validation of theoretical model. *Solar Energy Materials and Solar Cells*, *91*(1), 17–28. https://doi.org/10.1016/j.solmat.2006.06.061

Tiwari, A., Sodha, M. S., Chandra, A., & Joshi, J. C. (2006). Performance evaluation of photovoltaic thermal solar air collector for composite climate of India. *Solar Energy Materials and Solar Cells*, *90*(2), 175–189. https://doi.org/10.1016/j.solmat.2005.03.002

Tiwari, S., Agrawal, S., & Tiwari, G. N. (2018). PVT air collector integrated greenhouse dryers. *Renewable and Sustainable Energy Reviews*, *90*(June 2017), 142–159. https://doi.org/10.1016/j.rser.2018.03.043

Tonui, J. K., & Tripanagnostopoulos, Y. (2006). Improved PV/T solar collectors with heat extraction by forced or natural air circulation. *International Journal of Hydrogen Energy*, *31*(15), 2137–2146. https://doi.org/10.1016/j.ijhydene.2006.02.009

Tonui, J. K., & Tripanagnostopoulos, Y. (2007). Air-cooled PV/T solar collectors with low cost performance improvements. *Solar Energy*, *81*(4), 498–511. https://doi.org/10.1016/j.solener.2006.08.002

Tripanagnostopoulos, Y. (2007). Aspects and improvements of hybrid photovoltaic/thermal solar energy systems. *Solar Energy*, *81*(9), 1117–1131. https://doi.org/10.1016/j.solener.2007.04.002

Tripanagnostopoulos, Y., Nousia, T., Souliotis, M., & Yianoulis, P. (2002). Hybrid photovoltaic/thermal solar systems. *Solar Energy*, *72*(3), 217–234. https://doi.org/10.1016/S0038-092X(01)00096-2

United Nations. (2015). *Framework Convention on Climate Change*.

Vasan, N., & Stathopoulos, T. (2014). Experimental study of wind effects on unglazed transpired collectors. *Solar Energy*, *101*, 138–149. https://doi.org/10.1016/j.solener.2013.11.037

Vats, K., Tomar, V., & Tiwari, G. N. (2012). Effect of packing factor on the performance of a building integrated semitransparent photovoltaic thermal (BISPVT) system with air duct. *Energy and Buildings*, *53*, 159–165. https://doi.org/10.1016/j.enbuild.2012.07.004

Wang, Y., Shukla, A., & Liu, S. (2017). A state of art review on methodologies for heat transfer and energy flow characteristics of the active building envelopes. *Renewable and Sustainable Energy Reviews*, *78*(April), 1102–1116. https://doi.org/10.1016/j.rser.2017.05.015

Wolf, M. (1976). Performance analyses of combined heating and photovoltaic power systems for residences. *Energy Conversion*, *16*(1–2), 79–90. https://doi.org/10.1016/0013-7480(76)90018-8

Xu, P., Zhang, X., Shen, J., Wu, Y., Connelly, K., Yang, T., Tang, L., Xiao, M., & Wei, Y. (2017). A review of thermal absorbers and their integration methods for the combined solar photovoltaic/thermal (PV/T) modules. *Renewable and Sustainable Energy Reviews*, *75*(April 2016), 839–854. https://doi.org/10.1016/j.rser.2016.11.063

Yang, T., & Athienitis, A. K. (2014a). A study of design options for a building integrated photovoltaic/thermal (BIPV/T) system with glazed air collector and multiple inlets. *Solar Energy*, *104*, 82–92. https://doi.org/10.1016/j.solener.2014.01.049

Yang, T., & Athienitis, A. K. (2014b). A study of design options for a building integrated photovoltaic/thermal (BIPV/T) system with glazed air collector and multiple inlets. *Solar Energy*, *104*, 82–92. https://doi.org/10.1016/j.solener.2014.01.049

Yang, T., & Athienitis, A. K. (2015a). Experimental investigation of a two-inlet air-based building integrated photovoltaic/thermal (BIPV/T) system. *Applied Energy*, *159*, 70–79. https://doi.org/10.1016/j.apenergy.2015.08.048

Yang, T., & Athienitis, A. K. (2015b). Performance Evaluation of Air-based Building Integrated Photovolta-ic/Thermal (BIPV/T) System with Multiple Inlets in a Cold Climate. *Procedia Engineering*, *121*, 2060–2067. https://doi.org/10.1016/j.proeng.2015.09.207

Yang, T., & Athienitis, A. K. (2016). A review of research and developments of building-integrated photovoltaic/thermal (BIPV/T) systems. *Renewable and Sustainable Energy Reviews*, *66*, 886–912. https://doi.org/10.1016/j.rser.2016.07.011

Zogou, O., & Stapountzis, H. (2011). Energy analysis of an improved concept of integrated PV panels in an office building in central Greece. *Applied Energy*, *88*(3), 853–866. https://doi.org/10.1016/j.apenergy.2010.08.023

Zogou, O., & Stapountzis, H. (2012). Flow and heat transfer inside a PV/T collector for building application. *Applied Energy*, *91*(1), 103–115. https://doi.org/10.1016/j.apenergy.2011.09.019

Zondag, H. A. (2008). Flat-plate PV-Thermal collectors and systems: A review. *Renewable and Sustainable Energy Reviews*, *12*(4), 891–959. https://doi.org/10.1016/j.rser.2005.12.012

APPENDIX A: Flow measurements

A linear correlation between mass flow rate and average channel velocity was established according to the procedure described in Yang & Athienitis [30]. The ratio of flows for the single and double inlet configurations (Fig. A.1) was established through hot-wire anemometer measurements of air velocity at the locations indicated in Figure 10. It was found that for all flow rate setpoints, 68.1% (±1%) of the total flow entered though the bottom opening and the remaining from the second inlet (for the double-inlet configurations). This ratio was used to evaluate the Reynolds number for each section. For the case of the single-inlet configuration, the flow rate and therefore the Reynolds number were virtually the same, with slight variations due to the fact that the air density, ρ and viscosity, μ, were considered as temperature dependent parameters and were calculated based on the average air temperature of each respective section.

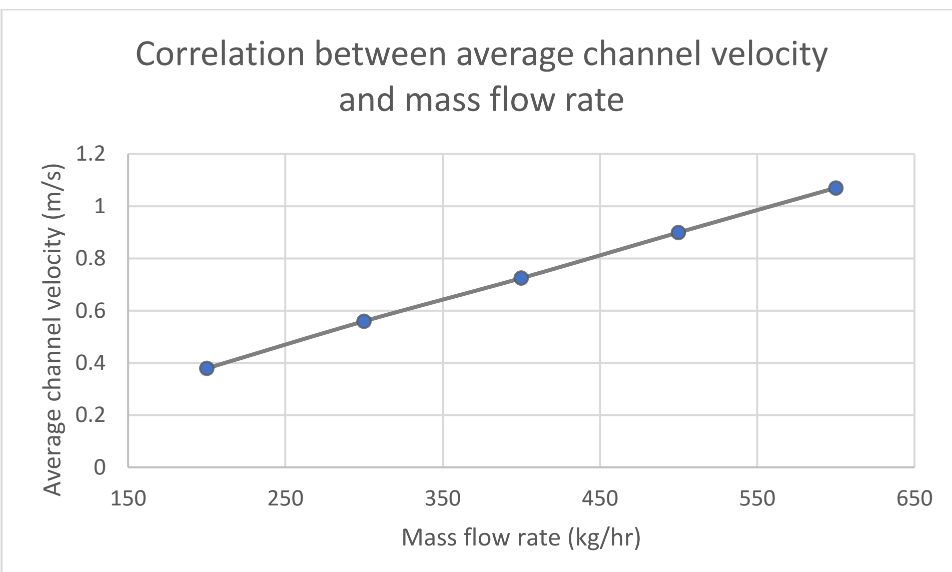

Figure A.1: Correlation between mass flow set point and recorded average channel velocity.

APPENDIX B: Energy balance, CHTC and Nu calculations

Figure B.1 shows the energy balance of a BIPV/T section (or control volume) which could represent either the bottom or top section, or the entire collector.

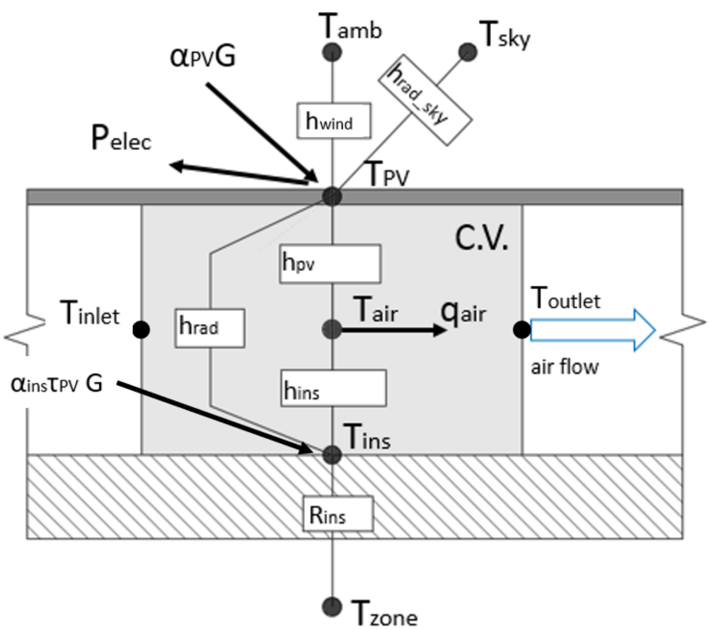

Figure B.1: Energy balance of a BIPV/T section (or control volume)

For the determination of the Nu of each respective section and surface, the following procedure was followed:

From the recorded temperature profiles of the PV, insulation and air, the respective average temperatures, as well as the inlet/outlet temperatures were calculated for each section.

The total amount of heat recovered from each section was calculated according to equation 2 (presented in section 5):

$$q_{air} = \dot{m} C_p \Delta T \qquad (2)$$

The amount of radiative heat transfer from the PV to the insulation surface for each section was calculated as follows (eq. B.1):

$$q_{rad\_PV\_ins} = \sigma \cdot \left(\frac{1}{\frac{1}{\varepsilon_{PV}}+\frac{1}{\varepsilon_{ins}}-1}\right) \cdot F_{PV-ins} \cdot (T_{PV}^4 - T_{ins}^4) \cdot A_c \qquad (B.1)$$

Where ε_{PV}, ε_{ins}, T_{PV} and T_{ins} the emissivity and absolute temperature (K) of the PV and insulation surface respectively, and $F_{PV\text{-}ins}$ the view factor between the PV and the insulation surface as calculated based on the geometry of the collector.

According to the energy balance, the amount of convective heat transfer from the insulation surface equals to the amount of radiative heat transfer from the PV to the insulation minus the conductive heat losses from the insulation (calculated based on the insulation RSI and the temperature difference from surface to surface, as measured by the thermocouples).

$$q_{ins\_air} = q_{rad\_PV\_ins} - \frac{1}{R_{ins}} \cdot (T_{ins} - T_{zone}) \cdot A_c \tag{B.2}$$

Followingly, the convective heat transfer coefficient of the insulation side (h_{ins}) was calculated according to equation 7:

$$h_{ins} = q_{ins-air}/((T_{ins} - T_{air})A_c) \tag{B.3}$$

Finally, the amount of convective heat transfer from the PV surface was evaluated deducting the amount of convective heat transfer from the total heat recovery (eq.8). The CHTC of the PV side was evaluated according to equation 9:

$$q_{PV-air} = q_{air} - q_{ins\_air} \tag{B.4}$$

$$h_{PV} = q_{PV-air}/((T_{PV} - T_{air})A_c) \tag{B.5}$$

The Nu of each respective section were determined using equation 5 (as presented in section 5.3)

APPENDIX C: Uncertainty Analysis

In this section, the uncertainties for the electrical and thermal efficiencies of the tested configurations were calculated according to the propagation of uncertainty methodology considering that the involved parameters were independent from each other:

$$\sigma_f = \sqrt{\left(\frac{\partial f}{\partial_{x_1}}\right)^2 {\sigma_{x_1}}^2 + \left(\frac{\partial f}{\partial_{x_2}}\right)^2 {\sigma_{x_2}}^2 + \cdots + \left(\frac{\partial f}{\partial_{x_n}}\right)^2 {\sigma_{x_n}}^2} \tag{C.1}$$

Electrical efficiency

The uncertainty in the assembly's electrical efficiency stems from the uncertainties in the power output of each of the two PV modules and the incident solar irradiance. The power output of each PV module was measured with a portable I-V curve tracer as:

$$P_{PV} = I_{max} \cdot V_{max} \tag{C.2}$$

where I_{max} and V_{max} the current and voltage at operating maximum power point respectively. The relative error in the voltage measurement is better than ±(0.2% of reading + 0.1% of full scale of range) with a range of 20 V. The relative error in the current measurement is ±(0.3% of reading + 0.1% of full scale of range) with a range of 22 Amperes. The uncertainty regarding the incident radiation is 2%, without considering the final uniformity.

The absolute uncertainty regarding the electrical efficiency (eq. 3) is then calculated as:

$$\sigma_{\eta_{el}} = \sqrt{\left(\frac{I_{\max1}}{G \cdot A_c} \cdot \sigma_{V_{max1}}\right)^2 + \left(\frac{V_{\max1}}{G \cdot A_c} \cdot \sigma_{I_{max1}}\right)^2 + \left(\frac{I_{\max2}}{G \cdot A_c} \cdot \sigma_{V_{max2}}\right)^2 + \left(\frac{V_{\max2}}{G \cdot A_c} \cdot \sigma_{I_{max2}}\right)^2 + \left(\frac{-I_{\max1} * V_{\max1} - I_{\max2} * V_{\max2}}{A_c \cdot G^2} \cdot \sigma_G\right)^2} \tag{C.3}$$

The absolute uncertainty regarding the electrical efficiency was found to be up to 0.26% (or up to 2.15% relative to the calculated electrical efficiency value).

Thermal efficiency

The uncertainty in the thermal efficiency (eq. 1) of the prototype involves uncertainties in the mass flow rate, the inlet-outlet temperature difference and the solar irradiance. The mass flow rate is measured by the Solar Air Collector Test Stand with an orifice flow meter which uses three differential pressure transducers of different ranges. The associated overall mass flow uncertainty is ±2 of the measured value (kg/hr or kg/s). The uncertainty associated with the temperature difference ΔT between the inlet and outlet of the air channel is calculated based on the uncertainty of the RTD probes (±0.1°C) as:

$$\sigma_{\Delta T} = \sqrt{0.1^2 + 0.1^2} = 0.14°\text{C} \tag{C.4}$$

$$\sigma_{\eta_{th}} = \sqrt{\left(\frac{C_p(\Delta T)}{G \cdot A_c} \cdot \sigma_{\dot{m}}\right)^2 + \left(\frac{\dot{m} * C_p}{G \cdot A_c} \cdot \sigma_{\Delta T}\right)^2 + \left(\frac{-2\dot{m} * C_p(\Delta T)}{A_c \cdot G^2} \cdot \sigma_G\right)^2} \tag{C.5}$$

The absolute uncertainty of the thermal efficiency was found to up to 1.5% (or 5.1% relative to the calculated electrical efficiency value).

PV temperatures

The uncertainty for the PV temperature measurements is taken as the uncertainty of the T-type thermocouples (special limit of errors with calibration: ±0.3°C).